

論文 / 著書情報
Article / Book Information

題目(和文)	熱処理によるCoO/CoPt多層膜の垂直磁気異方性および垂直交換バイアスの向上
Title(English)	Enhancement of Perpendicular Magnetic Anisotropy and Perpendicular Exchange Bias in CoO/CoPt Multilayer Films by Thermal Annealing
著者(和文)	郭磊
Author(English)	Lei Guo
出典(和文)	学位:博士(工学), 学位授与機関:東京工業大学, 報告番号:甲第10110号, 授与年月日:2016年3月26日, 学位の種別:課程博士, 審査員:史蹟,中村吉男,林幸,村石信二,中川茂樹
Citation(English)	Degree:Doctor (Engineering), Conferring organization: Tokyo Institute of Technology, Report number:甲第10110号, Conferred date:2016/3/26, Degree Type:Course doctor, Examiner:,,,,,
学位種別(和文)	博士論文
Type(English)	Doctoral Thesis

**Enhancement of Perpendicular Magnetic
Anisotropy and Perpendicular Exchange
Bias in CoO/CoPt Multilayer Films by
Thermal Annealing**

Lei Guo

Directed by

Prof. Ji Shi

Prof. Yoshio Nakamura

Department of Metallurgy and Ceramics Science

Tokyo Institute of Technology

December 2015

Preface

Perpendicular magnetic anisotropy (PMA) and perpendicular exchange bias (PEB) of $[\text{CoO}_x/\text{CoPt}_y]_n$ multilayer films have been studied systematically in this thesis. The influences of post-annealing temperature, CoPt thickness, CoO thickness, repetition period and CoO seed layer on PMA and PEB were studied step by step. Enhancement of PMA and PEB by thermal annealing has been confirmed in $[\text{CoO}_x/\text{CoPt}_y]_n$ multilayer films. We found 300°C-annealed $[\text{CoO}_x/\text{CoPt}_y]_n$ possess the strongest PMA and the best PEB.

According to the experiments, $\text{CoO}20\text{nm}/[\text{CoPt}5\text{nm}/\text{CoO}5\text{nm}]_5$ multilayer films show the best PMA performance and possess the highest thermal stability at the temperature region between -192°C and 400°C . This indicates $\text{CoO}20\text{nm}/[\text{CoPt}5\text{nm}/\text{CoO}5\text{nm}]_5$ multilayer films could be a potential candidate for the PMA application at middle-high temperature region between 300°C and 400°C . After perpendicular field cooling, 300°C-annealed $[\text{CoO}5\text{nm}/\text{CoPt}5\text{nm}]_5$ film shows the best PEB performance, having a PEB value of 1060 Oe. We hope this 300°C-annealed $[\text{CoO}5\text{nm}/\text{CoPt}5\text{nm}]_5$ multilayer film can have some potential applications in perpendicular magnetic tunneling junction.

The mechanism responsible for the magnetic anisotropy transition in $[\text{CoO}5\text{nm}/\text{CoPt}7\text{nm}]_5$ multilayer films has been studied in detail by analyzing CoO/CoPt interface and CoPt layer internal stress. It is found the effective PMA energy is proportional to the CoPt layer in-plane tensile stress but is inversely

proportional to the CoO/CoPt interface roughness. By means of low temperature experiment, we demonstrate the magnetic anisotropy transition observed in $[\text{CoO}5\text{nm}/\text{CoPt}7\text{nm}]_5$ multilayer film is mainly attributed to the change of CoPt layer in-plane tensile stress. In other words, it is magnetoelastically induced magnetic anisotropy transition in $[\text{CoO}5\text{nm}/\text{CoPt}7\text{nm}]_5$.

The effects of magnetoelastically induced PMA on PEB have been studied in $[\text{CoO}5\text{nm}/\text{CoPt}5\text{nm}]_5$ multilayer films. Significant enhancement of PMA was achieved in $[\text{CoO}5\text{nm}/\text{CoPt}5\text{nm}]_5$ multilayer films after annealing due to the increase of CoPt layer in-plane tensile stress. With the enhancement of magnetoelastically induced PMA, great improvement of PEB was also achieved in $[\text{CoO}5\text{nm}/\text{CoPt}5\text{nm}]_5$ multilayer films. We consider the enhanced PMA with more perpendicular spins alignment in CoPt layer results in the improved PEB in $[\text{CoO}5\text{nm}/\text{CoPt}5\text{nm}]_5$ multilayer films through enhanced perpendicular spins coupling at CoO/CoPt interfaces.

To our knowledge, the PMA surviving at temperature region between 300°C and 400°C in $[\text{CoO}_x/\text{CoPt}_y]_n$ multilayer film is obtained for the first time. On the other hand, the positive effect of PMA on PEB at FM/AFM interface in $[\text{CoO}_x/\text{CoPt}_y]_n$ multilayer films is also reported for the first time.

Contents

Preface.....	I
Contents.....	III
Chapter 1 Introduction.....	- 1 -
1.1 Challenge in longitudinal magnetic recording.....	- 1 -
1.2 History of perpendicular magnetic recording.....	- 3 -
1.3 Current perpendicular magnetic recording media.....	- 5 -
1.3.1 CoCrPt-SiO ₂	- 5 -
1.3.2 Co/Pd and CoPt/AlN.....	- 6 -
1.3.3 L ₁₀ CoPt and FePt.....	- 7 -
1.4 Magnetic anisotropy.....	- 8 -
1.4.1 Magnetocrystalline anisotropy.....	- 9 -
1.4.2 Interface anisotropy.....	- 10 -
1.4.3 Magnetoelastic anisotropy.....	- 10 -
1.4.4 Shape anisotropy.....	- 11 -
1.5 Exchange bias effect.....	- 11 -
1.5.1 Longitudinal exchange bias.....	- 13 -
1.5.2 Perpendicular exchange bias.....	- 16 -
1.6 Background of this work.....	- 17 -
1.7 Objectives of this work.....	- 19 -
1.8 Organization of this work.....	- 20 -
References.....	- 23 -
Chapter 2 Preparation and characterization of [CoO _x /CoPt _y] _n multilayer films.....	- 29 -
2.1 Preparation of [CoO _x /CoPt _y] _n film.....	- 29 -
2.1.1 RF magnetron sputtering of CoO layers.....	- 29 -
2.1.2 DC magnetron sputtering of CoPt layers.....	- 30 -
2.1.3 Post annealing of [CoO _x /CoPt _y] _n film.....	- 31 -
2.1.4 Field cooling of [CoO _x /CoPt _y] _n film.....	- 31 -
2.2 Structure characterization of [CoO _x /CoPt _y] _n film.....	- 32 -
2.2.1 Transmission electron microscopy.....	- 32 -
2.2.1.1 Fundamental of TEM.....	- 32 -
2.2.1.2 TEM of [CoO _x /CoPt _y] _n film.....	- 33 -
2.2.2 X-ray diffraction.....	- 34 -
2.2.2.1 Bragg's law and structure factor.....	- 35 -
2.2.2.2 CoPt structure.....	- 37 -
2.2.2.3 CoO structure.....	- 38 -
2.2.2.4 XRD of [CoO _x /CoPt _y] _n film.....	- 39 -
2.2.3 X-ray reflectivity.....	- 40 -
2.2.3.1 Fundamental of XRR.....	- 40 -
2.2.3.2 XRR of [CoO _x /CoPt _y] _n film.....	- 42 -
2.2.4 Atomic force microscopy.....	- 43 -
2.2.4.1 Fundamental of AFM.....	- 43 -

2.2.4.2 AFM of [CoO _x /CoPt _y] _n film.....	- 43 -
2.3 Magnetic property measurement.....	- 47 -
2.3.1 Ferromagnetic CoPt.....	- 47 -
2.3.2 Antiferromagnetic CoO.....	- 48 -
2.3.3 Co magnetic moments configuration at CoO/CoPt interface.....	- 49 -
2.3.4 Vibrating sample magnetometer.....	- 50 -
2.3.5 PMA magnetic hysteresis loops of [CoO _x /CoPt _y] _n film.....	- 51 -
2.3.6 PEB magnetic hysteresis loops of [CoO _x /CoPt _y] _n film.....	- 53 -
2.4 Summary.....	- 54 -
References.....	- 54 -
Chapter 3 Perpendicular magnetic anisotropy of [CoO _x /CoPt _y] _n multilayer films.....	- 57 -
3.1 Introduction.....	- 57 -
Keywords:.....	- 58 -
3.2 Experimental details.....	- 59 -
3.2.1 Preparation of [CoO _x /CoPt _y] _n multilayer films.....	- 59 -
3.2.2 Characterizations of [CoO _x /CoPt _y] _n multilayer films.....	- 59 -
3.3 Results and Discussion.....	- 61 -
3.3.1 [CoO _x /CoPt _y] _n with different CoPt thickness and different annealing temperature.....	- 61 -
3.3.2 [CoO _x /CoPt _y] _n with different CoO thickness.....	- 69 -
3.3.3 [CoO _x /CoPt _y] _n with different period.....	- 71 -
3.3.4 [CoO _x /CoPt _y] _n without and with CoO20nm seed layer.....	- 73 -
3.3.5 [CoPt _y /CoO _x] _n with CoO20nm seed layer but different CoPt thickness....	- 75 -
3.3.6 PMA thermal stability of CoO20nm/[CoPt5nm/CoO5nm] ₅	- 77 -
3.4 Conclusion.....	- 79 -
References.....	- 80 -
Chapter 4 Magnetoelastically induced magnetic anisotropy transition in [CoO5nm/CoPt7nm] ₅ multilayer films.....	- 81 -
4.1 Introduction.....	- 81 -
Keywords:.....	- 82 -
4.2 Experimental Details.....	- 83 -
4.2.1 Preparation of [CoO5nm/CoPt7nm] ₅ multilayer films.....	- 83 -
4.2.2 Characterizations of [CoO5nm/CoPt7nm] ₅ multilayer films.....	- 83 -
4.3 Results and Discussion.....	- 84 -
4.3.1 Hysteresis loops of [CoO5nm/CoPt7nm] ₅ multilayer films.....	- 84 -
4.3.2 AFM images of [CoO5nm/CoPt7nm] ₅ multilayer films.....	- 88 -
4.3.3 XRD of [CoO5nm/CoPt7nm] ₅ multilayer films.....	- 94 -
4.3.4 CoPt layer in-plane stress.....	- 95 -
4.3.5 Correlation between K_{eff} and R_{rms} , $\sigma_{//}$	- 99 -
4.4 Conclusion.....	- 105 -
References.....	- 106 -
Chapter 5 Perpendicular exchange bias of [CoO _x /CoPt _y] _n multilayer films.....	- 107 -
5.1 Introduction.....	- 107 -

Keywords:.....	- 108 -
5.2 Experimental details.....	- 109 -
5.2.1 Preparation of $[\text{CoO}_x/\text{CoPt}_y]_n$ multilayer films.....	- 109 -
5.2.2 Characterizations of $[\text{CoO}_x/\text{CoPt}_y]_n$ multilayer films.....	- 109 -
5.3 Results and Discussion.....	- 111 -
5.3.1 $[\text{CoO}_x/\text{CoPt}_y]_n$ with different post-annealing temperature.....	- 111 -
5.3.2 $[\text{CoO}_x/\text{CoPt}_y]_n$ with different CoPt thickness.....	- 114 -
5.3.3 $[\text{CoO}_x/\text{CoPt}_y]_n$ with different CoO thickness.....	- 116 -
5.3.4 $[\text{CoO}_x/\text{CoPt}_y]_n$ with different period.....	- 118 -
5.3.5 $[\text{CoPt}_y/\text{CoO}_x]_n$ with CoO20nm seed layer.....	- 120 -
5.4 Conclusion.....	- 122 -
References.....	- 122 -
Chapter 6 Magnetoelastically induced perpendicular magnetic anisotropy and perpendicular exchange bias of $[\text{CoO5nm}/\text{CoPt5nm}]_5$ multilayer films.....	- 123 -
6.1 Introduction.....	- 123 -
Keywords:.....	- 125 -
6.2 Experimental details.....	- 125 -
6.2.1 Preparation of $[\text{CoO5nm}/\text{CoPt5nm}]_5$ multilayer films.....	- 125 -
6.2.2 Characterizations of $[\text{CoO5nm}/\text{CoPt5nm}]_5$ multilayer films.....	- 126 -
6.3 Results and discussion.....	- 126 -
6.3.1 PMA of $[\text{CoO5nm}/\text{CoPt5nm}]_5$ multilayer films.....	- 126 -
6.3.2 PEB of $[\text{CoO5nm}/\text{CoPt5nm}]_5$ multilayer films.....	- 129 -
6.3.3 Cross-section TEM and top-surface AFM.....	- 131 -
6.3.4 XRD and CoPt layer in-plane stress.....	- 134 -
6.3.5 Correlation between CoPt layer stress, PMA and PEB.....	- 137 -
6.4 Conclusion.....	- 143 -
References.....	- 144 -
Chapter 7 Conclusions.....	- 145 -
Publications.....	- 148 -
Presentations.....	- 148 -
Acknowledgements.....	- 149 -

Chapter 1 Introduction

At present, the digital information storage devices can be classified mainly into optical storage (CD, DVD), semiconductor storage (flash memory, SD card) and magnetic storage (floppy disk, HDDs). In the past decades, hard disk drives (HDDs) grew rapidly because of the strong growth of the information society. The first HDDs could be dated back to late 1950s when IBM introduced random access method of accounting and control (RAMAC) with a areal density of 2 kb/in². Then, HDDs was improved over time and entered our personal computers in the 1980s. In 2008, the areal density of HDDs had reached 600 Gb/in², which was 300-million times of its ancestor. In our daily life, such a tremendous improvement in HDDs helps in many aspects, firstly the cost down per gigabit helps us to buy data storage at cheaper costs, secondly higher areal density of HDDs plays an important role in the development of electronic devices miniaturization^[1-7].

1.1 Challenge in longitudinal magnetic recording

Until recently, the HDDs industry has focused mainly on the longitudinal magnetic recording method, in which the magnetization of each data bit is aligned parallel to the disk. It is well known the total storage capacity of a HDDs

depends on how small we can make the grain needed to represent one bit of information: usually smaller grains generate greater capacity. However, there is a lowest limit to the size of grains. If the magnetic grains on the disk are too tiny, they would start to interfere with each other, and there will be a risk that the magnetization may spontaneously reverse due to excitation by the thermal energy^[8].

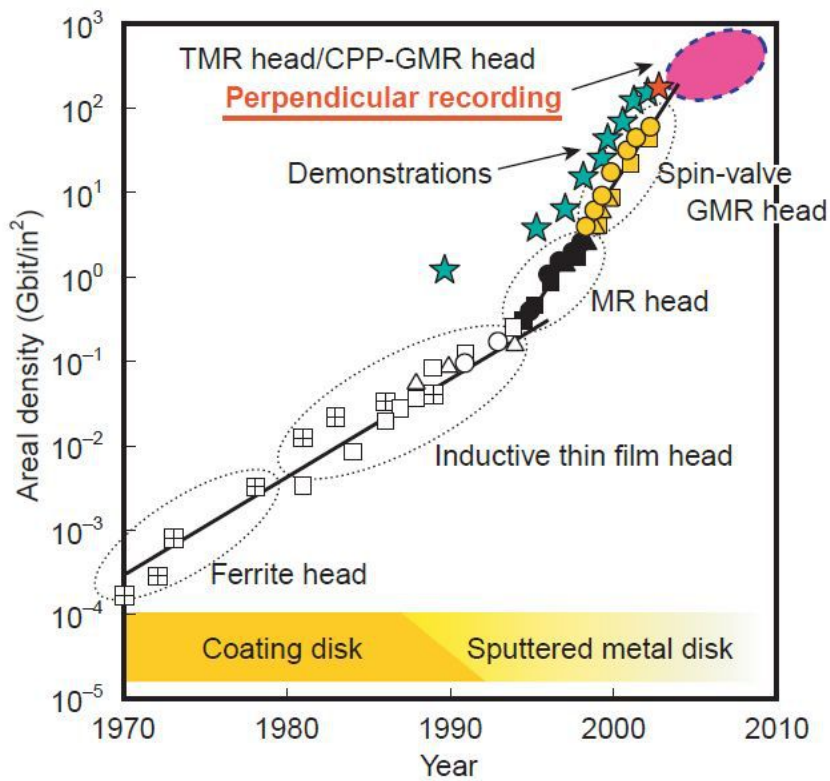


Fig 1-1 Areal density development of HDDs^[9].

As is known, the energy barrier that prevents the magnetization of a particle from flipping is proportional to anisotropy energy $K_u V$, where K_u is the anisotropy constant of the material and V is the volume of the grain. With the reduction of grain volume V , the anisotropy energy $K_u V$ and thus the energy barrier for magnetization reversal will be reduced. If the grain volume V is small

enough, the thermal energy $K_B T$ starts to compete with the anisotropy energy $K_u V$ and makes the magnetization thermally excited and reversed. This phenomenon, where the magnetic particles lose their ability to hold their magnetic orientations and reverse their magnetization without any external field, is known as the superparamagnetic effect (SPE)^[10-19].

According to the previous report, the original data in HDDs will be lost even if 5% of the magnetization reverses due to SPE. To our knowledge, SPE is the physical limit and also considered as the first threat to the areal density growth of longitudinal recording technology^[8].

1.2 History of perpendicular magnetic recording

Perpendicular magnetic recording (PMR) was first proven advantageous in 1970s by Iwasaki and his co-workers in Japan^[20-22]. Contrast with the conventional longitudinal magnetic recording, perpendicular magnetic recording is based on the media with perpendicular magnetic anisotropy (PMA).

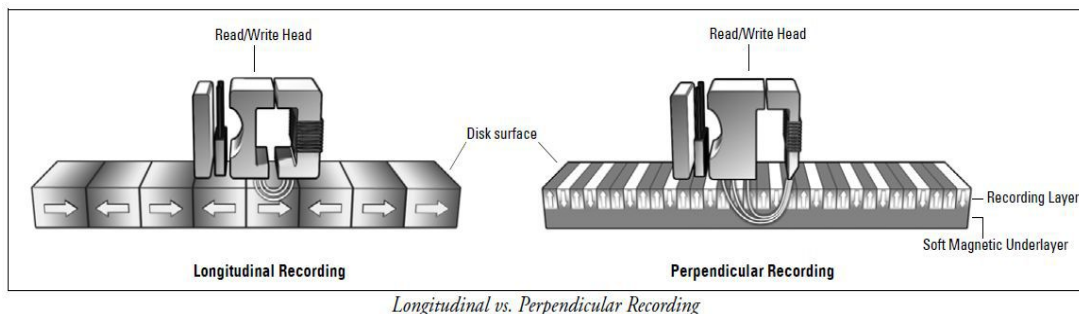


Fig 1-2 Configuration of longitudinal and perpendicular magnetic recording^[23].

As is shown in Fig1-2, generally a magnetic recording device has two key components: a recording medium to store information, a writer and reader head to produce localized magnetic field for writing information and to convert the magnetic signals of the recording medium to electrical signals for reading information. In a perpendicular magnetic recording disk, the magnetic bits keep perpendicular to the disk surface. So far, the well accepted explanation for the advantages of perpendicular magnetic recording is that it can achieve higher storage densities by aligning the magnetic elements perpendicularly to the surface of the disk, this means the magnetic elements can be placed closer on the disk, and thus more magnetic elements can be stored in a given area^[23].

Although perpendicular recording allows continued advances in areal density, the research on perpendicular recording until the last century was limited. It took about three decades to make a perpendicular recording product that has competing performance, reliability, and price advantage over the prevalent longitudinal recording technology^[24-32].

Perpendicular recording was first used by Toshiba in 3.5" floppy disks in 1989 to permit 2.88 MB of capacity. After that, the perpendicular recording has been improved greatly and its areal density shifts from 10Gb/in² in 1999 to 500Gb/in² recently. In 2005, the company Toshiba produced the first commercial perpendicular magnetic recording HDDs. By 2010, 667Gb/in² perpendicular magnetic recording HDDs was available^[33-37].

In the future, perpendicular magnetic recording technology is predicted to be dominated in the information storage field, so it is of great importance to study perpendicular magnetic recording media at present.

1.3 Current perpendicular magnetic recording media

Perpendicular magnetic recording technology is based on perpendicular magnetic recording media. So, it is necessary to introduce the popular perpendicular magnetic recording media firstly.

1.3.1 CoCrPt-SiO₂

The materials used as the perpendicular recording media has traditionally been a Co alloy. In the late 1970s, Iwasaki et al. proposed CoCr alloy as the original perpendicular magnetic recording media. Since then, offspring of Co alloy such as CoCrPt, CoCrTa, CoCrNb, CoCrPtNb, and CoCrPtB were developed successively^[8, 25, 26, 30, 32, 38-41].

In 2002, Oikawa et al. added SiO₂ into CoCrPt alloy to form SiO₂ boundaries which segregate the neighboring CoCrPt grains magnetic-interaction and thus achieve lower magnetic noise effectively^[42-47]. Since its favorable properties, nowadays CoCrPt-SiO₂ granular medium have been widely used in the commercial perpendicular magnetic recording HDDs.

Fig1-3 are the in-plane TEM image and the related hysteresis loop of

CoCrPt-SiO₂ medium^[9].

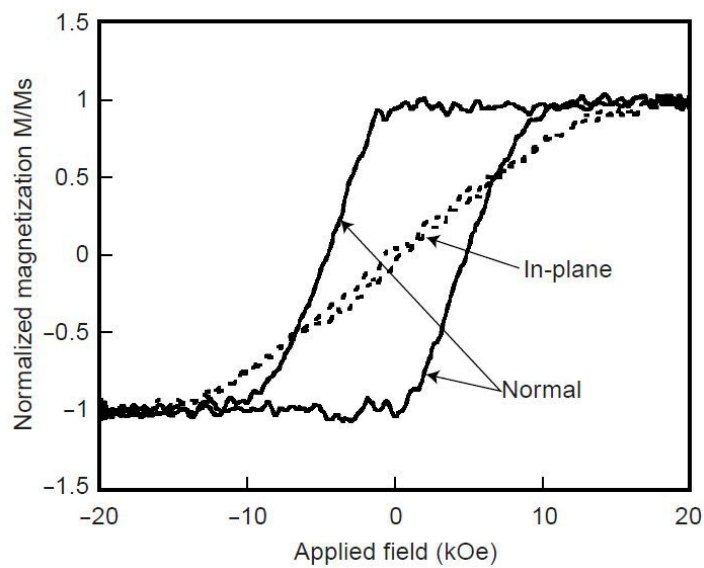
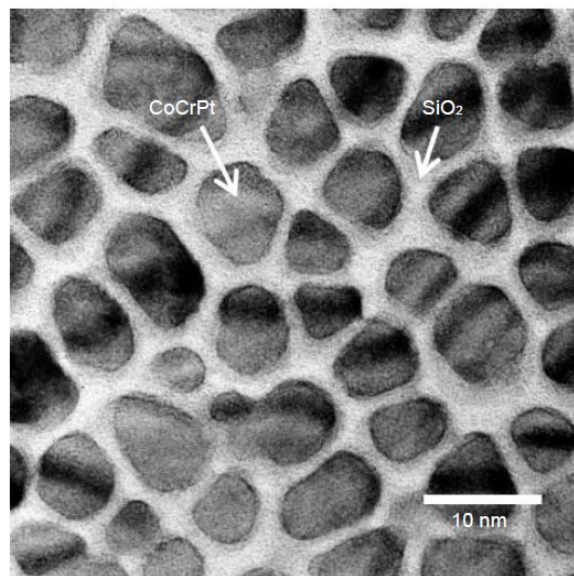


Fig 1-3 In-plane TEM image and hysteresis loop of CoCrPt-SiO₂ medium^[9].

1.3.2 Co/Pd and CoPt/AlN

In 1985, Carcia firstly reported PMA with layered structure in Co/Pd system and explained the mechanism responsible for PMA in terms of the interface

anisotropy^[48]. A few years later, PMA was also observed in Co/Au, Co/Pt and Co/Ru systems, of which the magnetic anisotropy could be enhanced by improving the interface quality^[49-51]. However, it is universal in the above metallic multilayer films that PMA always deteriorates at elevated temperatures higher than 250°C-300°C due to the interface diffusion, which limits their applications greatly^[52].

In order to overcome the interface diffusion in Co/metal, AlN and TiN were introduced instead of the metals recently, and PMA were obtained in CoPt/AlN, FePt/AlN and CoPt/TiN multilayer films. However, in such systems it is hard to get PMA without thermal annealing higher than 400°C^[53-55].

1.3.3 L1₀ CoPt and FePt

As is known, the magnetic anisotropy energy equals $K_u V$, where K_u is the magnetic anisotropy constant of the magnetic grain and V is the volume of the magnetic grain^[8]. To overcome the the superparamagnetic effect, the magnetic anisotropy energy $K_u V$ should be greater than the thermal energy $K_B T$. For the specified $K_u V$, it is easy to understand that the larger the magnetic anisotropy constant K_u is, the smaller the grain volume can be made to improve the recording areal density. So, it is significant to explore the materials that possess high magnetic anisotropy.

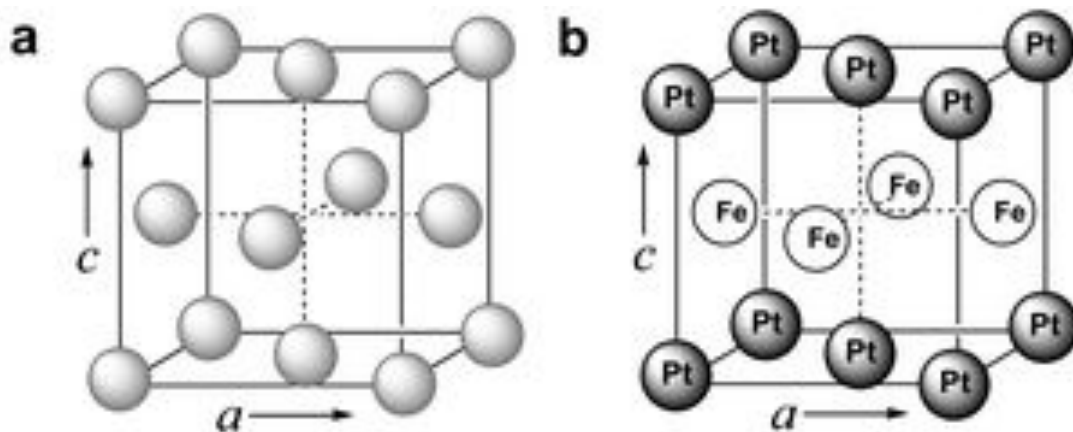


Fig1-4 FCC and FCT structures of FePt alloy.

Recently, face-centered-tetragonal ($L1_0$) CoPt and FePt alloy have been studied extensively due to their large coercivity and high magneto-crystalline anisotropy^[56, 57]. As is shown in Fig1-4(a), Fe or Pt atoms occupy the lattice points randomly in the FCC FePt solid solution alloy. After annealing, $L1_0$ transformation can be observed as shown in Fig1-4(b). However, $L1_0$ transformation usually needs post annealing higher than 600°C, which blocks its applications in some degree. At present, many researchers are focusing on how to reduce the transformation temperature^[58, 59].

1.4 Magnetic anisotropy

A magnetically isotropic material has no preferential direction for its magnetic moment unless there is an applied magnetic field. In contrast, the magnetic moment of magnetically anisotropic materials will tend to align with an "easy axis", which is an energetically favorable direction of spontaneous magnetization.

In a word, magnetic anisotropy is the directional dependence of a material's magnetic properties^[60].

To our knowledge, the sources responsible for magnetic anisotropy can be classified as: magnetocrystalline anisotropy, interface anisotropy, magnetoelastic anisotropy and shape anisotropy^[61, 62].

1.4.1 Magnetocrystalline anisotropy

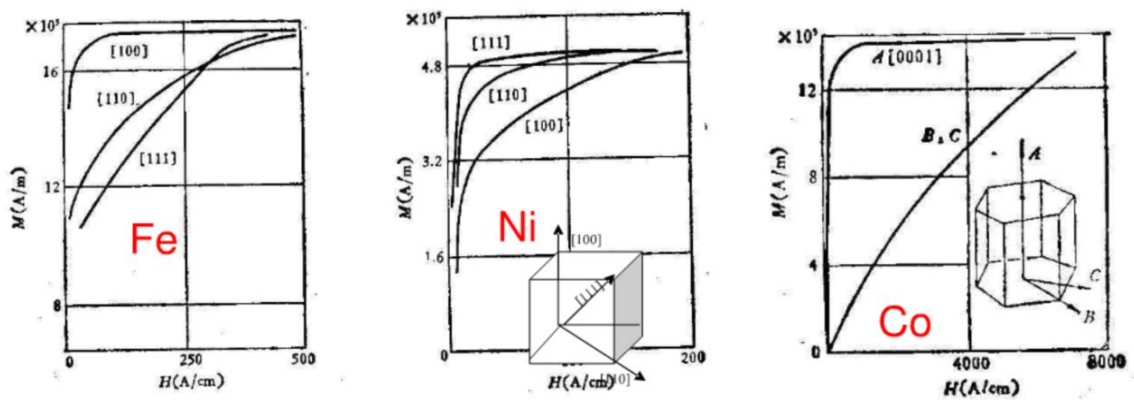


Fig1-5 Magnetocrystalline anisotropy of ideal single domain Fe, Ni and Co.

In physics, the spin-orbit interaction is the primary source of magnetocrystalline anisotropy and the atomic structure of a crystal introduces preferential directions for the magnetization. A ferromagnetic material is said to have magnetocrystalline anisotropy if it takes more energy to magnetize it in certain directions than in others. These directions are usually related to the principal axes of its crystal lattice. Based on the number of easy and hard axes, magnetocrystalline anisotropy can be classified as : uniaxial anisotropy which has only one easy axis, triaxial anisotropy which has a single easy axis,

an intermediate axis and a hard axis, cubic anisotropy which has three or four easy axes^[63-65]. For example, Fig1-5 shows the magnetocrystalline anisotropy of ideal single domain Fe, Ni and Co.

1.4.2 Interface anisotropy

In [Ferromagnet/X]_n ([F/X]_n) multilayer thin films, the atoms of ferromagnet layer located at the F/X interface usually show very different magnetocrystalline anisotropy from the atoms of the bulk ferromagnet due to the broken structure symmetry at F/X interface. Such anisotropy was predicted firstly by Neel in 1954 and named as interface anisotropy. After extensive researches, it is well accepted now in [F/X]_n multilayer thin films this F/X interface anisotropy plays important roles on the whole magnetic anisotropy of [F/X]_n^[66-68].

1.4.3 Magnetoelastic anisotropy

Magnetostriction is a property of ferromagnetic materials that causes them to change their shape or dimensions during the process of magnetization. It characterizes the shape change of a ferromagnetic material during magnetization. Magnetoelastic effect (inverse magnetostrictive effect) is the name given to the change of the magnetic susceptibility of a material when subjected to a mechanical stress. It characterizes the change of sample magnetization for given magnetizing field strength when mechanical stresses are applied to the sample^[69-73]. In [F/X]_n multilayer thin films, residual stress often

occurs in ferromagnet layer due to the existence of F/X interface. This residual stress will break the structure symmetry of ferromagnet layer, lead to different magnetocrystalline anisotropy and thus have great influences on the whole magnetic anisotropy of $[F/X]_n$ ^[74].

1.4.4 Shape anisotropy

Shape anisotropy is a typical long range anisotropy that originates from the magnetic dipolar interactions. When a particle is not perfectly spherical, the demagnetizing field will not be equal for all directions, creating one or more easy axes. In $[F/X]_n$ multilayer thin films, the strong demagnetizing field usually has great influences on the ferromagnet layer in-plane anisotropy^[75].

1.5 Exchange bias effect

When a multilayer film with ferromagnetic(FM)/antiferromagnetic(AFM) interfaces is cooled through the Neel temperature (T_N) of AFM in a external magnetic field the shift of FM hysteresis loop (H_{EB}) can be induced, which is so-called exchange bias effect (EB)^[76]. It is well accepted now the essential physics behind EB phenomenon is the coupling interaction between FM and AFM at their interface, as is shown in Fig1-6.

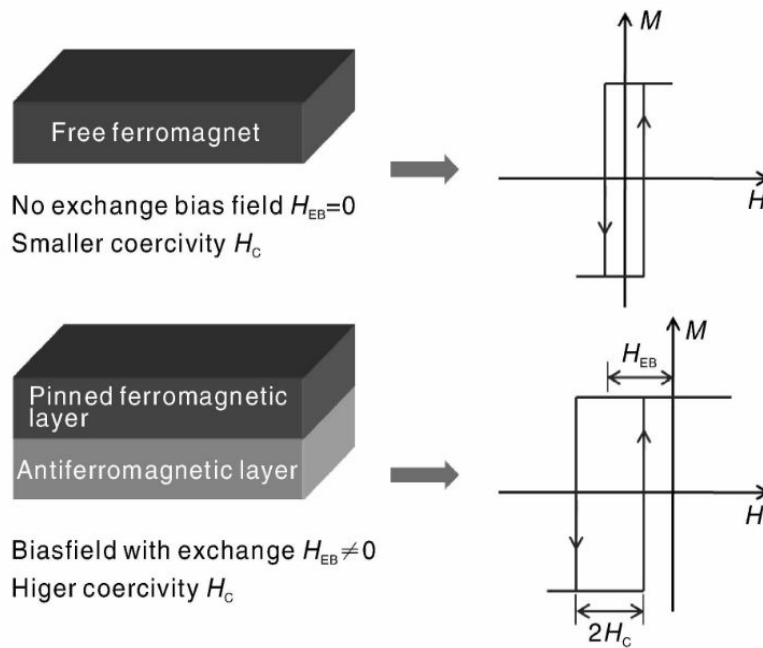


Fig1-6 Hysteresis loops of free FM and exchange biased FM^[77].

Since its discovery in 1956, EB phenomenon has been widely studied, due to its important roles in the development of fundamental physics, its complicated mechanism and technological application in spintronics field^[77]. The first commercial device introducing exchange bias was anisotropic magnetoresistance disk drive recording head made by IBM in the 1970s, but until the 1990s spin valve head was well on its way to displacing the anisotropic magnetoresistance disk drive recording head^[78-81].

In fact, in most cases EB is established in the film plane of FM/AFM multilayer, usually called longitudinal exchange bias (LEB). In the past few years, with the development of PMA, out-of-plane perpendicular exchange bias (PEB) was also introduced as an active topic since its discovery in 2000^[83]. So far,

several groups have shown that some systems with PMA can exhibit PEB after field cooling, such as CoPt/(CoO, FeMn, FeF₂) multilayer films^[82-84].

Despite the active research in this field, many aspects of EB are still controversial or unresolved so far. Considering its important value both in theory and application, we think it is significant to explore the nature of EB further.

1.5.1 Longitudinal exchange bias

LEB is associated with the exchange anisotropy generating at FM/AFM interfaces. It was discovered in 1956 by Meiklejohn and Bean, when they studied ferromagnetic Co particles embedded in antiferromagnetic CoO. Since then, LEB was observed in many systems with FM/AFM interfaces^[76].

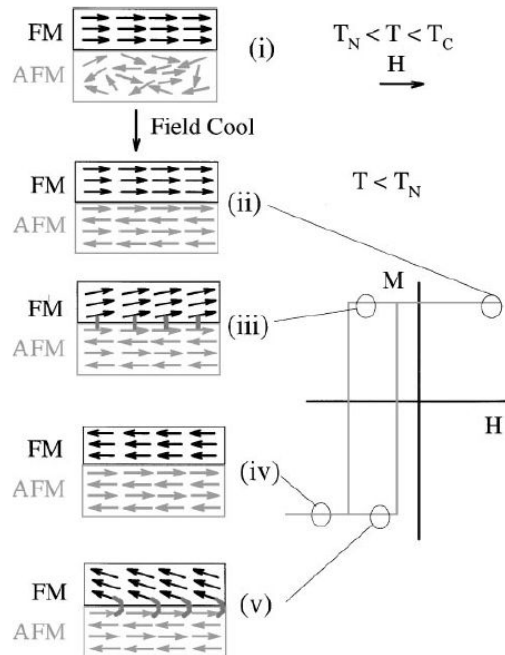


Fig1-7 FM/AFM interface spin configuration of LEB ideal model^[76].

Fig1-7 is the FM/AFM interface spin configuration in a LEB ideal model. Here, we assume that the Curie temperature (T_C) of FM is higher than Neel temperature (T_N) of AFM. When the FM/AFM interface is cooled down through T_N of AFM in a external magnetic field parallel to the interface, the spins plane of AFM next to the FM will align ferromagnetically to those of the FM due to the coupling interaction, and the other spin planes in the AFM will keep anti-parallel order (ii). If we reverse the external magnetic field, FM spins can be rotated by the reversed external magnetic field, but AFM spins remain unchanged or only weakly influenced by an externally applied magnetic field due to its intrinsic property (iii). Therefore, the AFM spins plane near to the interface will generate a microscopic torque which keeps FM spins in their original position (iv), and the reversal of FM moment will have an added energetic cost corresponding to overcome the microscopic torque from nearby AFM spins. In other words, FM spins have a hard rotation direction that needs larger external magnetic field to overcome the torque from AFM spins, and have a easy rotation direction in which FM spins can be rotated easily (v). Thus, the shift of FM hysteresis loop parallel to the interface can be induced as LEB^[76].

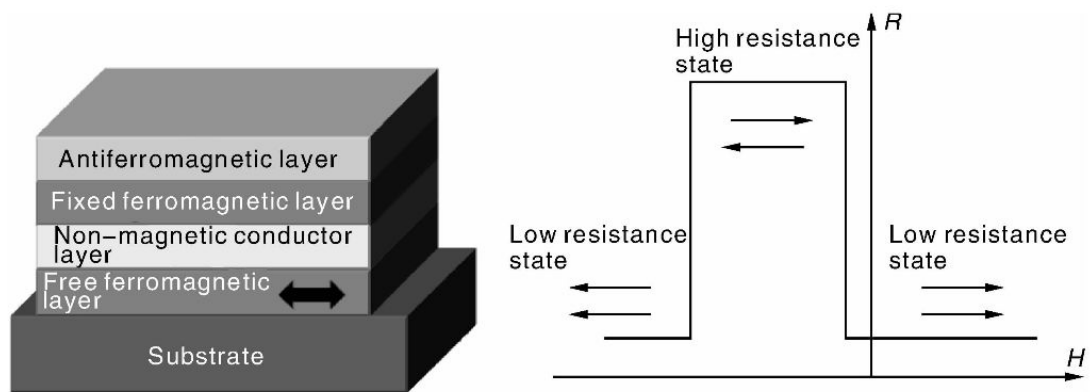


Fig1-8 Ideal spin valve and its R-H curve^[77].

So far, one successful application of LEB is spin valve which can be used as the core element in anisotropic magnetoresistance disk drive recording head^[78-81]. As is shown in Fig1-8, in a ideal spin valve, apart from the free ferromagnetic layer (which is magnetically soft), a fixed ferromagnetic layer that pinned by an antiferromagnetic layer is required (the fixed ferromagnetic layer is longitudinal exchange biased and it is magnetically hard). In addition, between free ferromagnetic layer and fixed ferromagnetic layer, a non-magnetic conductor layer is necessary to decouple the two ferromagnetic layers interactions^[77].

Based on the spin alignment configurations between free ferromagnetic and fixed ferromagnetic layers, the electrical resistance of spin valve can be changed from high to low value. Generally, antiparallel spin alignment between free ferromagnetic and fixed ferromagnetic layers leads to higher electrical resistance than the parallel spin state. Due to its special property, spin valve can be used in

magnetic sensors, hard disk read heads as well as magnetic random access memories^[82-85].

1.5.2 Perpendicular exchange bias

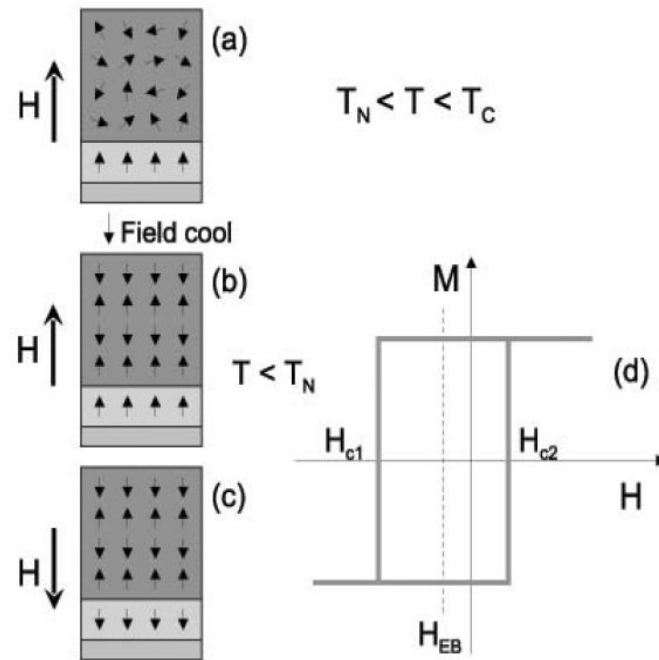


Fig1-9 FM/AFM interface spin configuration of PEB ideal model^[86].

To our knowledge, in the past decades researchers focused mainly on the LBE effect before the discovery of PEB in 2000^[88]. Recently, with the development of PMA, PEB was also introduced as an active topic which has been observed in CoPt/(CoO, FeMn, FeF₂) multilayer films^[87-89].

The spin configuration in PEB is shown in Fig1-9. We can find PEB is very similar to LEB and the main difference is all spins are keep perpendicular to the FM/AFM interface.

Nowadays, multilayer films with PEB are considered to be a potential effect used in the perpendicular spin valve and perpendicular magnetic tunneling junction e.g. With such industrial background as well as scientific interest, PEB has been widely studied in FM/AFM multilayer systems^[90].

1.6 Background of this work

1. According to our previous discussion in section 1.3.2, we have known that for Co/Pd, Co/Au, Co/Pt and Co/Ru metallic multilayer films their PMA always deteriorates at temperatures higher than 250°C-300°C due to the interface diffusion, which limits their applications greatly^[52]. On the other hand, in order to overcome the interface diffusion in Co/X metallic multilayer films, AlN and TiN are introduced to replace the X metal layer. After post thermal-annealing higher than 400°C, PMA can be obtained in CoPt/AlN, FePt/AlN and CoPt/TiN multilayer films. However, in such systems it is hard to get PMA without thermal-annealing higher than 400°C and this also blocks their applications in some degree^[53-55]. So, at present it is a challenge to develop PMA materials that can be used at middle-high temperature region between 300°C and 400°C.

2. Since their discoveries, PMA and PEB phenomenons have been widely studied, due to their complicated mechanisms and technological applications. In fact, despite the active researches in this field, many aspects of PMA and PEB are

still controversial so far. So, the influences of intrinsic and extrinsic factors (as following) on PMA and PEB still need further discussions. On the other hand, at present there are few works mentioning the correlation between PMA and PEB. So, considering the important values in theory and application, it is significant to further explore the nature of PEB as well as the correlation between PMA and PEB.

Intrinsic Factors
1. FM/AFM crystal texture
2. FM/AFM layer thickness
3. FM/AFM bilayer repetition period
4. FM/AFM interface roughness
5. FM/AFM internal stress
Extrinsic Factors
1. Thermal annealing
2. Cooling field

1.7 Objectives of this work

1. Study the influences of post-annealing temperature, CoPt layer thickness, CoO layer thickness, repetition period and CoO seed layer on PMA in $[\text{CoO}_x/\text{CoPt}_y]_n$ multilayer films systematically.
2. Study the thermal stability of PMA and find the most stable PMA performance in $[\text{CoO}_x/\text{CoPt}_y]_n$ multilayer films by optimizing the deposition conditions.
3. Explore the mechanism responsible for the PMA transition in $[\text{CoO}_x/\text{CoPt}_y]_n$ multilayer films theoretically and experimentally.
4. Study the influences of post-annealing temperature, CoPt layer thickness, CoO layer thickness, repetition period and CoO seed layer on PEB in $[\text{CoO}_x/\text{CoPt}_y]_n$ multilayer films systematically.
5. Find the best PEB performance in $[\text{CoO}_x/\text{CoPt}_y]_n$ multilayer films by optimizing the deposition conditions.
6. Explore the mechanism responsible for the PEB transition in $[\text{CoO}_x/\text{CoPt}_y]_n$ multilayer films. Try to explain the correlation between PMA and PEB in $[\text{CoO}_x/\text{CoPt}_y]_n$ multilayer films.

1.8 Organization of this work

Chapter 1 Introduction: The challenges in the development of longitudinal magnetic recording are introduced briefly. The development history and advantages of perpendicular magnetic recording as well as the current perpendicular magnetic recording media are introduced briefly. The magnetic anisotropy (including magnetocrystalline anisotropy, interface anisotropy, magnetoelastic anisotropy and shape anisotropy) as well as exchange bias effect (including longitudinal exchange bias and perpendicular exchange bias) are explained in details. The background, objective and organization of this thesis are listed respectively at the end of this chapter.

Chapter 2 Preparation and characterization of $[\text{CoO}_x/\text{CoPt}_y]_n$ multilayer films: First, preparation of $[\text{CoO}_x/\text{CoPt}_y]_n$ multilayer films (including magnetron sputtering, post annealing and field cooling) is introduced briefly. Second, the methods used to characterize $[\text{CoO}_x/\text{CoPt}_y]_n$ multilayer films (including transmission electron microscopy, X-ray diffraction, X-ray reflectivity and atomic force microscopy) are listed respectively. Third, the magnetic property measurement and the typical PMA and PEB hysteresis loops of $[\text{CoO}_x/\text{CoPt}_y]_n$ multilayer films are introduced briefly.

Chapter 3 Perpendicular magnetic anisotropy of $[\text{CoO}_x/\text{CoPt}_y]_n$ multilayer films: PMA of $[\text{CoO}_x/\text{CoPt}_y]_n$ multilayer films has been studied systematically in this chapter. In order to get the best PMA, the influences of post-annealing

temperature, CoPt thickness, CoO thickness, repetition period and CoO seed layer on PMA of $[\text{CoO}_x/\text{CoPt}_y]_n$ are studied step by step. According to our experiments, $\text{CoO}_{20\text{nm}}/[\text{CoPt}_{5\text{nm}}/\text{CoO}_{5\text{nm}}]_5$ multilayer films show the best PMA performance and possess the highest thermal stability at the temperature region between -192°C and 400°C . This indicates $\text{CoO}_{20\text{nm}}/[\text{CoPt}_{5\text{nm}}/\text{CoO}_{5\text{nm}}]_5$ multilayer films could be a potential candidate for the PMA application at elevated temperatures, in particular when they need to be processed at the middle high temperature region between 300°C and 400°C .

Chapter 4 Magnetoelastically induced magnetic anisotropy transition in $[\text{CoO}_{5\text{nm}}/\text{CoPt}_{7\text{nm}}]_5$ multilayer films: The magnetic anisotropy transition of $[\text{CoO}_{5\text{nm}}/\text{CoPt}_{7\text{nm}}]_5$ multilayer film with respect to post-annealing has been studied systematically in this chapter. The strongest PMA of $[\text{CoO}_{5\text{nm}}/\text{CoPt}_{7\text{nm}}]_5$ is achieved after post-annealing at 300°C and the tolerable post-annealing temperature with strong PMA is up to 400°C . The mechanism responsible for the transition of magnetic anisotropy has been investigated by analyzing CoO/CoPt interface and CoPt layer internal stress. It is found the effective PMA energy is proportional to the in-plane tensile stress of CoPt layer but is inversely proportional to the roughness of CoO/CoPt interface. Finally, by means of low temperature experiment we demonstrate experimentally that the magnetic anisotropy transition in this chapter is mainly attributed to the change of CoPt layer in-plane tensile stress.

Chapter 5 Perpendicular exchange bias of $[\text{CoO}_x/\text{CoPt}_y]_n$ multilayer films:

PEB of $[\text{CoO}_x/\text{CoPt}_y]_n$ multilayer films has been studied systematically in this chapter. In order to get the best PEB, the influences of annealing temperature, CoPt thickness, CoO thickness, repetition period and CoO seed layer on PEB in $[\text{CoO}_x/\text{CoPt}_y]_n$ were studied step by step. According to our experiments, 300°C-annealed $[\text{CoO}_{5\text{nm}}/\text{CoPt}_{5\text{nm}}]_5$ film shows the best PEB performance, having a PEB value of 1060 Oe.

Chapter 6 Magnetoelastically induced perpendicular magnetic anisotropy and perpendicular exchange bias of $[\text{CoO}_{5\text{nm}}/\text{CoPt}_{5\text{nm}}]_5$ multilayer films: In this chapter, the effects of magnetoelastically induced PMA on PEB have been studied in $[\text{CoO}_{5\text{nm}}/\text{CoPt}_{5\text{nm}}]_5$ multilayer films. We find the PMA strength of CoPt layer plays an important role on PEB at CoO/CoPt interfaces. With the enhancement of magnetoelastically induced PMA, great improvement of PEB was also achieved in $[\text{CoO}_{5\text{nm}}/\text{CoPt}_{5\text{nm}}]_5$ multilayer films, which increased from 130 Oe (as-deposited) up to 1060 Oe (300°C-annealed). We consider the enhanced PMA with more perpendicular spins alignment in CoPt layer results in the improved PEB in $[\text{CoO}_{5\text{nm}}/\text{CoPt}_{5\text{nm}}]_5$ multilayer films through enhanced perpendicular spins coupling at CoO/CoPt interfaces.

Chapter 7 Conclusions: The general conclusions are listed in this chapter.

References

- [1] S. Iwasaki, IEEE Trans. Magn. **20**, 657, 1984.
- [2] K. Ouchi and N. Honda, IEEE Trans. Magn. **36**, 16, 2000.
- [3] D. Litvinov, M. H. Kryder, and S. Khizroev, J. Magn. Magn. Mater. **232**, 84, 2001.
- [4] D. Litvinov and S. Khizroev, J. Appl. Phys. **97**, 071101, 2005.
- [5] S. Khizroev and D. Litvinov, J. Appl. Phys. **95**, 4521, 2004.
- [6] J. H. Judy, J. Magn. Magn. Mater. **287**, 16, 2004.
- [7] D. Litvinov, M. H. Kryder and S. Khizroev, J. Magn. Magn. Mater. **241**, 453, 2002.
- [8] S. N. Piramanayagam, J. Appl. Phys. **102**, 011301, 2007.
- [9] I. Kaitsu, R. Inamura, J. Toda and T. Morita, FUJITSU Sci. Tech. J. **42**, 122, 2006.
- [10] G. Bayreuther, P. Bruno, G. Lugert, and C. Turtur, Thin Solid Films **175**, 341, 1989.
- [11] H. J. Richter, S. Z. Wu, and R. Malmhall, IEEE Trans. Magn. **34**, 1540, 1998.
- [12] T. Pan and G. W. D. Spratt, IEEE Trans. Magn. **32**, 3623, 1996.
- [13] L. S. Prichard and K. O'Grady, J. Magn. Magn. Mater. **193**, 220, 1999.
- [14] S. M. Stinnett, W. D. Doyle, and C. Dawson, IEEE Trans. Magn. **34**, 1828, 1998.
- [15] A. Moser and D. Weller, IEEE Trans. Magn. **35**, 2808, 1999.
- [16] A. Moser, D. Weller, M. E. Best, and M. F. Doerner, J. Appl. Phys. **85**, 5018, 1999.
- [17] S. M. Stinnett, J. W. Harrell, A. F. Khapikov, and W. D. Doyle, IEEE Trans. Magn. **36**, 148, 2000.
- [18] M. Alex and D. Wachenschwanz, IEEE Trans. Magn. **35**, 2796, 1999.
- [19] M. P. Sharrock, J. Appl. Phys. **76**, 6413, 1994.

- [20] S. Iwasaki and K. Takemura, IEEE Trans. Magn. **11**, 1173, 1975.
- [21] S. Iwasaki and Y. Nakamura, IEEE Trans. Magn. **14**, 436, 1978.
- [22] S. Iwasaki, Y. Nakamura and K. Ouchi, IEEE Trans. Magn. **15**, 1456, 1979.
- [23] Western Digital Technologies, Perpendicular Magnetic Recording, USA, 2006.
- [24] M. Futamoto, Y. Honda, H. Kashiwase, and K. Yoshida, IEEE Trans. Magn. **21**, 1426, 1985.
- [25] Y. Hirayama, Y. Honda, T. Takeuchi, and M. Futamoto, IEEE Trans. Magn. **35**, 2766, 1999.
- [26] J. Ariake, N. Honda, K. Ouchi, and S. Iwasaki, IEEE Trans. Magn. **36**, 2411, 2000.
- [27] J. Ariake, N. Honda, K. Ouchi, and S. Iwasaki, IEEE Trans. Magn. **36**, 2399, 2000.
- [28] Y. Honda, A. Kikukawa, Y. Hirayama, and M. Futamoto, IEEE Trans. Magn. **36**, 2399, 2000.
- [29] Y. Hirayama, M. Futamoto, K. Ito, Y. Honda, and Y. Maruyama, IEEE Trans. Magn. **33**, 996, 1997.
- [30] Y. Hirayama, M. Futamoto, and K. Usami, IEEE Trans. Magn. **32**, 3807, 1996.
- [31] H. Muraoka, Y. Sonobe, K. Miura, A. M. Goodman, and Y. Nakamura, IEEE Trans. Magn. **38**, 1632, 2002.
- [32] H. Uwazumi, T. Shimatsu, Y. Sakai, A. Otsuki, I. Watanabe, H. Muraoka, and Y. Nakamura, IEEE Trans. Magn. **37**, 1595, 2001.
- [33] Rick Merritt, Hard drives go perpendicular, EE Times, 2005.
- [34] Introduction to the 82077, Floppy Disk Controller, Intel.

- [35] Review of drives with perpendicular recording, 2008.
- [36] Hitachi achieves nanotechnology milestone for quadrupling terabyte hard drive, Hitachi News Release.
- [37] Hard Drives Get New Record Density, Conceivably Tech.
- [38] Y. Hirayama, M. Futamoto, K. Ito, Y. Honda, and Y. Maruyama, IEEE Trans. Magn. **33**, 996, 1997.
- [39] N. Honda, J. Ariake, and K. Ouchi, IEEE Trans. Magn. **34**, 1651, 1998.
- [40] N. Honda, J. Ariake, K. Ouchi, and S. Iwasaki, IEEE Trans. Magn. **30**, 4023, 1994.
- [41] G. A. Bertero *et al.*, IEEE Trans. Magn. **38**, 1627, 2002.
- [42] T. Shimatsu *et al.*, IEEE Trans. Magn. **41**, 3175, 2005.
- [43] Y. Inaba, T. Shimatsu, T. Oikawa, H. Sato, H. Aoi, H. Muraoka, and Y. Nakamura, IEEE Trans. Magn. **40**, 2486, 2004.
- [44] H. Uwazumi, N. Nakajima, M. Masuda, T. Kawata, S. Takenoiri, S. Wa-tanabe, Y. Sakai, and K. Enomoto, IEEE Trans. Magn. **40**, 2392, 2004.
- [45] T. Shimatsu *et al.*, IEEE Trans. Magn. **41**, 566, 2005.
- [46] T. Shimatsu, T. Oikawa, Y. Inaba, H. Sato, I. Watanabe, H. Aoi, H. Muraoka, and Y. Nakamura, IEEE Trans. Magn. **40**, 2461, 2004.
- [47] Y. Inaba, T. Shimatsu, H. Muraoka, J. D. Dutson, and K. O'Grady, IEEE Trans. Magn. **41**, 3130, 2005.
- [48] P. F. Carcia, A. D. Meinhardt and A. Suna, Appl. Phys. Lett. **47**, 178, 1985.
- [49] C. Chappert and P. Bruno, J. Appl. Phys. **64**, 5736, 1988.

- [50] P. F. Carcia, J. Appl. Phys. **63**, 5066, 1988.
- [51] M. Sakurai, T. Takahata and I. Moritani, J. Magn. Soc. Japan **15**, 411, 1991.
- [52] Y. X. Yu, J. Shi and Y. Nakamura, Acta Materialia. **60**, 6770, 2012.
- [53] Y. Hodumi, J. Shi and Y. Nakamura, Appl. Phys. Lett. **90**, 212506, 2007.
- [54] C. Zhang, T. Sannomiya, S. Muraishi, J. Shi and Y. Nakamura, Appl. Phys. A. **116**, 1695, 2014.
- [55] H. Y. An, Q. Xie, J. Wang, T. Sannomiya, S. Muraishi, Z. J. Zhang, Y. Nakamura and J. Shi, J. Vac. Sci. Tec. A. **33**, 021512, 2015.
- [56] M. Kryder, E. Gage, T. McDaniel, W. Challener, R. Rottmayer, G. Ju, Y. Hsia, and M. Erden, Proc. IEEE **96**, 1810, 2008.
- [57] D. Weller, A. Moser, L. Folks, M. Best, W. Lee, M. Toney, M. Schwichert, J. Thiele, and M. Doemer, IEEE Trans. Magn. **36**, 10, 2000.
- [58] K. Barmak, J. Kim, L. H. Lewis, K. R. Coffey, M. F. Toney, A. J. Kellock, and J. U. Thielz, J. Appl. Phys. **98**, 033904, 2005.
- [59] Y. K. Takahashi, K. Hono, T. Shima, and K. Takanashi, J. Magn. Magn. Mater. **267**, 248, 2003.
- [60] A. Amikam, Introduction to the Theory of Ferromagnetism, Clarendon Press, ISBN 0-19-851791-2 (1996).
- [61] Donahue Michael J and Porter Donald G, IEEE Transactions on Magnetics, **38**(5), 2468, 2002.

- [62] M. Malcolm, Permanent magnets in theory and practice, Pentech press, ISBN 0-7273-1604-4 (1977).
- [63] B. D. Cullity and C. D. Graham, Introduction to Magnetic Materials. John Wiley & Sons, ISBN 0-201-01218-9, (2005).
- [64] G. H. O. Daalderop and M. F. H. Schuurmans, Phys. Rev. B **41** (17) 11919, 1990.
- [65] L. D. Landau, E. M. Lifshitz and L. P. Pitaevski, *Electrodynamics of Continuous Media*. Course of Theoretical Physics **8**, Elsevier. ISBN 0-7506-2634-8 (2004).
- [66] L. Neel, J. Phys. Radium **15**, 225, 1954.
- [67] A. J. Bennett and B. R. Cooper, Phys. Rev. B, **3**, 1642, 1971.
- [68] U. Gradmann and J. Muller, Phys. Status Solidi, **27**, 313, 1968.
- [69] Mohri, K. and Korekoda, S. *IEEE Transactions on Magnetics* **14**, 1071, 1978.
- [70] James, R. D., and Wuttig, M. Magnetostriction of martensite. Philosophical Magazine A, **77**(5), 1273, 1998.
- [71] Salach, J.; Szewczyk, R.; Bienkowski, A.; Frydrych, P. *Journal of Electrical Engineering* **61** (7): 93, 2010.
- [72] Bydzovsky, J.; Kollar, P.; et al. *Journal of Electrical Engineering* **52**, 205, 2001.
- [73] Bienkowski, A.; Rozniatowski, K.; Szewczyk, R. *Journal of Magnetism and Magnetic Materials* **254**, 547, 2003.
- [74] R. Bozorth, *Ferromagnetism*. Van Nostrand (1951).
- [75] B. D. Cullity, Introduction to Magnetic Materials, Addison-Wesley, Reading Massachusetts (1972).

- [76] J. Nogues and I. K. Schuller, *J. Magn. Magn. Mater.* **192**, (1999) 203.
- [77] S. N. Dong, X. H. Huang and X. G. Li, *Materials China*, **30**, 46, 2011.
- [78] W. H. Meiklejohn and C. P. Bean, *Physical Review* **105** (3), 904 (1957).
- [79] A. E. Berkowitz and K. Takano, *J. Magn. Magn. Matls.* **200**, 552 (1999).
- [80] Kiwi Miguel, *J. Magn. Magn. Matls.* **234** (3), 584, (2001).
- [81] J. Hong, T. Leo, D. J. Smith and A. E. Berkowitz, *Phys. Rev. Lett.* **96**, 117204 (2006).
- [82] R. Coehoorn, *Giant magnetoresistance and magnetic interactions in exchange-biased spin-valves*. Technische Universiteit Eindhoven. 2011.
- [83] Brown, Elliot and Wormington, Matthew, *The International Centre for Diffraction Data*. pp. 290–294. 2011.
- [84] B. C. Dodrill, and B. J. Kelley, *Magnetic In-line Metrology for GMR Spin-Valve Sensors*, 2011.
- [85] U. Hartmann, *Magnetic Multilayers and Giant Magnetoresistance*. Springer Series in Surface Sciences 37. Springer. (2000).
- [86] C. N. Helio et al, *Brazilian Journal of Physics*, **39**, 150, 2009.
- [87] F. Garcia, G. Casali, B. Rodmacq and B. Dieny, *J. Appl. Phys.* **91**, (2002) 6905.
- [88] S. Maat, K. Takano, and E. E. Fullerton, *Phys. Rev. Lett.* **87**, (2001) 087202.
- [89] B. Kagerer, C. Binek and W. Kleemann, *J. Magn. Magn. Mater.* **217**, (2000) 139.
- [90] L. Guo, Y. Wang, J. Wang, S. Muraishi, T. Sannomiya, Y. Nakamura and J. Shi, *J. Magn. Magn. Mater.* **394**, (2015) 349.

Chapter 2 Preparation and characterization of [CoO_x/CoPt_y]_n multilayer films

In this chapter, the preparation and characterization methods of [CoO_x/CoPt_y]_n multilayer films are introduced in detail. [CoO_x/CoPt_y]_n multilayer films were deposited on glass substrate by magnetron sputtering at room temperature, then vacuum annealed at different temperatures after deposition. The micro-structural characterizations of [CoO_x/CoPt_y]_n multilayer films, including crystallinity, cross-section, top-surface and interface, were carried out by x-ray diffraction (XRD), transmission electron microscope (TEM), atomic force microscope (AFM) and x-ray reflectivity (XRR) respectively. The magnetic anisotropy of [CoO_x/CoPt_y]_n multilayer films were measured by vibrating sample magnetometer (VSM) at room temperature and the exchange bias of [CoO_x/CoPt_y]_n multilayer films were measured at low temperature after field cooling with liquid N₂.

2.1 Preparation of [CoO_x/CoPt_y]_n film

2.1.1 RF magnetron sputtering of CoO layers

Magnetron sputtering is a method used for physical vapor deposition of thin films. Nowadays, it has been widely used for the deposition of important industry coatings[1]. In present work, antiferromagnetic CoO layers were deposited by

radio frequency magnetron sputtering (RF). The base pressure before deposition was around 5×10^{-5} Pa. As is shown in Fig 2-1, pure Co target was used for the deposition of CoO layers in the atmosphere of 0.8Pa Ar plus 0.2Pa O₂. CoO layers were deposited directly on the glass substrates at room temperature with a deposition rate around 0.33nm/m.

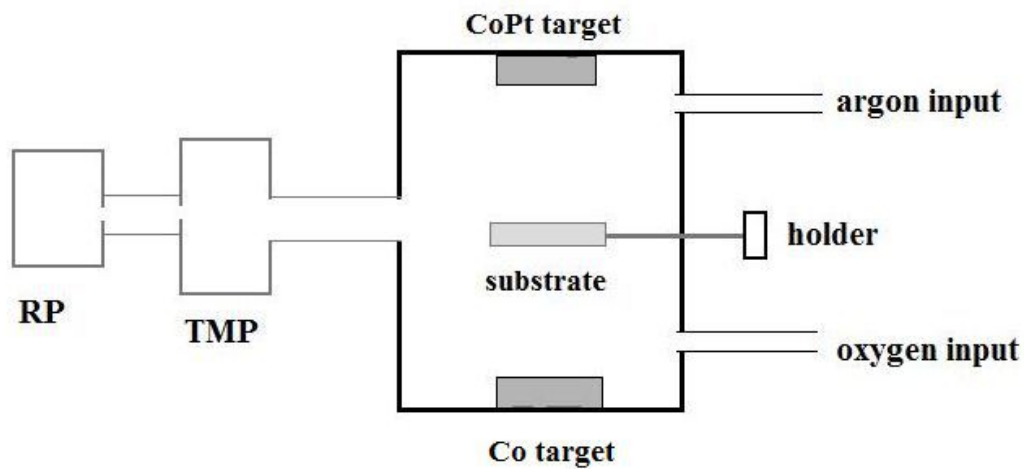


Fig 2-1 Configuration of magnetron sputtering used for [CoO_x/CoPt_y]_n multilayer film deposition (Co target is used for CoO layers deposition, CoPt target was used for CoPt layers deposition).

2.1.2 DC magnetron sputtering of CoPt layers

After the deposition of each CoO layer, Ar and O₂ mixed gas inside the chamber would be removed by turbo molecular pump (TMP) and rotary pump (RP), glass substrate would be rotated 180° through outside holder. Then, the ferromagnetic CoPt alloy layer would be deposited by direct current magnetron sputtering (DC) in the atmosphere of 0.8Pa Ar. The deposition rate of CoPt alloy layer was around 2.5nm/m. Energy dispersive spectrometer was used to

determine the chemical composition of CoPt alloy layer and it was identified as $\text{Co}_{0.43}\text{Pt}_{0.57}$.

During the deposition, glass substrate would be rotated through outside holder periodically and CoO/CoPt bilayer was repeated for n times to get $[\text{CoO}_x/\text{CoPt}_y]_n$ multilayer films. The as-deposited $[\text{CoO}_x/\text{CoPt}_y]_n$ multilayer film with size of $1\text{cm}\times 1\text{cm}$ is shown in Fig 2-2.

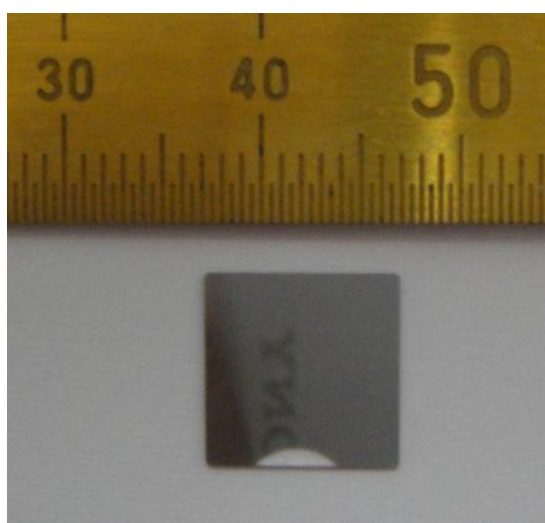


Fig 2-2 As-deposited $[\text{CoO}_x/\text{CoPt}_y]_n$ multilayer film ($1\text{cm}\times 1\text{cm}$).

2.1.3 Post annealing of $[\text{CoO}_x/\text{CoPt}_y]_n$ film

After deposition, the as-deposited $[\text{CoO}_x/\text{CoPt}_y]_n$ multilayer films would be post-annealed at different temperatures for 3h. By varying the post-annealing temperature, the micro-structures of $[\text{CoO}_x/\text{CoPt}_y]_n$ multilayer films were also changed, allowing us to obtain different magnetic properties.

2.1.4 Field cooling of $[\text{CoO}_x/\text{CoPt}_y]_n$ film

In chapter 1, we have known that the exchange bias effect is an interfacial phenomenon associated with exchange coupling created at the FM/AFM interface, when the system is field-cooled through AFM Néel temperature (T_N). So, in the case of $[\text{CoO}_x/\text{CoPt}_y]_n$ multilayer film here, its EB was determined at low temperature around 80K, after field cooling by liquid N_2 through AFM CoO Néel temperature ($T_N \sim 290\text{K}$).

2.2 Structure characterization of $[\text{CoO}_x/\text{CoPt}_y]_n$ film

2.2.1 Transmission electron microscopy

2.2.1.1 Fundamental of TEM

Transmission electron microscopy (TEM) is a microscopy technique that are used to image at a significantly higher resolution by accelerated electrons. The electrons transmitting through an ultra-thin specimen will interact with the specimen and obtain the micro-structure information of the transmitted specimen, including electron density, phase, periodicity and so on. Then, an micro-structure image of the specimen is formed from the interaction of the electrons and detected by a sensor such as a CCD camera[2].

The great advantage of TEM is that its resolution is tens of thousands times higher than the optical microscopes and can even observe the atom arrangements in the specimen, due to the smaller de Broglie wavelength of electrons[3].

2.2.1.2 TEM of $[\text{CoO}_x/\text{CoPt}_y]_n$ film

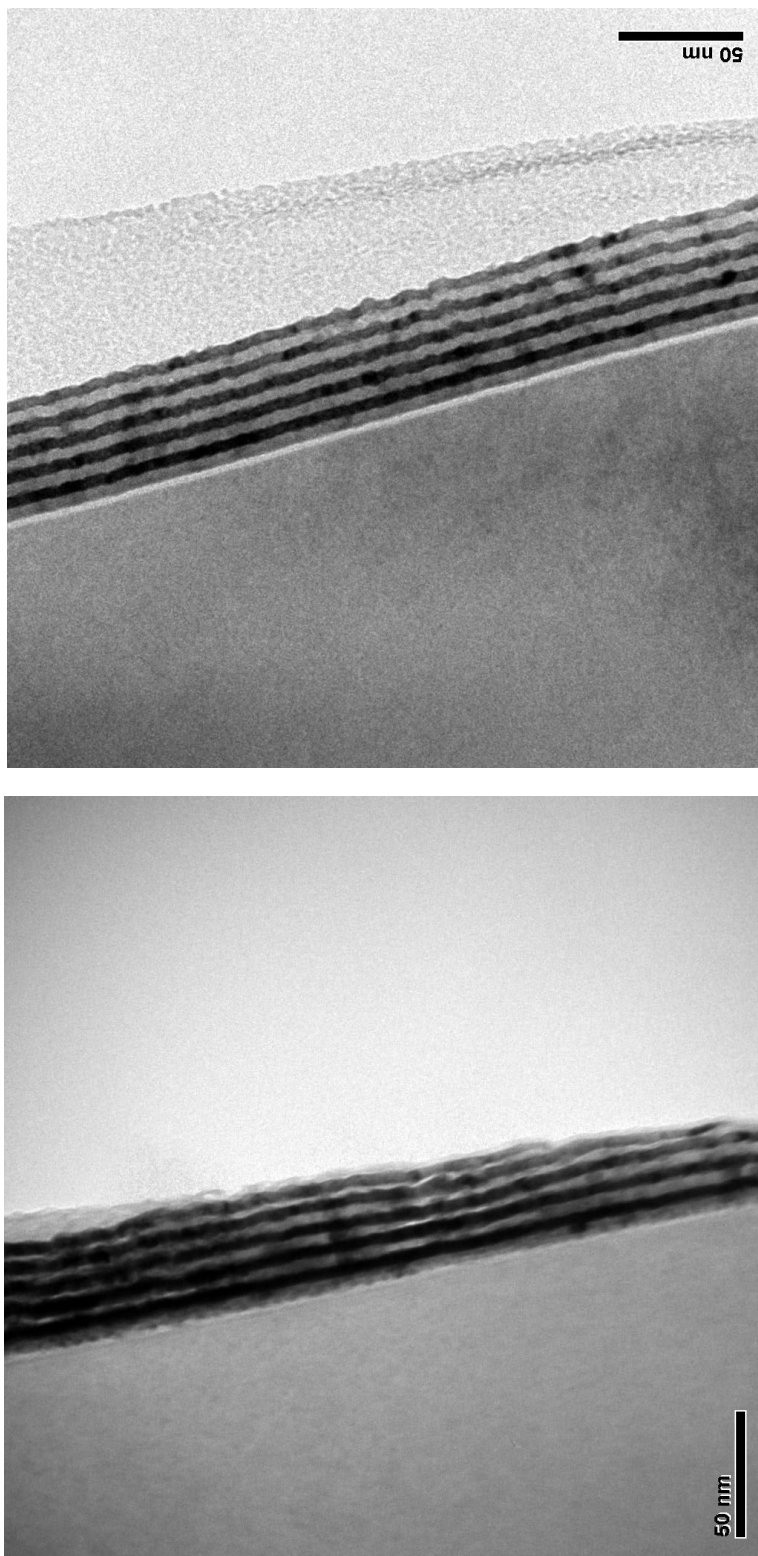


Fig 2-3 Cross-section TEM images of as-deposited and 300°C-annealed $[\text{CoO}5\text{nm}/\text{CoPt}5\text{nm}]_5$ films (dark layer is CoPt).

In present work, the cross-section of $[\text{CoO}_x/\text{CoPt}_y]_n$ film was observed by TEM in order to determine the CoO and CoPt layer thickness and monitor the micro-structure change of $[\text{CoO}_x/\text{CoPt}_y]_n$ film with post annealing. Fig 2-3 shows the cross-section TEM images of as-deposited and 300°C-annealed $[\text{CoO}5\text{nm}/\text{CoPt}5\text{nm}]_5$ films. It is clear in the first TEM image that for the as-deposited $[\text{CoO}5\text{nm}/\text{CoPt}5\text{nm}]_5$ film, the continuous CoO5nm/CoPt5nm bilayer is repeated periodically with sharp layer transition at each interface. However, in the second TEM image CoO layers become fuzzy after 300°C annealing, according to our subsequent experiments this is due to the gradual decomposition of CoO at high temperature.

2.2.2 X-ray diffraction

X-ray diffraction (XRD) is a tool used for identifying the crystal structure. By measuring the intensities and angles of diffracted X-ray beams, a three-dimensional electrons density picture of the crystal can be achieved, and thus the mean positions of the atoms and various other information in the crystal can be determined from this electron density picture[4-6].

2.2.2.1 Bragg's law and structure factor

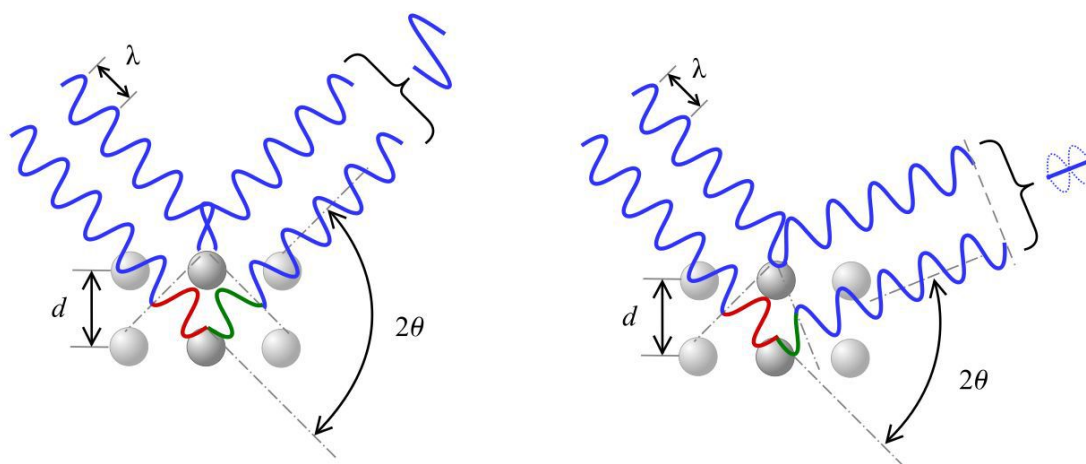


Fig 2-4 Constructive interference (left) and destructive interference (right) between diffracted X-ray beams. https://en.wikipedia.org/wiki/Bragg%27s_law

According to Bragg's law, the strong constructive interference known as Bragg peaks can be obtained in the diffraction pattern when the scattering angles satisfy Bragg condition:

$$2d_{(hkl)} \sin \theta_n = n\lambda$$

where λ is incident X-ray wavelength, d_{hkl} is lattice plane distance, θ is X-ray incident angle[7]. Fig 2-4 shows the constructive interference and destructive interference between diffracted X-ray beams. It is well known the constructive interference corresponds to the related diffraction peak in the XRD pattern.

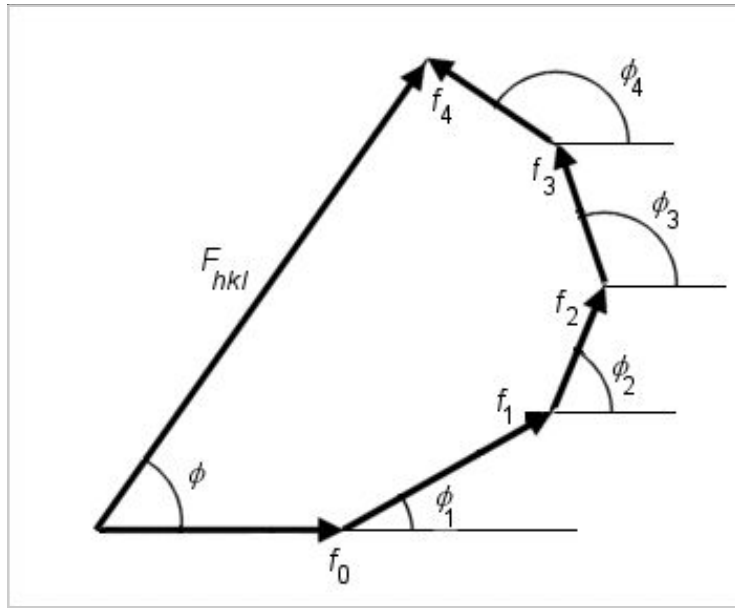


Fig 2-5 Structure factor F_{hkl} .

http://reference.iucr.org/dictionary/Structure_factor

On the other hand, for the crystal unit cell that contains several atoms, the intensity of a diffracted beam I_{hkl} is directly related to the amplitude of the structure factor F_{hkl} :

$$I_{hkl} \propto |F_{hkl}|^2$$

$$|F_{hkl}|^2 = \left[\sum_{j=1}^N f_j \cos 2\pi(hx_j + ky_j + lz_j) \right]^2 + \left[\sum_{j=1}^N f_j \sin 2\pi(hx_j + ky_j + lz_j) \right]^2$$

where F_{hkl} is a complex function (it has amplitude and phase) describing the sum of diffracted X-rays by all atoms in the unit cell, h, k, l are Miller indices, x_j, y_j, z_j are the position of the j atom, f_j is the scattering factor of the j atom[8-13].

2.2.2.2 CoPt structure

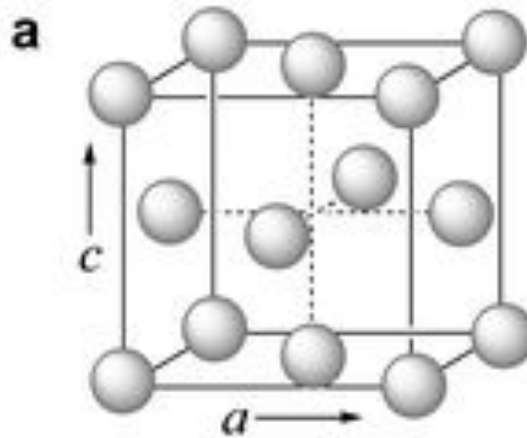


Fig 2-6 Crystal structure of FCC CoPt alloy (Co or Pt occupies each lattice point randomly).

In present work, CoPt layer is solid solution alloy with composition of $\text{Co}_{0.43}\text{Pt}_{0.57}$. It has preferred face centered cubic structure (FCC), which can be attributed to the addition of Pt, since CoPt alloy with Pt component is energetically favorable to form strong FCC texture[14]. Fig 2-6 is the crystal structure of FCC CoPt alloy, in which Co or Pt atom occupies each lattice point randomly and form solid solution state.

For the specified FCC CoPt unit cell, it contains four atoms with positions as: $(0,0,0)$, $(1/2,1/2,0)$, $(1/2,0,1/2)$, $(0,1/2,1/2)$. So, according to the definition of structure factor F_{hkl} mentioned above, the diffracted peak intensities I_{hkl} of FCC CoPt can be expressed as follow:

$$16f^2 \quad (\text{if } h,k,l \text{ all are even or all are odd, strong peak})$$

$$I_{hkl} = |F_{hkl}|^2 =$$

$$0 \quad (\text{the others, no peak})$$

2.2.2.3 CoO structure

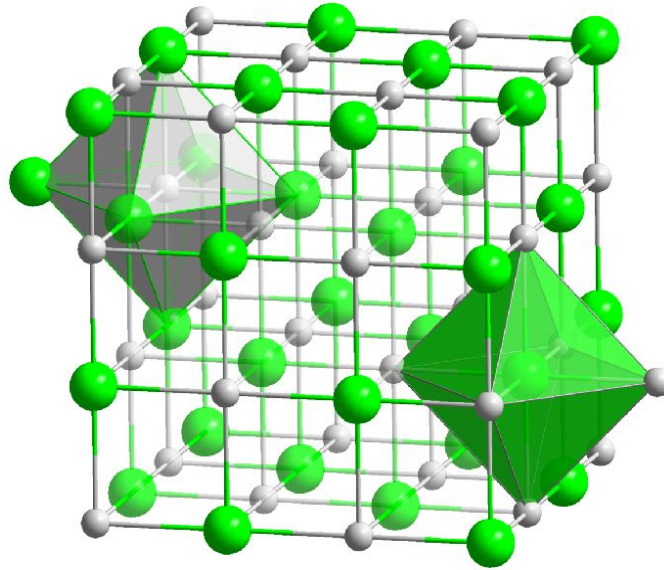


Fig 2-7 Crystal structure of FCC CoO (black balls represent Co atoms).

CoO layer is also FCC structure, but it is a little different from the FCC CoPt alloy. As is shown in Fig 2-7, the FCC CoO lattice contains of two interpenetrating FCC Co^{2+} sublattice and FCC O^{2-} sublattice. Each lattice point includes both Co^{2+} and O^{2-} , forming a oxygen octahedron with Co^{2+} in the center.

So, different from FCC CoPt, for the specified FCC CoO unit cell it contains four Co atoms with positions as: $(0,0,0)$, $(1/2,1/2,0)$, $(1/2,0,1/2)$, $(0,1/2,1/2)$ and four O atoms with positions as: $(1/2,1/2,1/2)$, $(1/2,0,0)$, $(0,0,1/2)$, $(0,1/2,0)$. According to the definition of structure factor F_{hkl} mentioned above, the diffracted peak intensities I_{hkl} of FCC CoO can be expressed as follow:

$$I_{hkl} = |F_{hkl}|^2 = \begin{array}{ll} 16(f_{\text{Co}} + f_{\text{O}})^2 & \text{(if } h, k, l \text{ all are even, strong peak)} \\ 16(f_{\text{Co}} - f_{\text{O}})^2 & \text{(if } h, k, l \text{ all are odd, weak peak)} \\ 0 & \text{(the others, no peak)} \end{array}$$

2.2.2.4 XRD of $[\text{CoO}_x/\text{CoPt}_y]_n$ film

$[\text{CoO}_x/\text{CoPt}_y]_n$ multilayer films were deposited directly on glass substrate by magnetron sputtering at room temperature, then vacuum annealed at different temperatures for 3h after deposition. By varying the post-annealing temperature, the micro-structures of $[\text{CoO}_x/\text{CoPt}_y]_n$ multilayer films were also changed, allowing us to obtain different crystallinity.

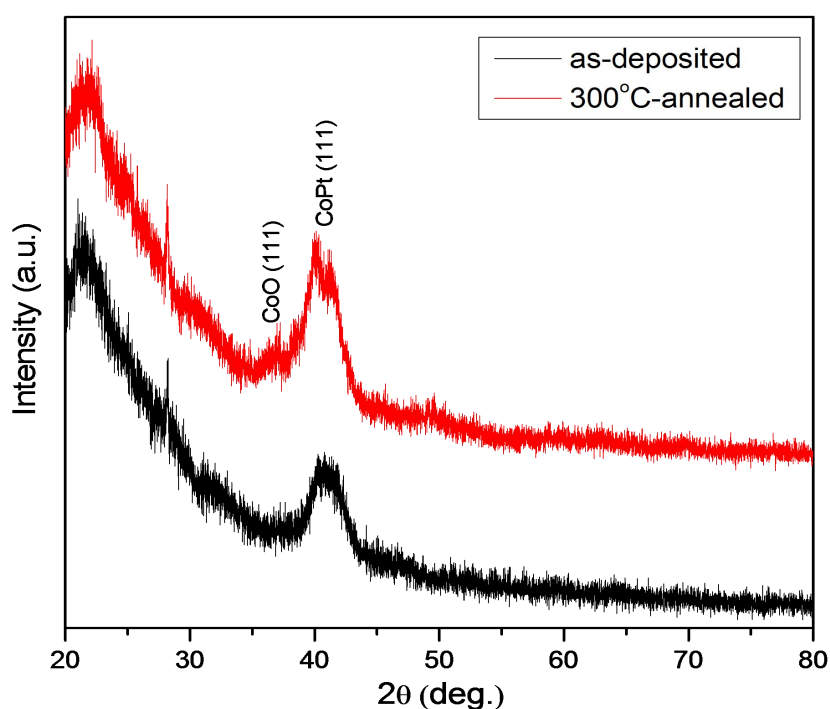


Fig 2-8 Out-of-plane XRD profile of $\text{CoO}_{20\text{nm}}/[\text{CoPt}_{5\text{nm}}/\text{CoO}_{5\text{nm}}]_5$ film.

A typical out-of-plane XRD profile of $[\text{CoO}_x/\text{CoPt}_y]_n$ film is shown in Fig 2-8. Firstly, it is clear to see that both as-deposited and 300°C-annealed $\text{CoO}_{20\text{nm}}/[\text{CoPt}_{5\text{nm}}/\text{CoO}_{5\text{nm}}]_5$ films are well crystallized with preferred FCC CoPt (111) orientation. As to the 300°C-annealed sample, its CoPt (111) peak becomes stronger, indicating the improvement of CoPt crystallinity by annealing. Since

<111> directions are the easy magnetization axes of FCC CoPt, we believe the strong <111> orientation of CoPt layers is favorable for the development of strong PMA in $[\text{CoO}_x/\text{CoPt}_y]_n$ multilayer films. Secondly, we can find an evident split in 300°C-annealed CoPt (111) peak, and this is due to the modulation from the periodic multilayer structure.

On the other hand, although CoO is also FCC structure with (111) orientation, its (111) peak is much lower than CoPt (111) peak. Firstly, this can be attributed to the influence of structure factor F_{hkl} mentioned above. According to our previous analysis, the (111) diffracted peak intensity $I_{\text{CoPt}(111)}$ of FCC CoPt can be expressed as $I_{\text{CoPt}(111)} = |F_{\text{CoPt}(111)}|^2 = 16f^2$ (if h, k, l all are even or all are odd, **strong peak**), and the (111) diffracted peak intensity $I_{\text{CoO}(111)}$ of FCC CoO can be expressed as $I_{\text{CoO}(111)} = |F_{\text{CoO}(111)}|^2 = 16(f_{\text{Co}} - f_{\text{O}})^2$ (if h, k, l all are odd, **weak peak**). We can find CoPt (111) is a strong peak but CoO (111) is a weak peak. Secondly, in $\text{CoO}_{20\text{nm}}/[\text{CoPt}_{5\text{nm}}/\text{CoO}_{5\text{nm}}]_5$ film, the top-surface is CoPt layer and it is easy to understand this also leads to the stronger CoPt (111) peak.

2.2.3 X-ray reflectivity

2.2.3.1 Fundamental of XRR

X-ray reflectivity (XRR) is a technique used for interface characterization of thin films in a nondestructive manner, and it can determine film density, surface or interface roughness and film thickness roughly[15].

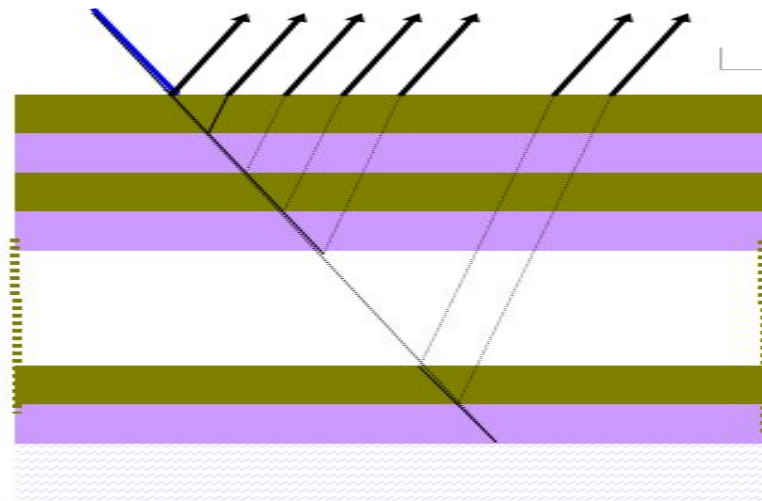


Fig 2-9 X-ray reflectivity of multilayer film.

X-ray reflectivity of multilayer film is shown in Fig 2-9. At every interface, a portion of X-ray is reflected and all of these partially reflected X-ray beams will create an interference pattern as a function of incidence angle (over an angle range close to the critical angle).

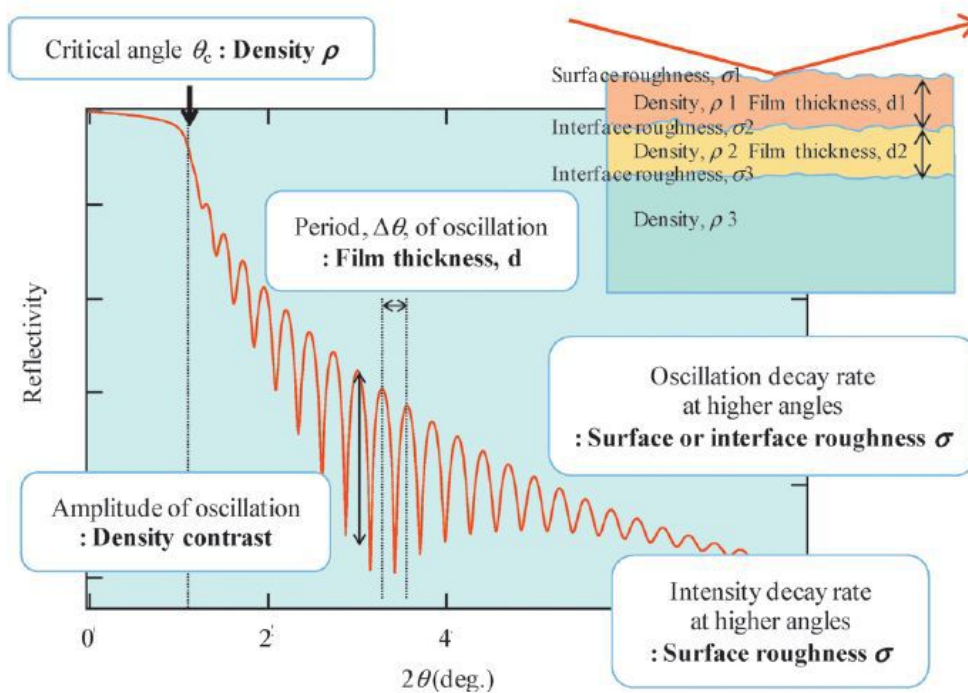


Fig 2-10 Information provided by XRR^[15].

Generally, the XRR profile of a film as shown in Fig 2-10 provides information of critical angle, slope and periodicity of interference peak, which correspond to the density of thin film, surface or interface roughness, and thin film thickness, respectively[15].

2.2.3.2 XRR of $[\text{CoO}_x/\text{CoPt}_y]_n$ film

In present work, XRR was only an assistant tool used to characterize the CoO/CoPt interface quality of $[\text{CoO}_x/\text{CoPt}_y]_n$ film and measure the change of CoO/CoPt interface with post-annealing.

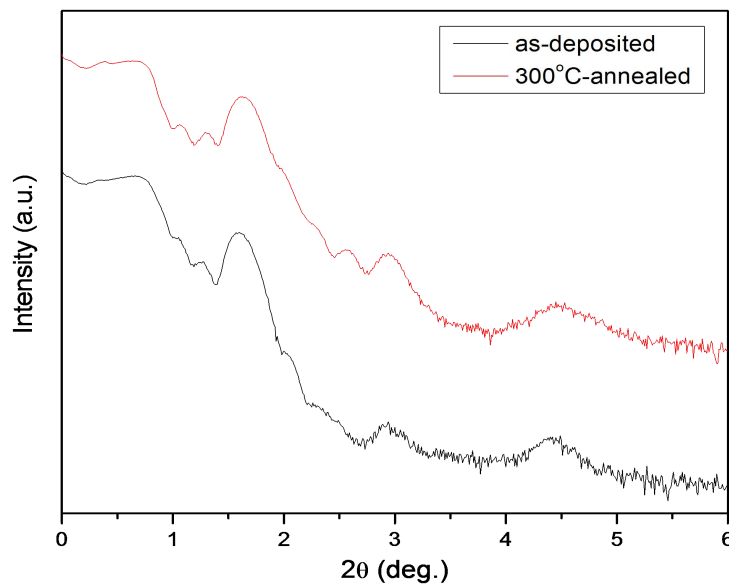


Fig 2-11 XRR profile of $\text{CoO}_{20\text{nm}}/[\text{CoPt}_{5\text{nm}}/\text{CoO}_{5\text{nm}}]_5$ film.

A typical XRR profile of $[\text{CoO}_x/\text{CoPt}_y]_n$ film is shown in Fig 2-11. Firstly, it is clear that three Bragg main peaks which generate from the modulation of periodic structure can be seen in both samples, indicating good periodicity and good

interface quality in $\text{CoO}_{20\text{nm}}/[\text{CoPt}_{5\text{nm}}/\text{CoO}_{5\text{nm}}]_5$ films. Secondly, compared with the as-deposited sample, the slight decreasing of slope with enhanced Kiessig fringes in 300°C -annealed $\text{CoO}_{20\text{nm}}/[\text{CoPt}_{5\text{nm}}/\text{CoO}_{5\text{nm}}]_5$ film indicates that the $\text{CoPt}_{5\text{nm}}/\text{CoO}_{5\text{nm}}$ interfaces become smoother after annealing at 300°C .

2.2.4 Atomic force microscopy

2.2.4.1 Fundamental of AFM

Atomic force microscopy (AFM) is a kind of high-resolution scanning probe microscopy. It can provide a three-dimensional surface profile at a high resolution and is possible to quantify the surface roughness at the same time. The detector on AFM is a cantilever with a sharp tip at its end which is used to scan the specimen surface. When the tip of cantilever touches the sample surface, forces between the tip and the sample will lead to a bend of the cantilever. AFM processes the bend of cantilever and converts it into an electrical signal. In addition, most AFM can work well in ambient air environment, and samples viewed by AFM usually do not need any special treatments which would damage the sample inevitably[16-18].

2.2.4.2 AFM of $[\text{CoO}_x/\text{CoPt}_y]_n$ film

In present work, to quantify the post-annealing induced interface change, $[\text{CoO}_x/\text{CoPt}_y]_n$ film top-surface topography was measured by AFM as an intuitive

reference of CoO/CoPt interface. We also derived the $[\text{CoO}_x/\text{CoPt}_y]_n$ film top surface root-mean-square roughness from AFM images, which is an important parameter in judging the magnetic property of $[\text{CoO}_x/\text{CoPt}_y]_n$ film.

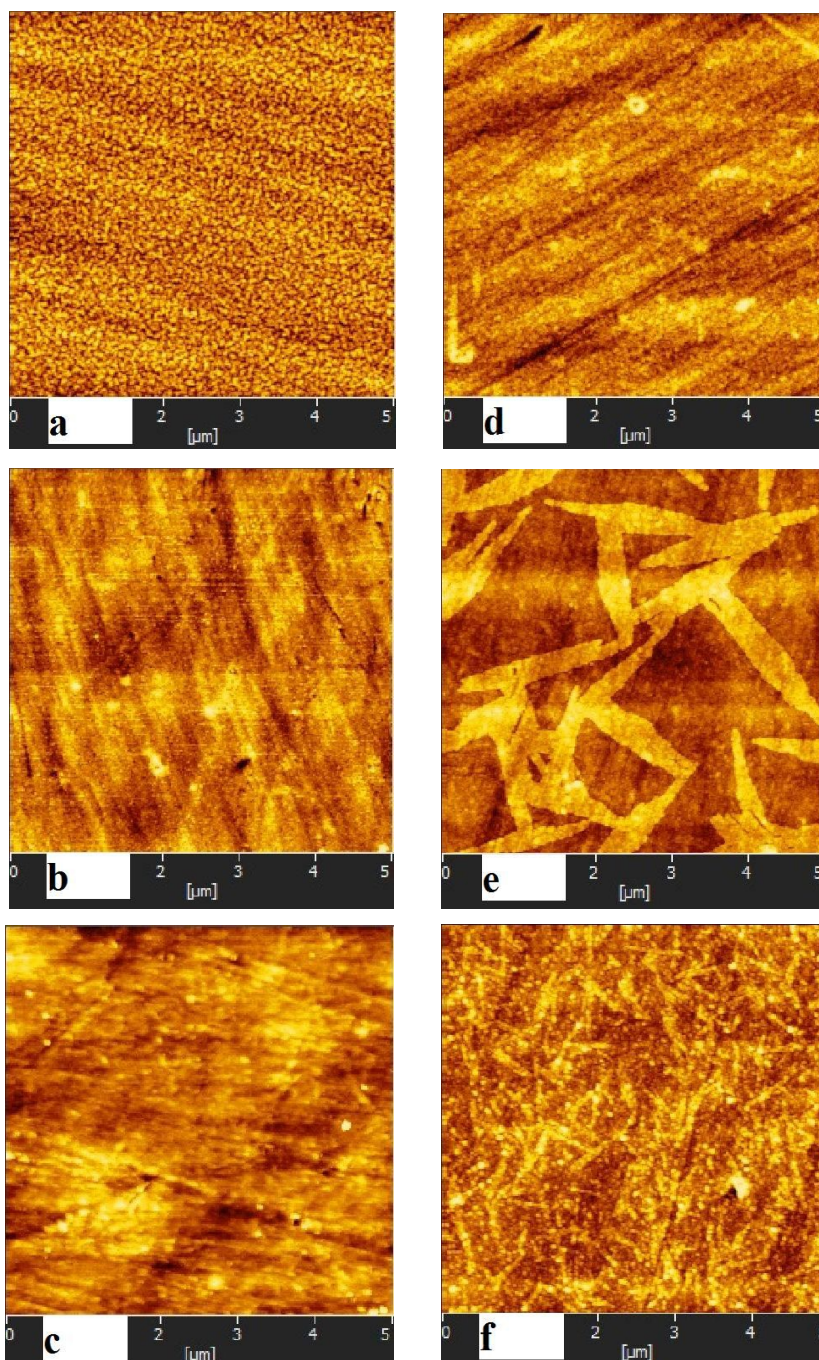


Fig 2-12 Two-dimensional AFM images of $[\text{CoO}5\text{nm}/\text{CoPt}2.5\text{nm}]_5$ film (a: as-deposited, b: 250°C-annealed, c: 300°C-annealed, d: 350°C-annealed, e: 400°C-annealed, f: 500°C-annealed).

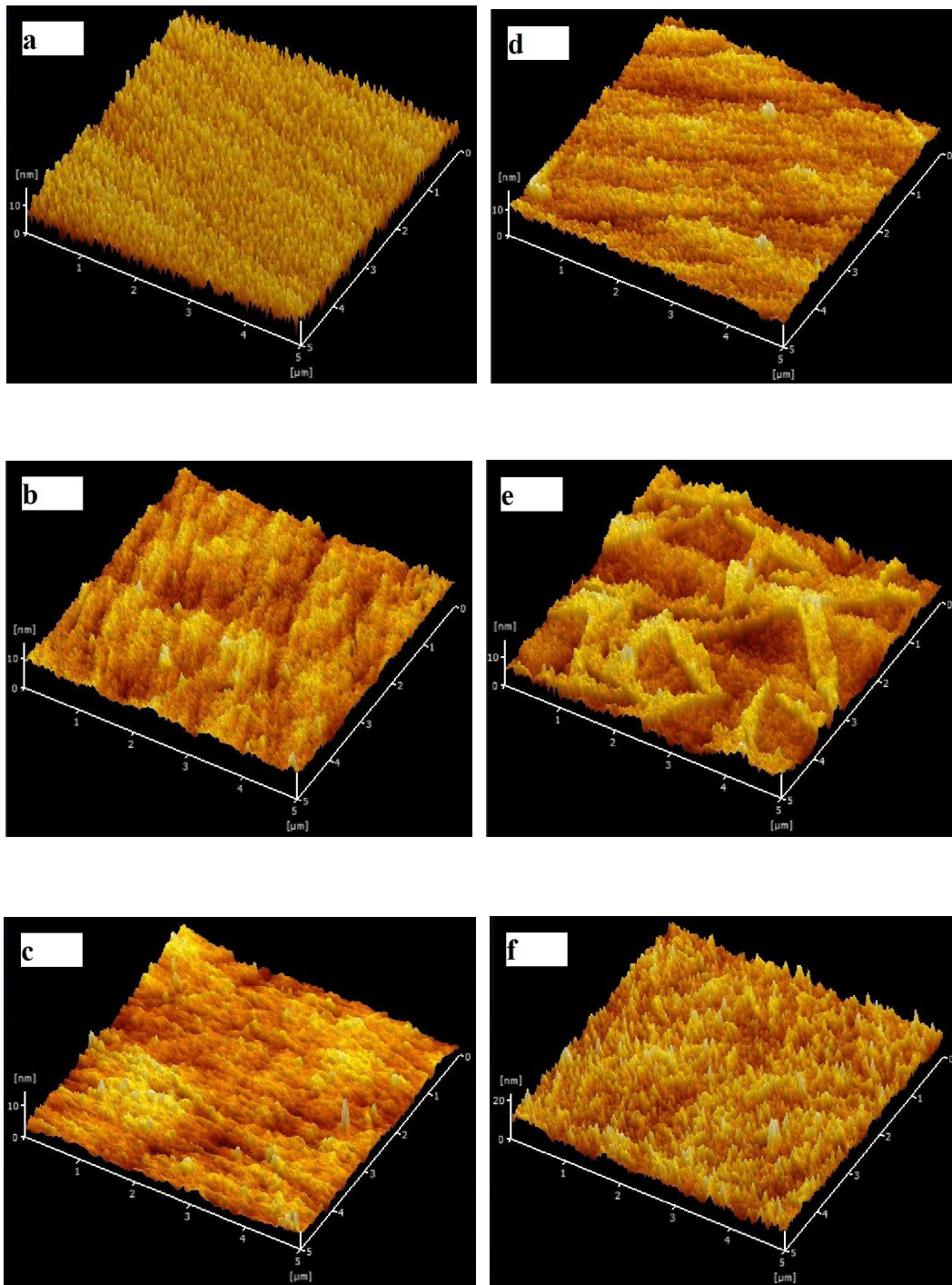


Fig 2-13 Three-dimensional AFM images of [CoO5nm/CoPt2.5nm]₅ film (a: as-deposited, b: 250°C-annealed, c: 300°C-annealed, d: 350°C-annealed, e: 400°C-annealed, f: 500°C-annealed).

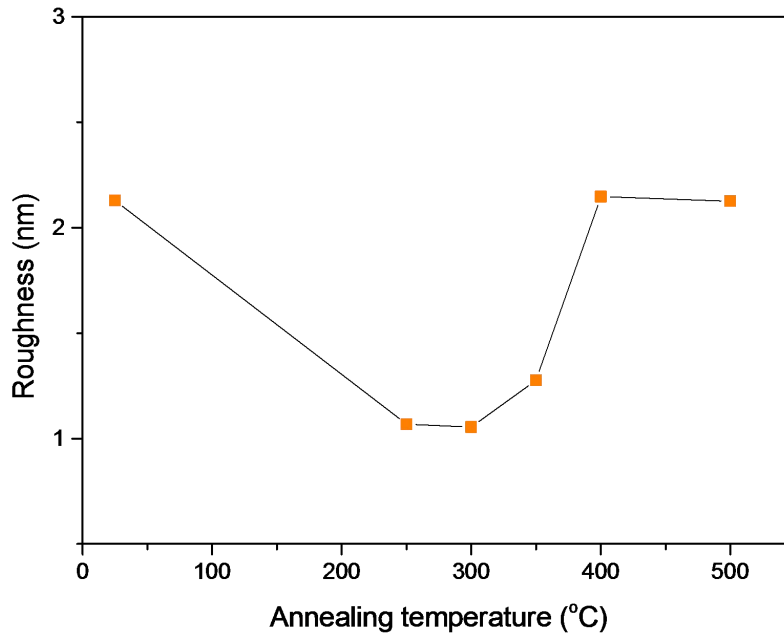


Fig 2-14 The dependence of $[\text{CoO}5\text{nm}/\text{CoPt}2.5\text{nm}]_5$ top-surface roughness on post-annealing temperature.

A typical AFM profile of $[\text{CoO}_x/\text{CoPt}_y]_n$ film is shown as above. It includes the two-dimensional AFM images (Fig 2-12), the three-dimensional AFM images (Fig 2-13) as well as the derived top-surface roughness values from AFM images (Fig 2-14).

It is clear in Fig 2-14 that when the annealing temperature is below 300°C the top-surface roughness of $[\text{CoO}5\text{nm}/\text{CoPt}2.5\text{nm}]_5$ can be reduced by annealing, due to the coalescence of grains and the removal of defects. On the contrary, when the annealing temperature is above 300°C the $[\text{CoO}5\text{nm}/\text{CoPt}2.5\text{nm}]_5$ top-surface becomes rougher and rougher with the increasing of annealing temperature. According to our experience, this results from the gradual decomposition of underneath CoO layer at high temperature.

2.3 Magnetic property measurement

2.3.1 Ferromagnetic CoPt

Ferromagnets are very important in modern industry, and they are the basis for many electrical and electro-mechanical devices such as generators, transformers, electric motors, electromagnets as well as hard disk magnetic storage. The common ferromagnets in nature are iron, nickel, cobalt and most of their alloys[19, 20].

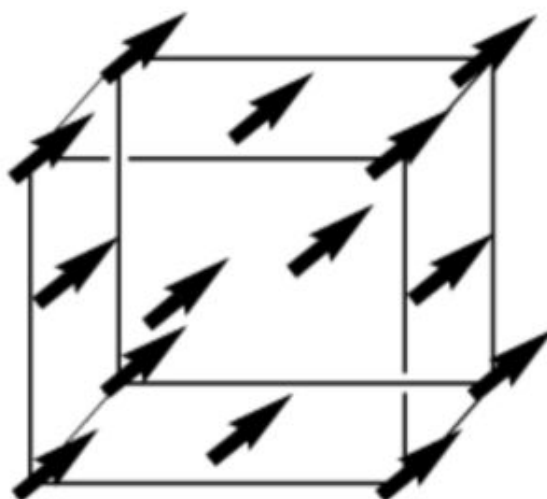


Fig 2-15 Magnetic moments of Co atoms in FCC ferromagnetic CoPt lattice.

In present work, ferromagnetic CoPt alloy is FCC crystal structure. As is shown in Fig 2-15, in each CoPt magnetic domain (usually it contains several CoPt lattices), the magnetic moments of all Co atoms keep parallel and point in the $[111]$ direction. So, $\langle 111 \rangle$ directions are the so-called easy magnetization axes of FCC CoPt. In $[\text{CoO}_x/\text{CoPt}_y]_n$ films, each CoPt layer is made of tens of thousands of CoPt magnetic domains and the moments of separate domains point

in different directions. So, without external magnetic field, all the CoPt magnetic domains are arranged randomly, and thus the magnetization of a $[\text{CoO}_x/\text{CoPt}_y]_n$ film is zero at its virgin state. The Curie temperatures of Co is around 1388 K.

2.3.2 Antiferromagnetic CoO

Antiferromagnets occur commonly among transition metal compounds, especially oxides, when they are cooled below a critical temperature known as the Neel temperature. They can couple with ferromagnets at FM/AFM interfaces through a mechanism known as exchange bias[21-23].

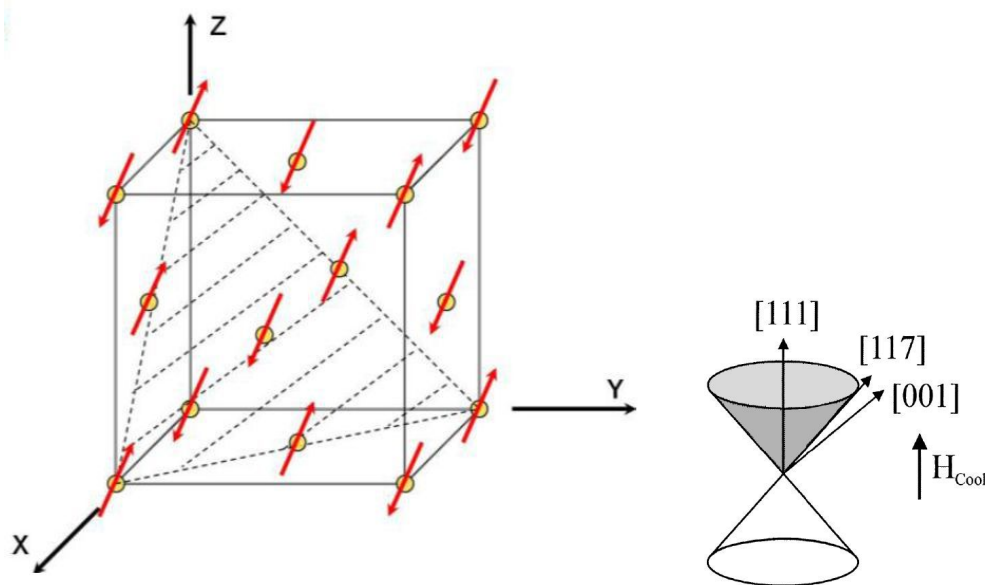


Fig 2-16 Magnetic moments of Co atoms in FCC antiferromagnetic CoO lattice^[24].

In present work, antiferromagnetic CoO is also FCC crystal structure. The Neel temperatures of CoO is around 290K. As is shown in Fig 2-16, when the temperature is below 290K, CoO (111) planes are the uncompensated Co magnetic

moment planes and all Co magnetic moments in (111) planes point in the [117] direction. But, the Co magnetic moments locating in (222) planes align antiparallel to the neighboring magnetic moments locating in (111) planes. In each CoO magnetic domain, the half-apex angle between [111] and [117] is around 43° [25, 26].

2.3.3 Co magnetic moments configuration at CoO/CoPt interface

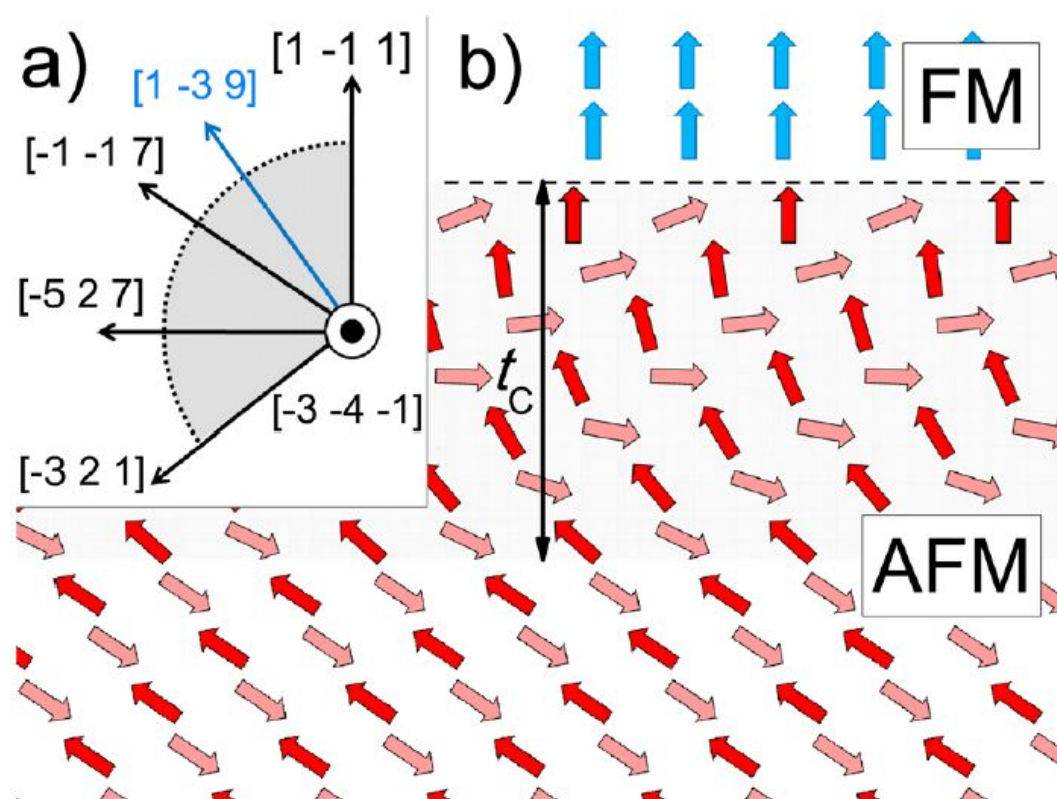


Fig 2-17 The schematic picture of Co magnetic moments configuration at CoO/CoPt interface (blue arrows represent the Co magnetic moments of FM CoPt layer, red arrows represent the Co magnetic moments of AFM CoO layer)^[26].

Here, we assume the perfect CoPt (1 -1 1) and CoO (1 -1 1) textures are obtained at CoO/CoPt (AFM/FM) interface. So, after perpendicular field cooling down through CoO Neel temperature, all the Co magnetic moments of CoPt layer

will keep parallel and point to $[1 -1 1]$ direction. On the other hand, all the Co magnetic moments of CoO layer will keep antiparallel and point to $[-1 -1 7]$ direction, having a 43° half-apex angle with $[1 -1 1]$ direction. Most importantly, among the Co magnetic moments of CoO layer, those locating close enough to the CoO/CoPt interface will align in $[1 -1 1]$ direction due to the coupling interaction between CoPt and CoO[26].

2.3.4 Vibrating sample magnetometer

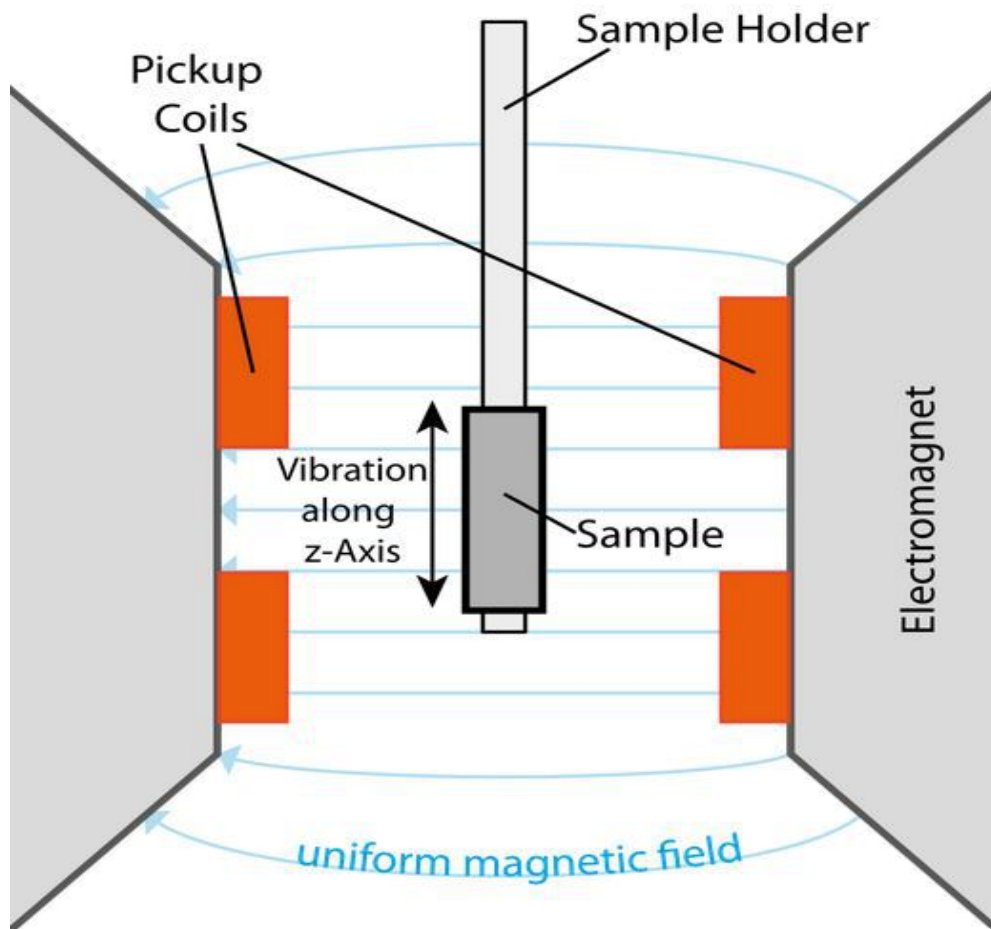


Fig 2-18 The schematic diagram of VSM.

https://commons.wikimedia.org/wiki/File:VSM_en.svg

In present work, vibrating sample magnetometer (VSM) was used to measure the magnetic property of $[\text{CoO}_x/\text{CoPt}_y]_n$ films. VSM was invented in 1955 by Simon Foner at Lincoln Laboratory MIT. It measures the magnetization of a small magnetic sample placed in an external magnetizing field by converting the dipole field of the magnetic sample into an electrical signal[27]. Fig 2-18 is the schematic diagram of VSM. Sample is vibrated physically along Z-axis with sample holder inside a magnetic field which magnetizes the sample. The signal induced in the pick-up coils by sample magnetic field is compared with a standard specimen, and the hysteresis loop of magnetic sample can be obtained.

2.3.5 PMA magnetic hysteresis loops of $[\text{CoO}_x/\text{CoPt}_y]_n$ film

A typical hysteresis loop profile of as-deposited, 100°C-annealed, 300°C-annealed and 400°C-annealed $\text{CoO}20\text{nm}/[\text{CoPt}5\text{nm}/\text{CoO}5\text{nm}]_5$ films with strong PMA is shown in Fig 2-19 (measured at RT).

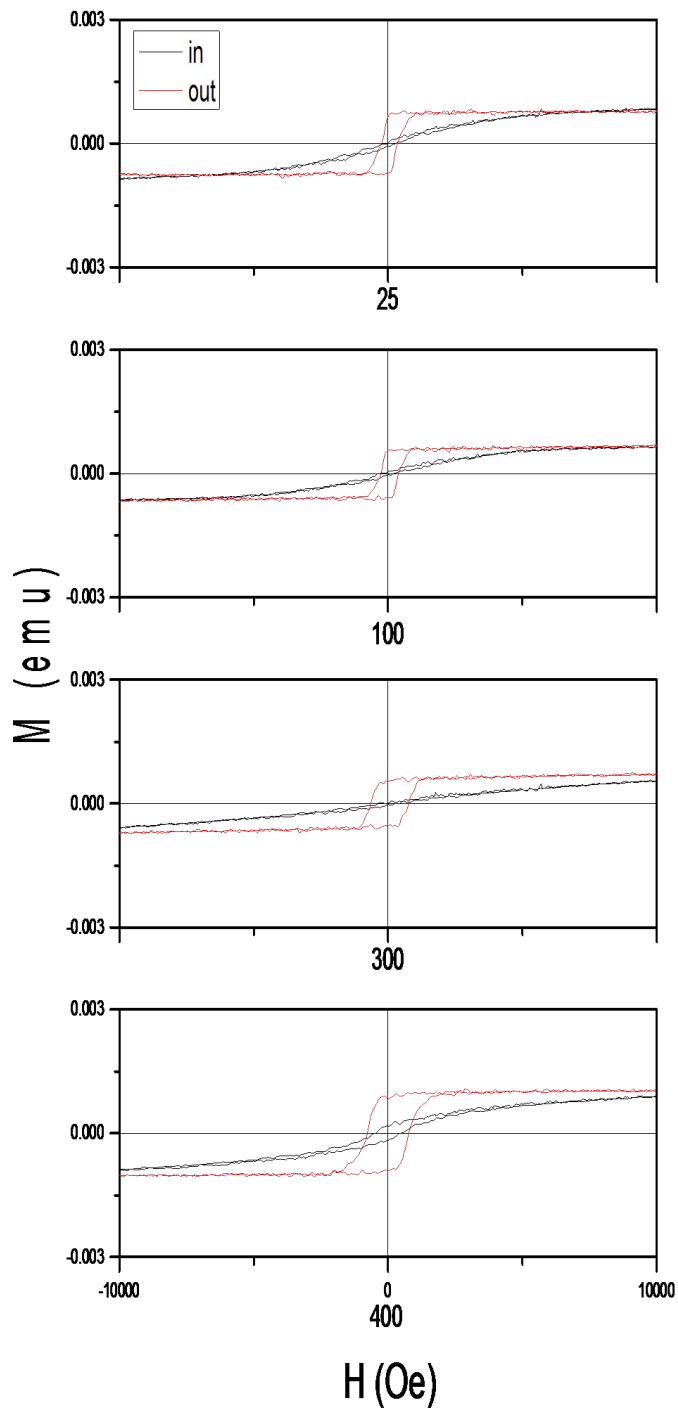


Fig 2-19 Hysteresis loops of as-deposited, 100°C-annealed, 300°C-annealed and 400°C-annealed CoO20nm/[CoPt5nm/CoO5nm]₅ films (measured at RT).

2.3.6 PEB magnetic hysteresis loops of $[\text{CoO}_x/\text{CoPt}_y]_n$ film

Fig 2-20 (right column) shows the perpendicular exchange bias effect in 300°C -annealed $[\text{CoO}5\text{nm}/\text{CoPt}2.5\text{nm}]_5$, 300°C -annealed $[\text{CoO}5\text{nm}/\text{CoPt}5\text{nm}]_5$ and 300°C -annealed $[\text{CoO}5\text{nm}/\text{CoO}7\text{nm}]_5$ films, measured at LT around -192°C after perpendicular field cooling.

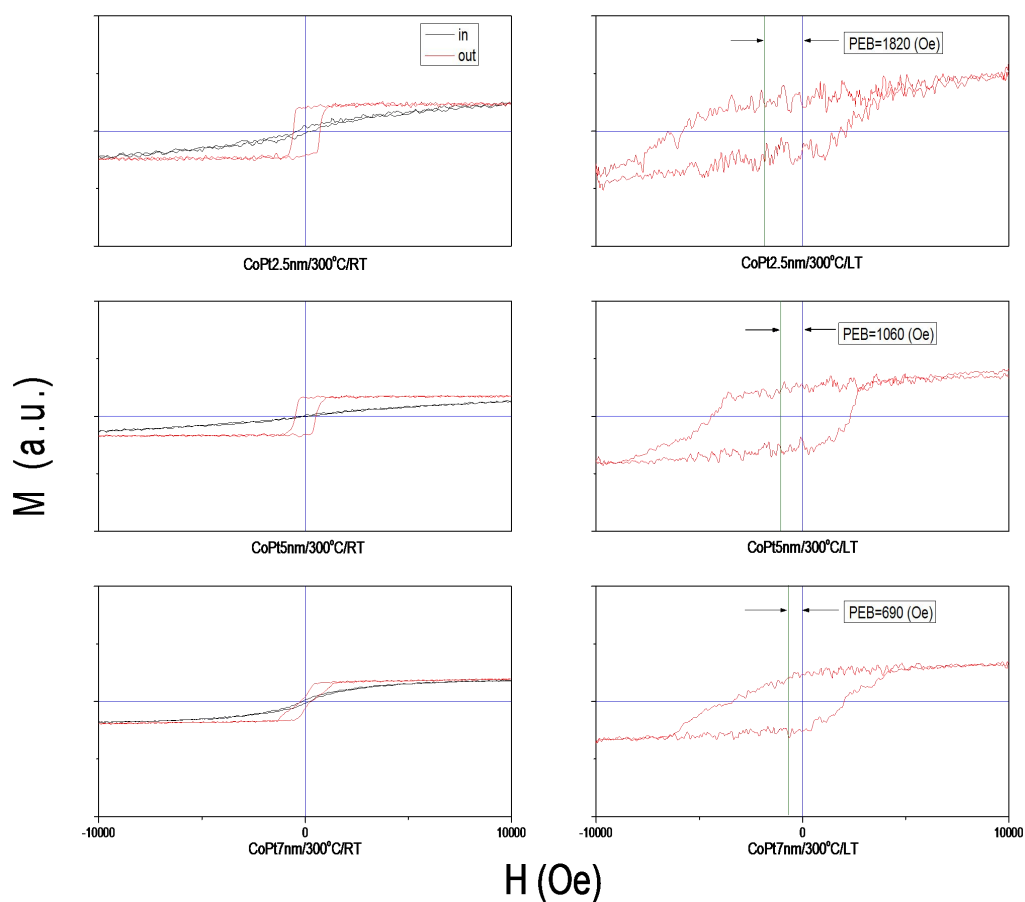


Fig 2-20 Hysteresis loops of 300°C -annealed $[\text{CoO}5\text{nm}/\text{CoPt}2.5\text{nm}]_5$, 300°C -annealed $[\text{CoO}5\text{nm}/\text{CoPt}5\text{nm}]_5$ and 300°C -annealed $[\text{CoO}5\text{nm}/\text{CoO}7\text{nm}]_5$ films (left column was measured at RT, right column was measured at LT after perpendicular field cooling).

2.4 Summary

First, preparation of $[\text{CoO}_x/\text{CoPt}_y]_n$ multilayer films (including magnetron sputtering, post annealing and field cooling) is introduced briefly. Second, the methods used to characterize $[\text{CoO}_x/\text{CoPt}_y]_n$ multilayer films (including transmission electron microscopy, X-ray diffraction, X-ray reflectivity and atomic force microscopy) are listed respectively. Third, the magnetic property measurement and the typical PMA and PEB hysteresis loops of $[\text{CoO}_x/\text{CoPt}_y]_n$ multilayer films are introduced briefly.

References

- [1] P. J. Kelly and R. D. Arnell, *Vacuum*, 56, 159, (2000).
- [2] R. Egerton, *Physical principles of electron microscopy*. Springer. (2005) ISBN 0-387-25800-0.
- [3] B. Fultz and J. Howe, *Transmission Electron Microscopy and Diffractometry of Materials*. Springer. (2007). ISBN 3-540-73885-1.
- [4] W. H. Bragg, *Nature*, 77, 270, (1995).
- [5] I. I. Shafranovskii, and N. V. Belov, *50 Years of X-Ray Diffraction* (Springer): 351. (1962) ISBN 90-277-9029-9.
- [6] W. H. Zachariasen, *Theory of X-ray Diffraction in Crystals*. New York: Dover Publications. (1945). LCCN 67026967.

- [7] H. P. Myers, *Introductory Solid State Physics*. Taylor & Francis. (2002)
ISBN 0-7484-0660-3.
- [8] Structure factor, *Online dictionary of crystallography*, The International Union of Crystallography, 2013.
- [9] I. Teraoka, *Polymer Solutions: An Introduction to Physical Properties*. John Wiley & Sons. (2002).
- [10] A. Guinier, *X-ray Diffraction In Crystals, Imperfect Crystals, and Amorphous Bodies*. W. H. Freeman and Co. (1963).
- [11] D. Chandler, *Introduction to Modern Statistical Mechanics*. Oxford University Press. (1987).
- [12] N. Als-Nielsen, and D. McMorrow, *Elements of Modern X-ray Physics* (2nd edition). John Wiley & Sons. (2011).
- [13] J. P. Hansen and I. R. McDonald, *Theory of Simple Liquids* (3rd edition). Academic Press. (2005).
- [14] J. Wang, T. Omi, T. Sannomiya, S. Muraishi, J. Shi and Y. Nakamura, *Appl. Phys. Lett.* **103**, 042401, (2013) .
- [15] M. Yasaka, *X-ray thin film measurement techniques V*, *The Rigaku Journal*, **26**(2), 2010.
- [16] G. Binnig, C. F. Quate and C. Gerber, *Physical Review Letters*, **56**, 930, (1986).
- [17] Giessibl and J. Franz, *Reviews of Modern Physics* **75**, 949, (2003).
- [18] P. J. Bryant, R. G. Miller and R. Yang, *Appl. Phys. Lett.*, **52**, 2233, 1988.

- [19] Chikazumi and Soshin, Physics of ferromagnetism. Oxford University Press (2009). ISBN 9780199564811.
- [20] Bozorth and M. Richard, Ferromagnetism, IEEE Press (1993). ISBN 0-7803-1032-2.
- [21] B. D. Cullity and C. D. Graham, Introduction to Magnetic Materials, Wiley-IEEE Press (2008).
- [22] Duo, Lamberto, Marco Finazzi and Franco Ciccacci, Magnetic Properties of Antiferromagnetic Oxide Materials. KGaA, Weinheim: Wiley-VCH Verlag GmbH & Co. (2010).
- [23] Spaldin and Nicola, Magnetic Materials Fundamentals and Device Applications. Cambridge, United Kingdom: The Press Syndicate of the University of Cambridge. (2003).
- [24] J. Wang, Study of longitudinal and perpendicular exchange bias in sputter-deposited Co-Pt/CoO multilayer films, Ph.D. thesis, Tokyo Institute of Technology, 2013.
- [25] S. Maat, K. Takano, S. S. P. Parkin and Eric E. Fullerton, Physical Review Letters, **87**, 087202-1, (2001).
- [26] D. Le Roy, R. Morel, A. Brenac, S. Pouget and L. Notin, Journal of Applied Physics, **111**, 083901, (2012).
- [27] D. O. Smith, Rev. Sci. Instrum. **27**, 261 (1956).

Chapter 3 Perpendicular magnetic anisotropy of [CoO_x/CoPt_y]_n multilayer films

3.1 Introduction

Perpendicular magnetic recording, which is based on up and down magnetization in perpendicular magnetic anisotropy (PMA) thin film, was firstly proposed in the late 1970s[1,2]. After that, PMA has been proposed in various configurations during the past decades, since it is of great importance in high density perpendicular magnetic recording[3-10].

In 1985, Carcia reported PMA with layered structure in Co/Pd system and explained the mechanism responsible for PMA in terms of the interface anisotropy[3]. A few years later, PMA was also observed in Co/Au, Co/Pt and Co/Ru systems, of which the magnetic anisotropy could be enhanced by improving the interface quality [4-6]. However, it is universal in the above metallic multilayer films that PMA always deteriorates at elevated temperatures higher than 250°C-300°C due to the interface diffusion, which limits their applications greatly[7].

Recently, AlN and TiN were used to avoid interface diffusion and PMA was obtained in CoPt/AlN, FePt/AlN and CoPt/TiN multilayer films with tolerable temperature up to 600°C. However, in such systems it is hard to get PMA without

thermal annealing higher than 400°C, which also blocks their applications in some degree [8-10].

So, at present it is significant to develop PMA materials that can be used at middle-high-temperature-region between 300°C and 400°C.

In this chapter, PMA of $[\text{CoO}_x/\text{CoPt}_y]_n$ multilayer films has been studied systematically. In order to get the best PMA, the influences of annealing-temperature, CoPt thickness, CoO thickness, period and seed layer on $[\text{CoO}_x/\text{CoPt}_y]_n$ PMA were studied step by step. According to our experiments, $\text{CoO}_{20\text{nm}}/[\text{CoPt}_{5\text{nm}}/\text{CoO}_{5\text{nm}}]_5$ multilayer films show the best PMA performance and possess the highest thermal stability at the temperature region between -192°C and 400°C. This indicates $\text{CoO}_{20\text{nm}}/[\text{CoPt}_{5\text{nm}}/\text{CoO}_{5\text{nm}}]_5$ multilayer films could be a potential candidate for the PMA application at elevated temperatures, in particular when they need to be processed at the middle high temperature region between 300°C and 400°C.

Keywords:

PMA of $[\text{CoO}_x/\text{CoPt}_y]_n$ multilayer film,

$\text{CoO}_{20\text{nm}}/[\text{CoPt}_{5\text{nm}}/\text{CoO}_{5\text{nm}}]_5$ multilayer film,

PMA thermal stability between -192°C and 400°C,

PMA application at temperature region between 300°C and 400°C.

3.2 Experimental details

3.2.1 Preparation of [CoO_x/CoPt_y]_n multilayer films

In order to find the best PMA performance, a series of [CoO_x/CoPt_y]_n multilayer films with different CoPt thickness, different CoO thickness, different period and different seed layer were prepared. [CoO_x/CoPt_y]_n multilayer films were deposited on glass substrate at room temperature (RT) by magnetron sputtering. Ferromagnetic Co_{0.43}Pt_{0.57} alloy layers were deposited by DC sputtering with 0.8Pa Ar, antiferromagnetic CoO layers were deposited by RF sputtering with gas mixture of 0.8Pa Ar and 0.2Pa O₂, the base pressure before deposition was around 5×10^{-5} Pa. After deposition, [CoO_x/CoPt_y]_n multilayer films were vacuum annealed at different temperatures for 3h, respectively.

The related preparation details of [CoO_x/CoPt_y]_n multilayer films are shown clearly in Table 3-1~Table 3-6.

3.2.2 Characterizations of [CoO_x/CoPt_y]_n multilayer films

The RT M-H hysteresis loops of [CoO_x/CoPt_y]_n multilayer films were measured by vibrating sample magnetometer (VSM) directly.

The low temperature M-H hysteresis loops were measured at -192°C by VSM after cooling by liquid N₂.

Table 3-1. [CoO_x/CoPt_y]_n with different CoPt thickness and different annealing temperature

	25°C-deposited	250°C-annealed	300°C-annealed	350°C-annealed	400°C-annealed	500°C-annealed
[CoO _{5nm} /CoPt _{2.5nm}] ₅	●	●	●	●	●	●
[CoO _{5nm} /CoPt _{5nm}] ₅	●	●	●	●	●	●
[CoO _{5nm} /CoPt _{7nm}] ₅	●	●	●	●	●	●
[CoO _{5nm} /CoPt _{9nm}] ₅	●	●	●	●	●	●
[CoO _{5nm} /CoPt _{12nm}] ₅	●	●	●	●	●	●

Table 3-2. [CoO_x/CoPt_y]_n with different CoO thickness

	25°C-deposited	250°C-annealed	300°C-annealed	350°C-annealed		
[CoO _{5nm} /CoPt _{5nm}] ₅	●	●	●	●		
[CoO _{10nm} /CoPt _{5nm}] ₃	●	●	●	●		

Table 3-3. [CoO_x/CoPt_y]_n with different period

			300°C-annealed			
[CoO _{5nm} /CoPt _{5nm}] ₁			●			
[CoO _{5nm} /CoPt _{5nm}] ₃			●			
[CoO _{5nm} /CoPt _{5nm}] ₅			●			
[CoO _{5nm} /CoPt _{5nm}] ₇			●			
[CoO _{5nm} /CoPt _{5nm}] ₁₀			●			
[CoO _{5nm} /CoPt _{5nm}] ₁₂			●			

Table 3-4. [CoO_x/CoPt_y]_n without and with CoO_{20nm} seed layer

	25°C-deposited	100°C-annealed	300°C-annealed	350°C-annealed		
[CoO _{5nm} /CoPt _{5nm}] ₅	●	●	●	●		
CoO _{20nm} /[CoPt _{5nm} /CoO _{5nm}] ₅	●	●	●	●		

Table 3-5. [CoPt_y/CoO_x]_n with CoO_{20nm} seed layer but different CoPt thickness

	-192°C-cooled	25°C-deposited	300°C-annealed			
CoO _{20nm} /[CoPt _{5nm} /CoO _{5nm}] ₅	●	●	●			
CoO _{20nm} /[CoPt _{6nm} /CoO _{5nm}] ₅	●	●	●			

Table 3-6. PMA thermal stability of CoO_{20nm}/[CoPt_{5nm}/CoO_{5nm}]₅

	-192°C-cooled	25°C-deposited	100°C-annealed	300°C-annealed	350°C-annealed	400°C-annealed
CoO _{20nm} /[CoPt _{5nm} /CoO _{5nm}] ₅	●	●	●	●	●	●

3.3 Results and Discussion

3.3.1 [CoO_x/CoPt_y]_n with different CoPt thickness and different annealing temperature

	25°C-deposited	250°C-annealed	300°C-annealed	350°C-annealed	400°C-annealed	500°C-annealed
[CoO _{5nm} /CoPt _{2.5nm}] ₅	●	●	●	●	●	●
[CoO _{5nm} /CoPt _{5nm}] ₅	●	●	●	●	●	●
[CoO _{5nm} /CoPt _{7nm}] ₅	●	●	●	●	●	●
[CoO _{5nm} /CoPt _{9nm}] ₅	●	●	●	●	●	●
[CoO _{5nm} /CoPt _{12nm}] ₅	●	●	●	●	●	●

[CoO_x/CoPt_y]_n multilayer films with different CoPt thickness y and different post-annealing temperature were studied in section 3.3.1. The related M-H hysteresis loops of [CoO_{5nm}/CoPt_y]₅ multilayer films are listed in Fig 3-1, Fig 3-2, Fig 3-3, Fig 3-4 and Fig 3-5, individually. The comprehensive comparison of their M-H hysteresis loops is shown in Fig 3-6.

Based on the results, it can be seen both CoPt thickness and post-annealing temperature play important roles in developing strong PMA. In Fig 3-6, for the specified CoPt thickness, the strongest PMA can be obtained in 300°C-annealed sample. Apart from post-annealing, ferromagnetic CoPt layer thickness y is also

very important, in particular γ has great influences on the magnetic anisotropy of the as-deposited $[\text{CoO}_{5\text{nm}}/\text{CoPt}_y]_5$ sample. However, PMA shows evident degradation tendency when the annealing temperature is above 350°C . To our knowledge, this is due to the gradual decomposition of CoO layer at high temperatures.

On the other hand, the effective PMA energy K_{eff} was also listed in Fig 3-6. Based on the K_{eff} shown in Fig 3-6, it is clear to see that 300°C is the best annealing temperature to get the strongest PMA, and 5nm is the best CoPt thickness to get stable PMA.

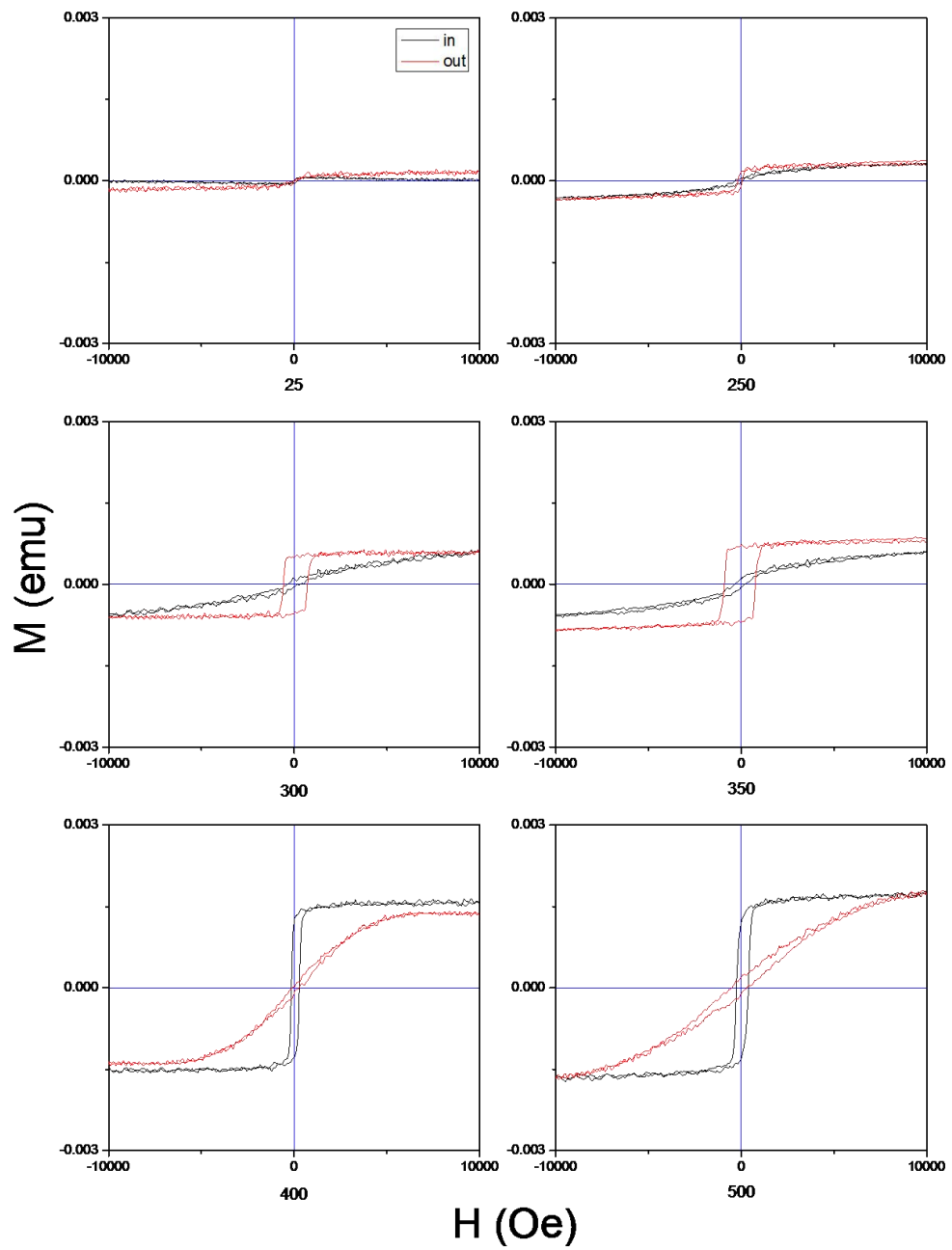


Fig 3-1 Hysteresis loops of as-deposited, 250°C-annealed, 300°C-annealed, 350°C-annealed, 400°C-annealed and 500°C-annealed $[CoO5nm/CoPt2.5nm]_5$ samples (measured at RT).

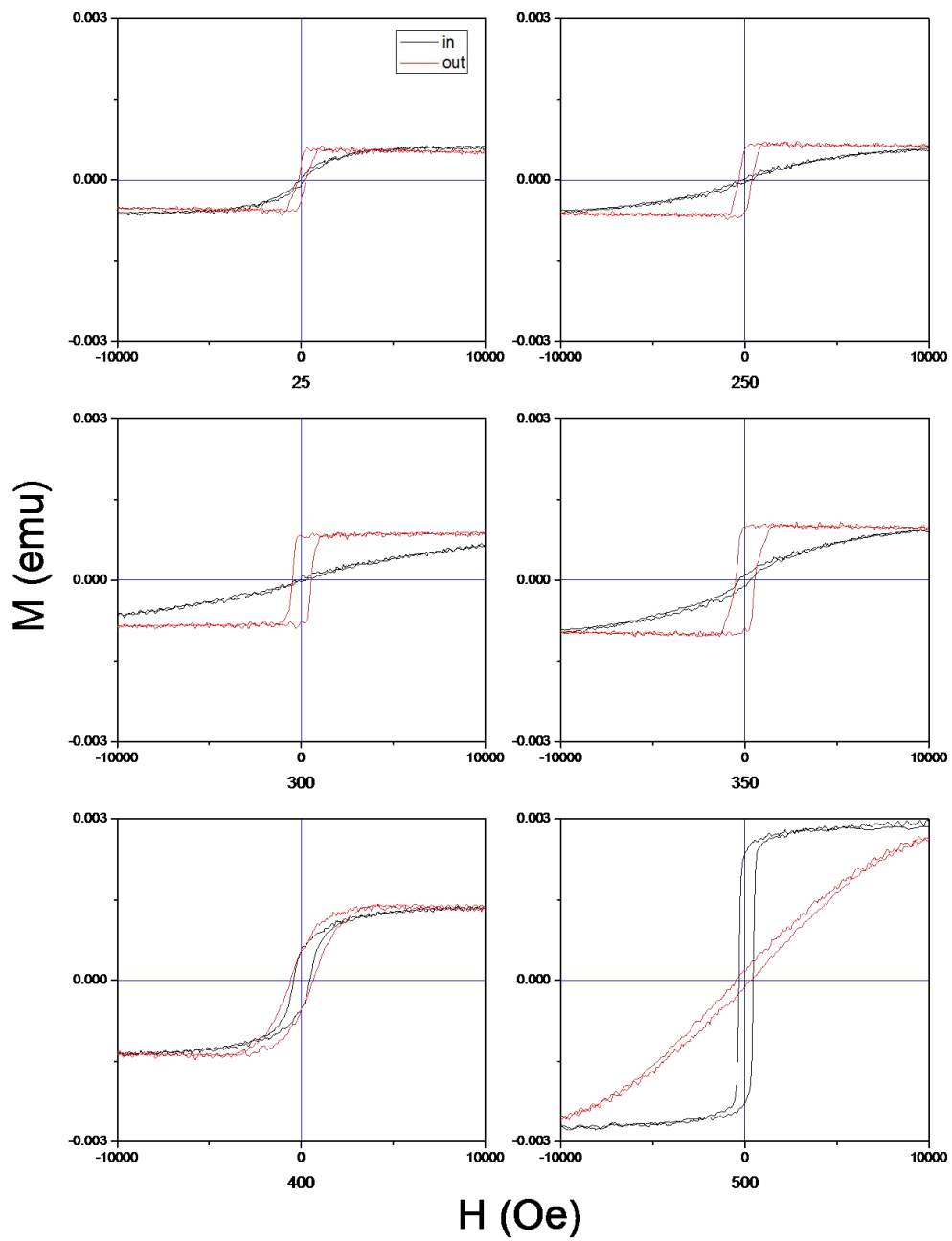


Fig 3-2 Hysteresis loops of as-deposited, 250°C-annealed, 300°C-annealed, 350°C-annealed, 400°C-annealed and 500°C-annealed $[\text{CoO}5\text{nm}/\text{CoPt}5\text{nm}]_5$ samples (measured at RT).

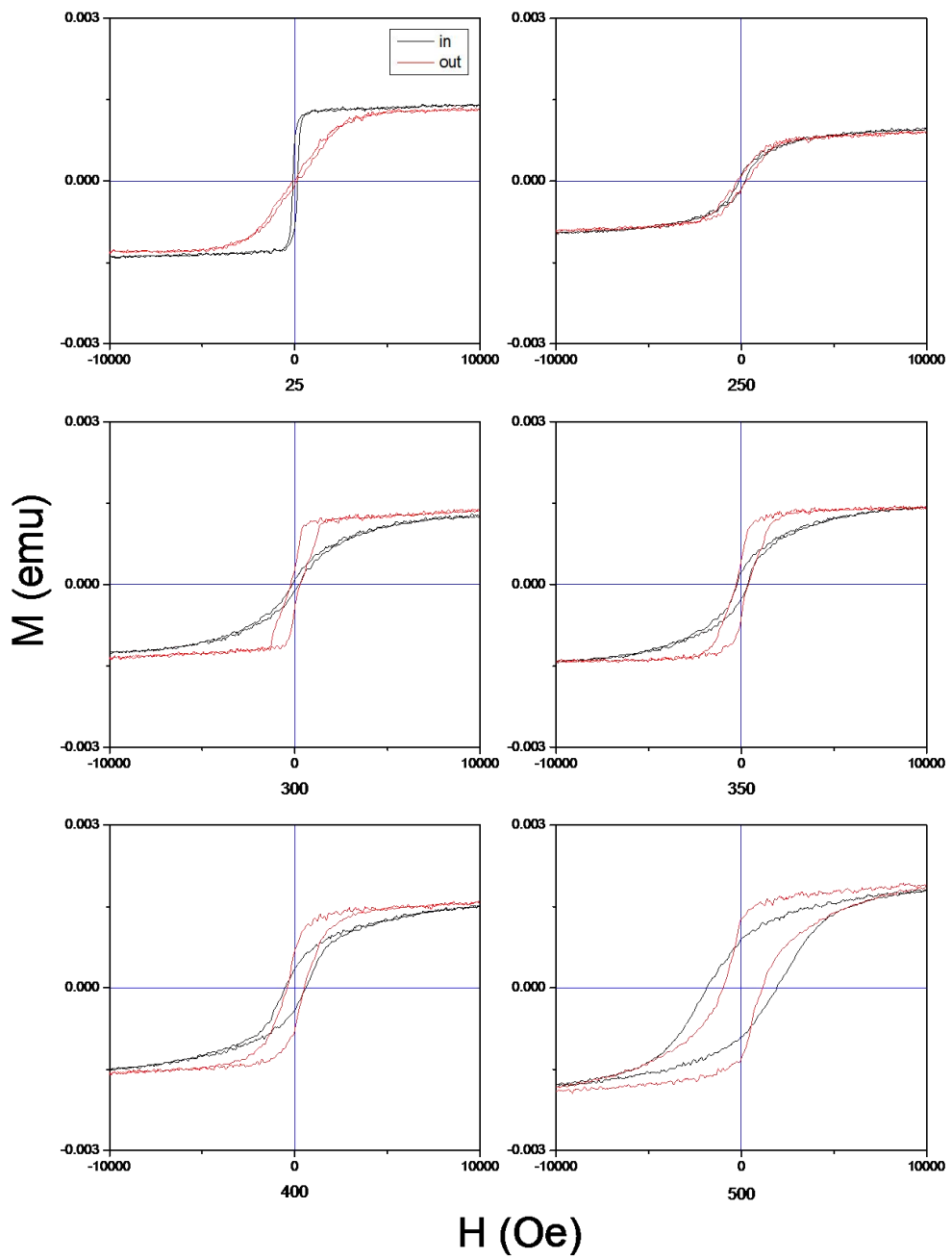


Fig 3-3 Hysteresis loops of as-deposited, 250°C-annealed, 300°C-annealed, 350°C-annealed, 400°C-annealed and 500°C-annealed $[\text{CoO}5\text{nm}/\text{CoPt}7\text{nm}]_5$ samples (measured at RT).

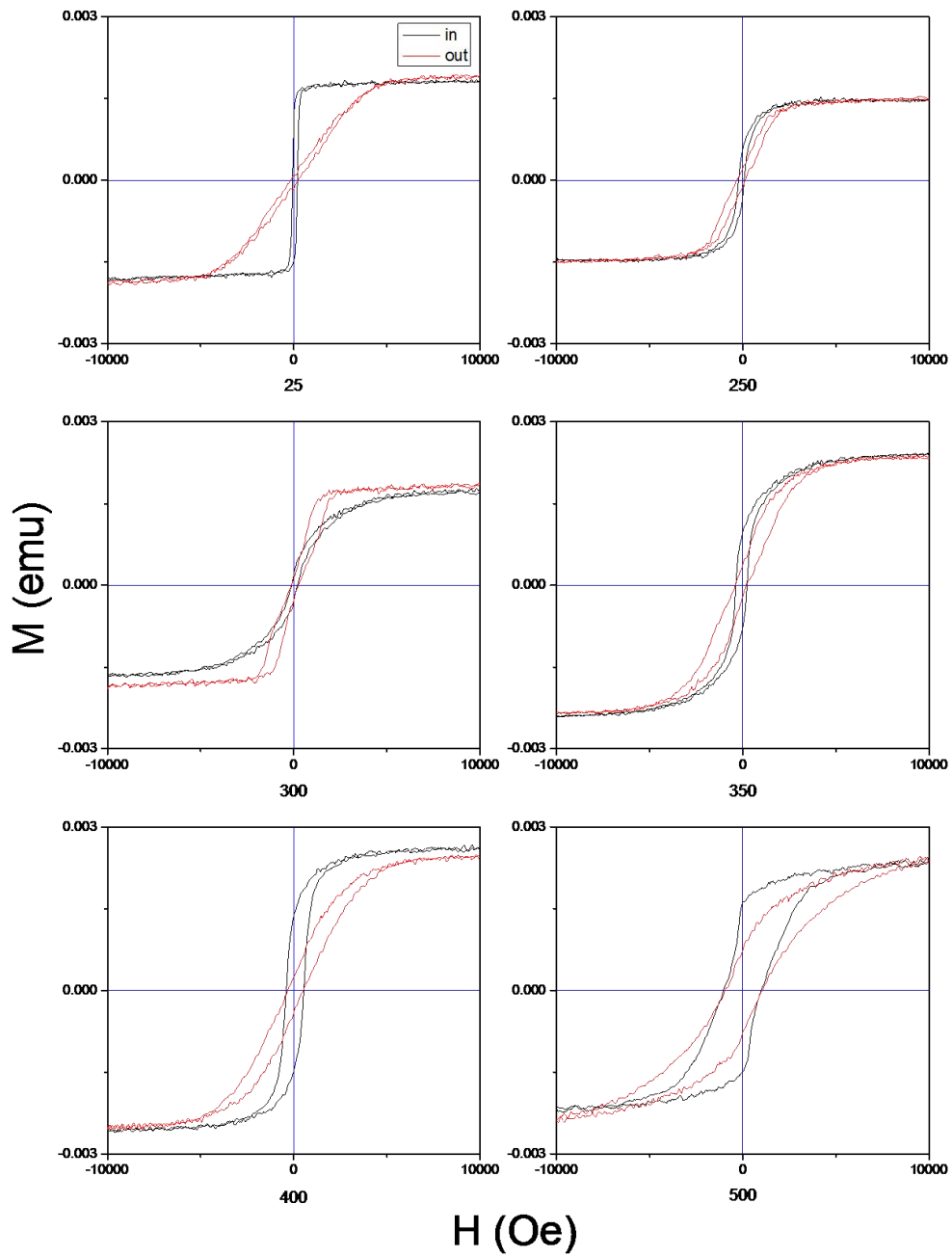


Fig 3-4 Hysteresis loops of as-deposited, 250°C-annealed, 300°C-annealed, 350°C-annealed, 400°C-annealed and 500°C-annealed $[\text{CoO}5\text{nm}/\text{CoPt}9\text{nm}]_5$ samples (measured at RT).

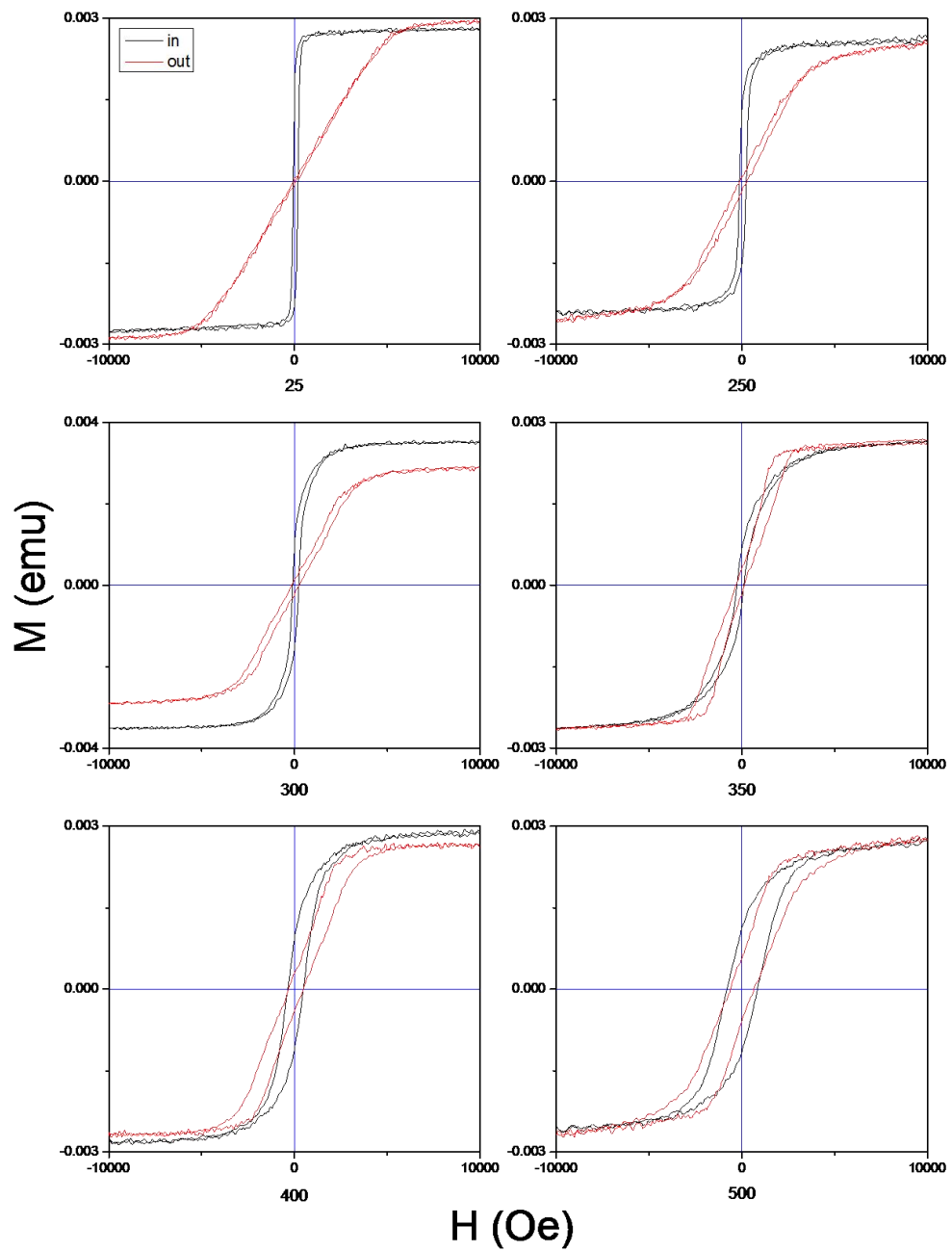


Fig 3-5 Hysteresis loops of as-deposited, 250°C-annealed, 300°C-annealed, 350°C-annealed, 400°C-annealed and 500°C-annealed $[\text{CoO}5\text{nm}/\text{CoPt}12\text{nm}]_5$ samples (measured at RT).

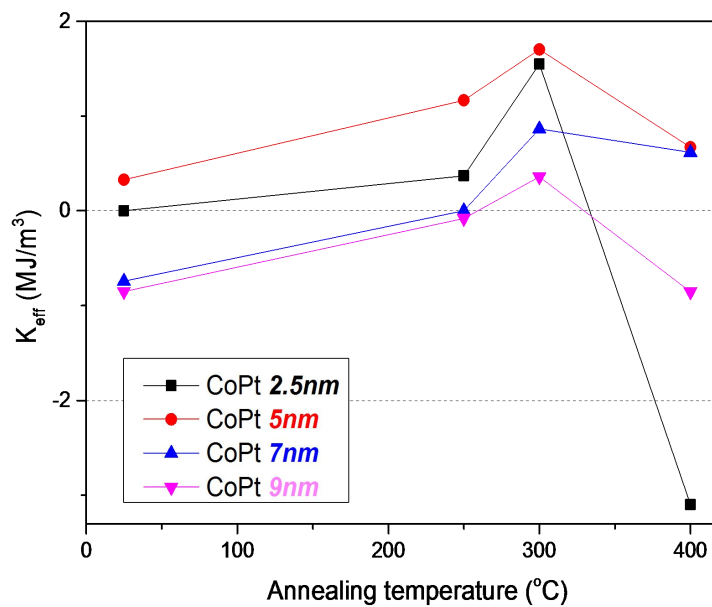
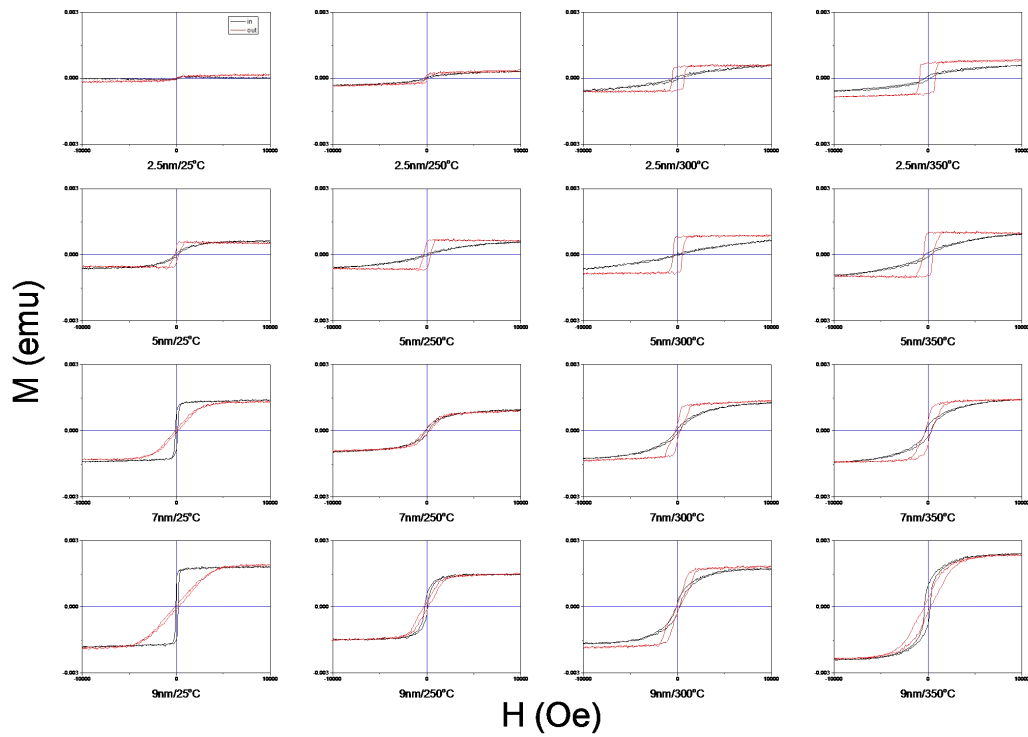


Fig 3-6 Hysteresis loops and K_{eff} of $[\text{CoO}_{5\text{nm}}/\text{CoPt}_y]_5$ with different CoPt thickness $y=$

2.5nm, 5nm, 7nm and 9nm (measured at RT).

3.3.2 [CoO_x/CoPt_y]_n with different CoO thickness

	25°C-deposited	250°C-annealed	300°C-annealed	350°C-annealed		
[CoO _{5nm} /CoPt _{5nm}] ₅	●	●	●	●		
[CoO _{10nm} /CoPt _{5nm}] ₃	●	●	●	●		

[CoO_x/CoPt_y]_n multilayer films with different CoO thickness x and different post-annealing temperature were studied in section 3.3.2. The related M-H hysteresis loops are listed in Fig 3-7.

According to Fig 3-7, we can find 5nm is the better CoO thickness to get stable PMA, and 300°C is also the best annealing temperature to get the strongest PMA.

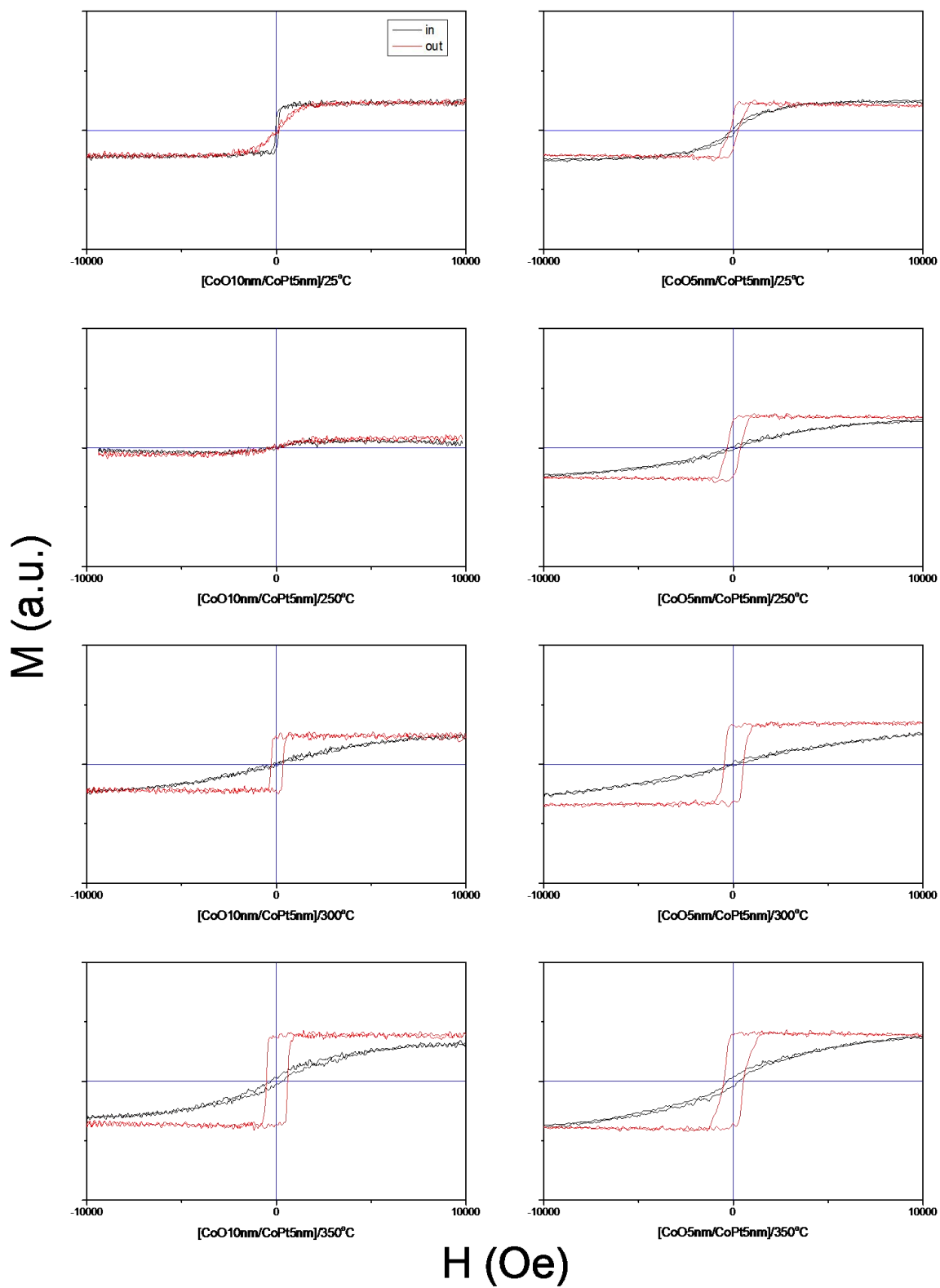


Fig 3-7 **Left:** hysteresis loops of $[\text{CoO}_{10\text{nm}}/\text{CoPt}_{5\text{nm}}]_3$ samples (measured at RT).

Right: hysteresis loops of $[\text{CoO}_{5\text{nm}}/\text{CoPt}_{5\text{nm}}]_5$ samples (measured at RT).

3.3.3 [CoO_x/CoPt_y]_n with different period

			300°C-annealed			
[CoO _{5nm} /CoPt _{5nm}] ₁			•			
[CoO _{5nm} /CoPt _{5nm}] ₃			•			
[CoO _{5nm} /CoPt _{5nm}] ₅			•			
[CoO _{5nm} /CoPt _{5nm}] ₇			•			
[CoO _{5nm} /CoPt _{5nm}] ₁₀			•			
[CoO _{5nm} /CoPt _{5nm}] ₁₂			•			

300°C-annealed [CoO_x/CoPt_y]_n multilayer films with different period were studied in section 3.3.3. The related M-H hysteresis loops of 300°C-annealed [CoO_{5nm}/CoPt_{5nm}]_n multilayer films are listed in Fig 3-8.

According to Fig 3-8, we can find $n=5$ is the best repetition-period to get the strongest PMA.

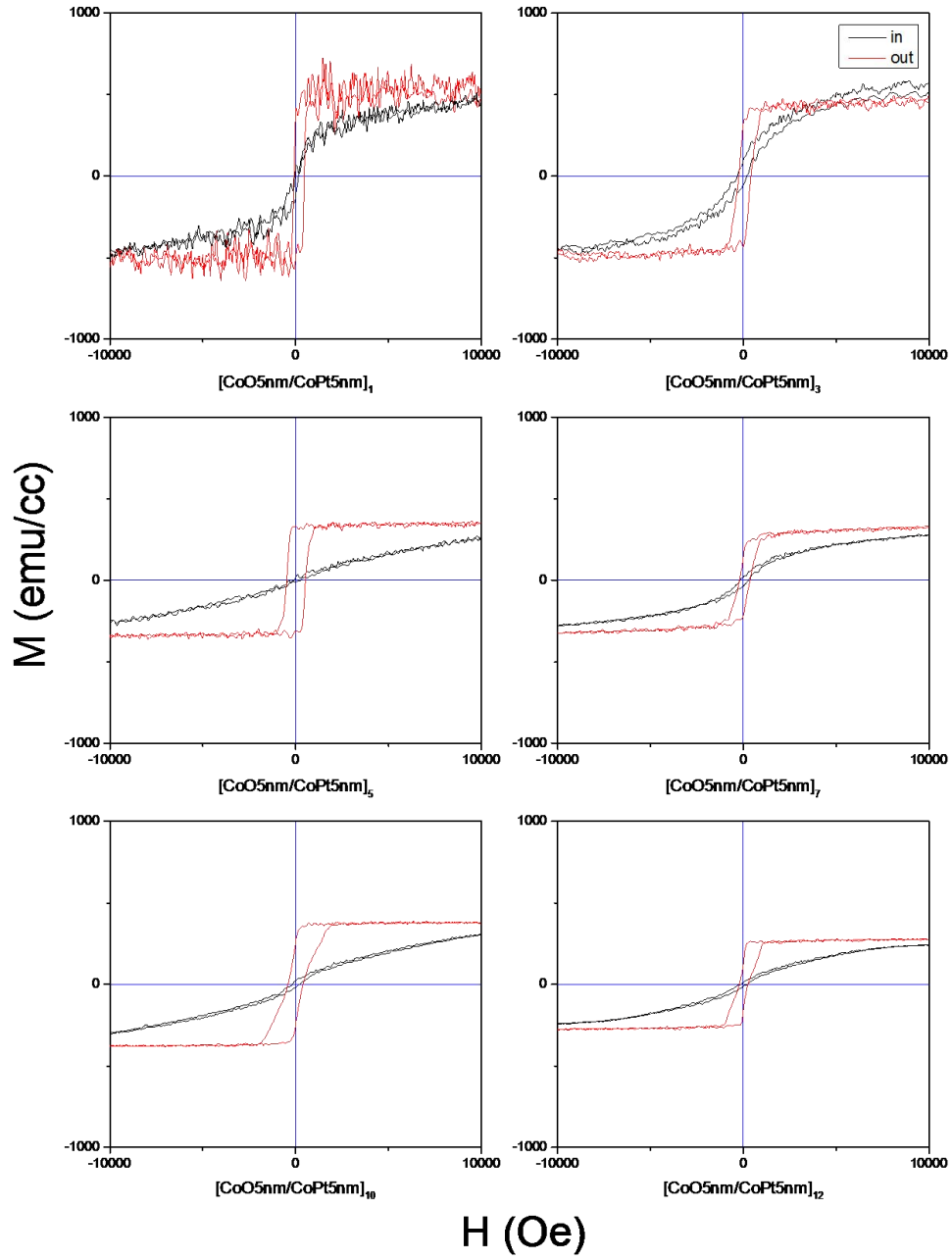


Fig 3-8 Hysteresis loops of 300°C-annealed $[\text{CoO5nm}/\text{CoPt5nm}]_n$ with different period $n=1, 3, 5,$

7, 10, 12 (measured at RT).

3.3.4 [CoO_x/CoPt_y]_n without and with CoO_{20nm} seed layer

	25°C-deposited	100°C-annealed	300°C-annealed	350°C-annealed		
[CoO _{5nm} /CoPt _{5nm}] ₅	●	●	●	●		
<u>CoO_{20nm}</u> /[CoPt _{5nm} /CoO _{5nm}] ₅	●	●	●	●		

[CoO_x/CoPt_y]_n multilayer films without and with CoO_{20nm} seed layer were studied in section 3.3.4. The related M-H hysteresis loops of [CoO_{5nm}/CoPt_{5nm}]₅ without CoO_{20nm} seed layer and CoO_{20nm}/[CoPt_{5nm}/CoO_{5nm}]₅ with CoO_{20nm} seed layer are listed in Fig 3-9.

According to Fig 3-9, we can find CoO_{20nm}/[CoPt_{5nm}/CoO_{5nm}]₅ multilayer film with CoO_{20nm} seed layer possesses better PMA performances than [CoO_{5nm}/CoPt_{5nm}]₅ multilayer film, especially for the 25°C-deposited and 100°C-annealed samples.

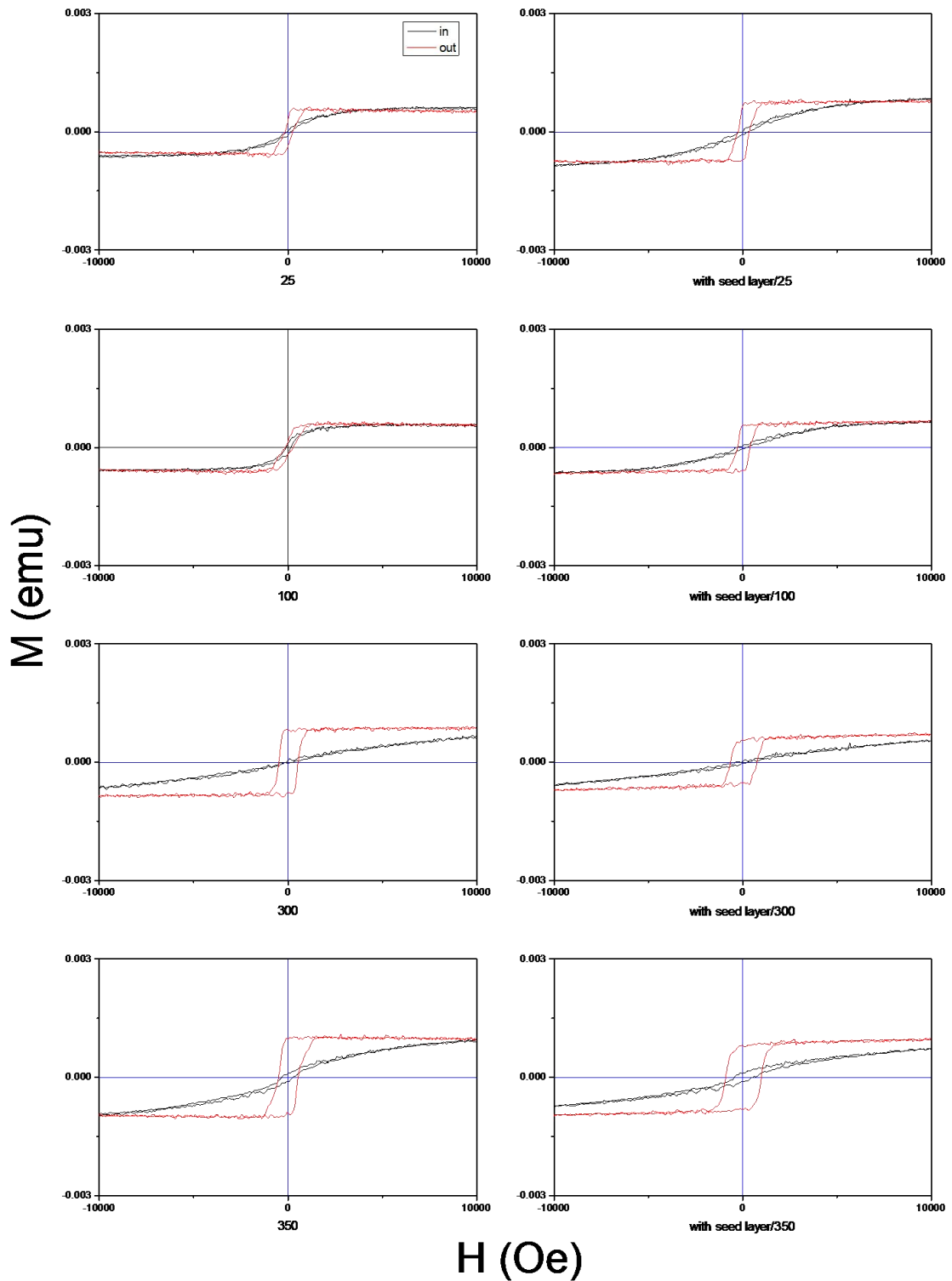


Fig 3-9 **Left:** hysteresis loops of $[\text{CoO}_{5\text{nm}}/\text{CoPt}_{5\text{nm}}]_5$ samples (measured at RT).

Right: hysteresis loops of $\text{CoO}_{20\text{nm}}/[\text{CoPt}_{5\text{nm}}/\text{CoO}_{5\text{nm}}]_5$ samples (measured at RT).

3.3.5 [CoPt_y/CoO_x]_n with CoO_{20nm} seed layer but different CoPt thickness

	-192°C-cooled	25°C-deposited	300°C-annealed			
<u>CoO_{20nm}</u> /[CoPt _{5nm} /CoO _{5nm}] ₅	●	●	●			
<u>CoO_{20nm}</u> /[CoPt _{6nm} /CoO _{5nm}] ₅	●	●	●			

[CoPt_y/CoO_x]_n multilayer films with CoO_{20nm} seed layer but different CoPt thickness were studied in section 3.3.5. The related M-H hysteresis loops of CoO_{20nm}/[CoPt_y/CoO_{5nm}]₅ are listed in Fig 3-10.

According to Fig 3-10, we can find CoO_{20nm}/[CoPt_{5nm}/CoO_{5nm}]₅ multilayer film possesses better PMA performances than CoO_{20nm}/[CoPt_{6nm}/CoO_{5nm}]₅ multilayer film, especially for the 25°C-deposited sample.

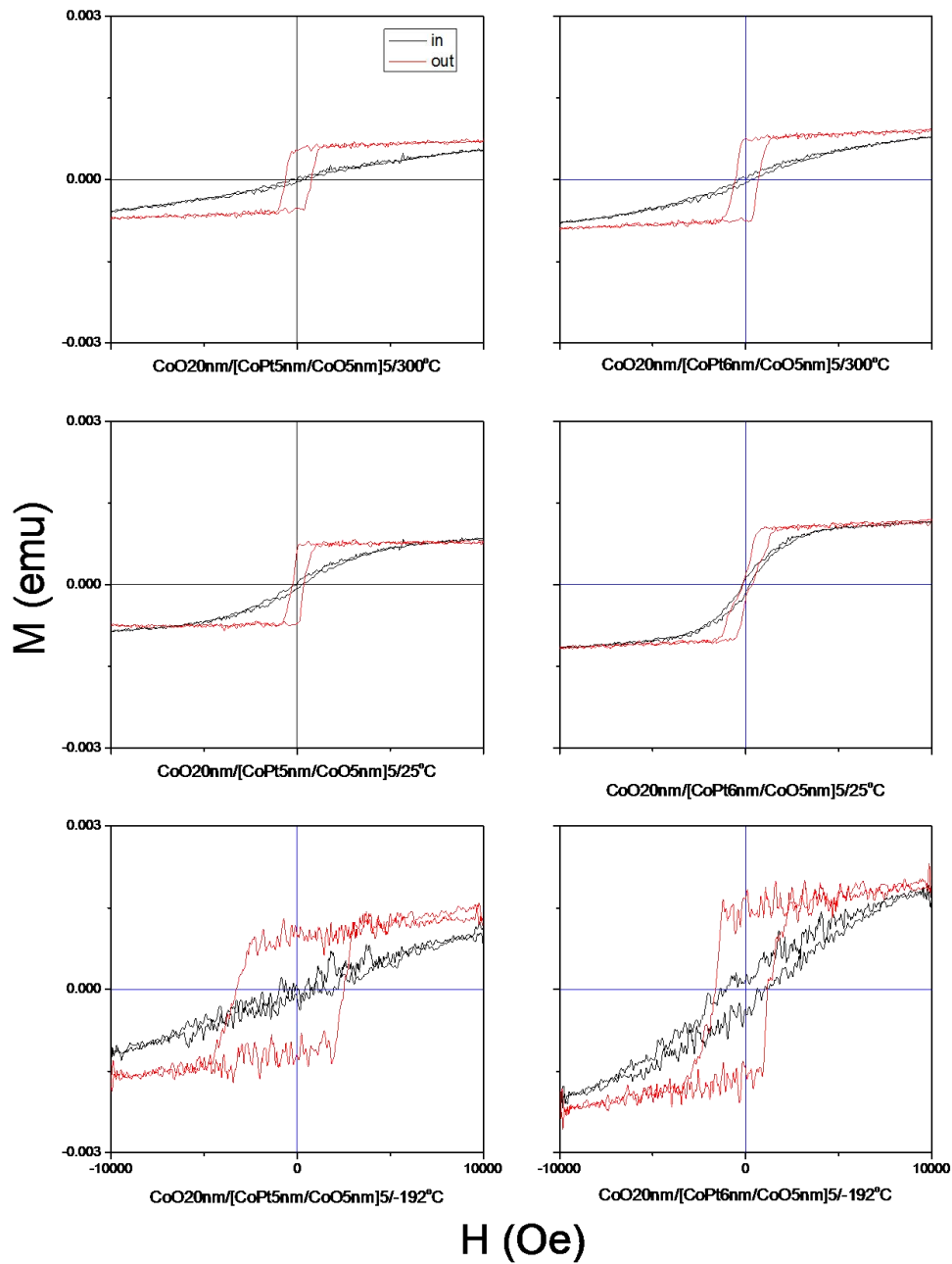


Fig 3-10 Left: hysteresis loops of $\text{CoO}_{20\text{nm}}/[\text{CoPt}_{5\text{nm}}/\text{CoO}_{5\text{nm}}]_5$ samples.

Right: hysteresis loops of $\text{CoO}_{20\text{nm}}/[\text{CoPt}_{6\text{nm}}/\text{CoO}_{5\text{nm}}]_5$ samples.

3.3.6 PMA thermal stability of $\text{CoO}_{20\text{nm}}/[\text{CoPt}_{5\text{nm}}/\text{CoO}_{5\text{nm}}]_5$

	-192°C-cooled	25°C-deposited	100°C-annealed	300°C-annealed	350°C-annealed	400°C-annealed
$\text{CoO}_{20\text{nm}}/[\text{CoPt}_{5\text{nm}}/\text{CoO}_{5\text{nm}}]_5$	●	●	●	●	●	●

In section 3.3.1~3.3.5, the influences of annealing temperature, CoPt thickness, CoO thickness, repetition period and seed layer on $[\text{CoO}_x/\text{CoPt}_y]_n$ PMA were studied step by step. By optimizing the deposition conditions, we found $\text{CoO}_{20\text{nm}}/[\text{CoPt}_{5\text{nm}}/\text{CoO}_{5\text{nm}}]_5$ multilayer films show the best PMA performance.

In this section, PMA thermal stability of $\text{CoO}_{20\text{nm}}/[\text{CoPt}_{5\text{nm}}/\text{CoO}_{5\text{nm}}]_5$ multilayer films were further studied. The related M-H hysteresis loops of $\text{CoO}_{20\text{nm}}/[\text{CoPt}_{5\text{nm}}/\text{CoO}_{5\text{nm}}]_5$ are listed in Fig 3-11.

According to Fig 3-11, we can find $\text{CoO}_{20\text{nm}}/[\text{CoPt}_{5\text{nm}}/\text{CoO}_{5\text{nm}}]_5$ multilayer film possesses very high PMA thermal stability at the temperature region between -192°C and 400°C. This indicates $\text{CoO}_{20\text{nm}}/[\text{CoPt}_{5\text{nm}}/\text{CoO}_{5\text{nm}}]_5$ multilayer films could be a potential candidate for the PMA application at middle high temperature region between 300°C and 400°C.

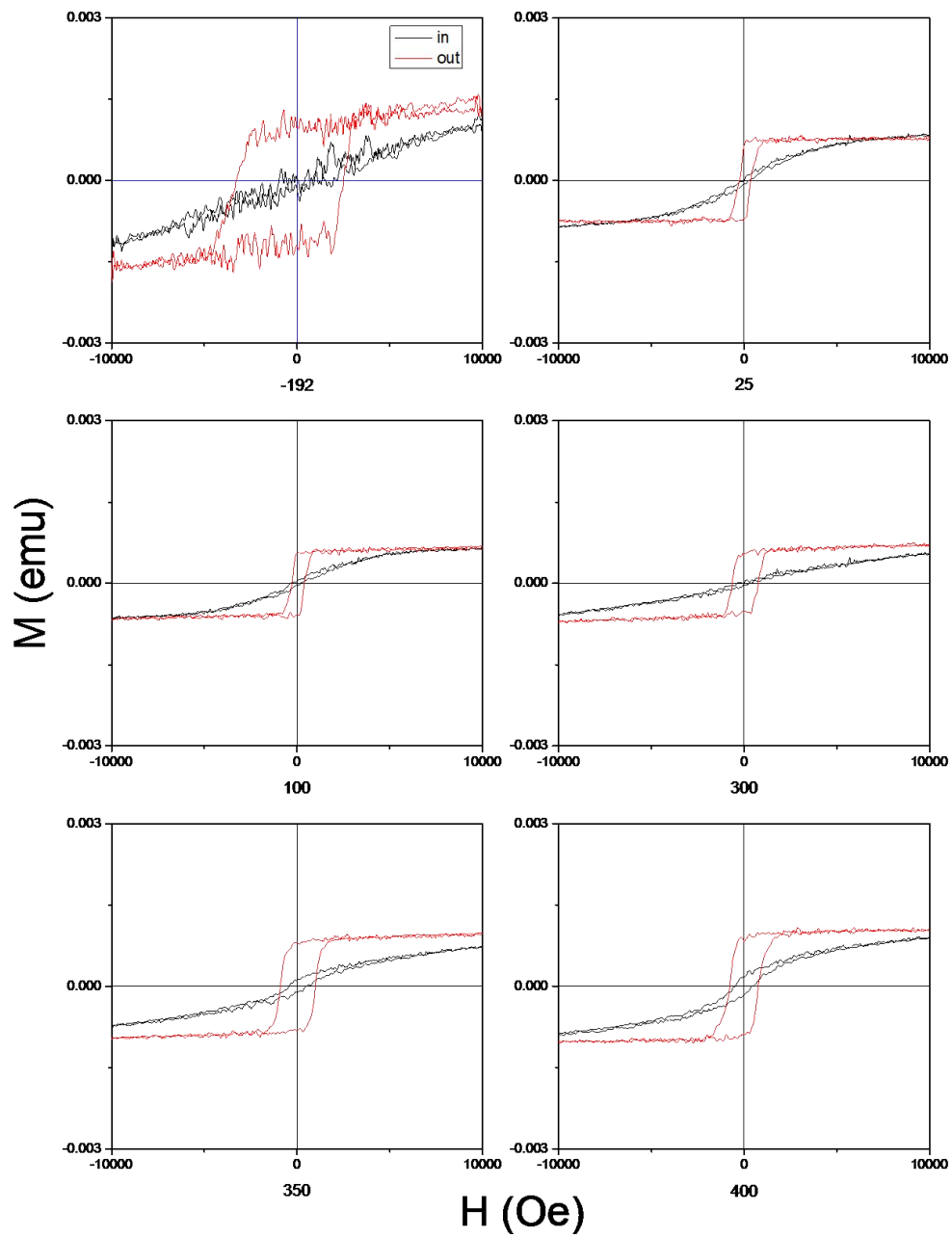


Fig 3-11 Hysteresis loops of -192°C-cooled, as-deposited, 100°C-annealed, 300°C-annealed, 350°C-annealed and 400°C-annealed $\text{CoO}_{20\text{nm}}/[\text{CoPt}_{5\text{nm}}/\text{CoO}_{5\text{nm}}]_5$ samples.

3.4 Conclusion

1. To get the strongest PMA in $[\text{CoO}_x/\text{CoPt}_y]_n$ multilayer films, the influences of post-annealing temperature, CoPt thickness y , CoO thickness x , repetition period n and CoO seed layer on PMA of $[\text{CoO}_x/\text{CoPt}_y]_n$ multilayer films have been studied systematically.
2. Enhanced PMA can be obtained in the annealed $[\text{CoO}_x/\text{CoPt}_y]_n$ multilayer films. Especially, the strongest PMA can be obtained in the 300°C-annealed $[\text{CoO}_x/\text{CoPt}_y]_n$ multilayer films.
3. By optimizing the deposition conditions, $\text{CoO}_{20\text{nm}}/[\text{CoPt}_{5\text{nm}}/\text{CoO}_{5\text{nm}}]_5$ multilayer films show the best PMA performance and possess the highest thermal stability at the temperature region between -192°C and 400°C.
4. To our knowledge, PMA surviving at temperature region between 300°C and 400°C is obtained for the first time in $[\text{CoO}_x/\text{CoPt}_y]_n$ multilayer films.
5. In our opinion, $\text{CoO}_{20\text{nm}}/[\text{CoPt}_{5\text{nm}}/\text{CoO}_{5\text{nm}}]_5$ multilayer films could be a potential candidate for the PMA application at elevated temperatures, in particular when they need to be processed at the middle high temperature region between 300°C and 400°C.

References

- [1] S. Iwasaki and K. Takemura, IEEE Trans. Magn. **11**, (1975) 1173.
- [2] S. N. Piramanayagam, J. Appl. Phys. **102**, (2007) 011301.
- [3] P. F. Carcia, A. D. Meinhaldt and A. Suna, Appl. Phys. Lett. **47**, (1985) 178.
- [4] C. Chappert and P. Bruno, J. Appl. Phys. **64**, (1988) 5736.
- [5] P. F. Carcia, J. Appl. Phys. **63**, (1988) 5066.
- [6] M. Sakurai, T. Takahata and I. Moritani, J. Magn. Soc. Japan **15**, (1991) 411.
- [7] Y. X. Yu, J. Shi and Y. Nakamura, Acta Materialia. **60**, (2012) 6770.
- [8] Y. Hodumi, J. Shi and Y. Nakamura, Appl. Phys. Lett. **90**, (2007) 212506.
- [9] C. Zhang, T. Sannomiya, S. Muraishi, J. Shi and Y. Nakamura, Appl. Phys. A. **116**, (2014) 1695.
- [10] H. Y. An, Q. Xie, J. Wang, T. Sannomiya, S. Muraishi, Z. J. Zhang, Y. Nakamura and J. Shi, J. Vac. Sci. Tec. A. **33** (2015) 021512.

Chapter 4 Magnetoelastically induced magnetic anisotropy transition in [CoO5nm/CoPt7nm]₅ multilayer films

4.1 Introduction

During the past decades, multilayer films with perpendicular magnetic anisotropy (PMA) have been proposed in various configurations [1-7]. In 1985, Carcia firstly reported PMA for layered structure in Co/Pd system, and explained the mechanism responsible for PMA in terms of the interface anisotropy originated from the broken symmetry at the interface [1]. A few years later, PMA was also observed in Co/Au, Co/Pt and Co/Ru systems, of which the magnetic anisotropy could be enhanced by improving the interface quality [2-4].

Recently, AlN was used instead of noble metal layer to avoid interdiffusion and PMA was obtained in CoPt/AlN and FePt/AlN systems after thermal annealing at temperatures up to 600°C [5-7]. In such multilayer films, it was considered that both interface anisotropy and magnetoelastic effect played important roles in promoting PMA.

In this chapter, the magnetic anisotropy of [CoO5nm/CoPt7nm]₅ multilayer film with respect to post-annealing has been studied systematically. [CoO5nm/CoPt7nm]₅ multilayer film undergoes a smooth transition from

longitudinal magnetic anisotropy (LMA) to perpendicular magnetic anisotropy (PMA) upon annealing and returns backward to LMA at high temperature of 550°C. The strongest PMA of [CoO5nm/CoPt7nm]₅ is achieved after post-annealing at 300°C and the tolerable post-annealing temperature with strong PMA is up to 400°C.

The mechanism responsible for the transition of magnetic anisotropy has been investigated by analyzing CoO/CoPt interface and CoPt layer internal stress. It is found the effective PMA energy is proportional to the in-plane tensile stress of CoPt layer but is inversely proportional to the roughness of CoO/CoPt interface.

Finally, by means of low temperature experiment we demonstrate experimentally that the magnetic anisotropy transition in this chapter is mainly attributed to the change of CoPt layer in-plane tensile stress. In other words, it is a magnetoelastically induced magnetic anisotropy transition in [CoO5nm/CoPt7nm]₅ multilayer films.

Keywords:

[CoO5nm/CoPt7nm]₅ multilayer film,

transition of magnetic anisotropy,

magnetoelastic effect.

4.2 Experimental Details

4.2.1 Preparation of [CoO5nm/CoPt7nm]₅ multilayer films

[CoO5nm/CoPt7nm]₅ multilayer films were deposited on glass substrate at room temperature (RT) by magnetron sputtering. Ferromagnetic Co_{0.43}Pt_{0.57} alloy layers were deposited by DC sputtering with 0.8Pa Ar, antiferromagnetic CoO layers were deposited by RF sputtering with a gas mixture of 0.8Pa Ar and 0.2Pa O₂. The base pressure before deposition was around 5×10^{-5} Pa. After deposition, [CoO5nm/CoPt7nm]₅ multilayer films were vacuum annealed at 200°C, 250°C, 300°C, 350°C, 400°C, 500°C and 550°C for 3h respectively, then cooled down to RT.

4.2.2 Characterizations of [CoO5nm/CoPt7nm]₅ multilayer films

After cooling down from annealing-temperature to RT, the M-H hysteresis loops of [CoO5nm/CoPt7nm]₅ were measured at RT by vibrating sample magnetometer (VSM) and the effective PMA energy (K_{eff}) was extracted by calculating the area between out-of-plane and in-plane M-H hysteresis loops.

The low temperature M-H hysteresis loops of 200°C-annealed [CoO5nm/CoPt7nm]₅ were further measured after cooling with liquid N₂.

By varying the post-annealing temperature, the microstructure of [CoO5nm/CoPt7nm]₅ multilayer film was also changed, allowing us to obtain different crystallinity, interface and in-plane stress. The microstructure

characterizations of [CoO5nm/CoPt7nm]₅, including crystallinity and top-surface topography, were carried out by x-ray diffraction (XRD) and atomic force microscope (AFM). [CoO5nm/CoPt7nm]₅ top-surface root-mean-square roughness (R_{rms}) was derived from AFM as an intuitive reference of CoO/CoPt interface. CoO/CoPt interface was characterized by XRR. CoPt in-plane grain diameter was calculated by Scherrer formula. CoPt layer internal stress was calculated by $\sin^2\phi$ method through analyzing its in-plane (11-1) and the out-of-plane (111) lattice distances.

4.3 Results and Discussion

4.3.1 Hysteresis loops of [CoO5nm/CoPt7nm]₅ multilayer films

The M-H hysteresis loop evolution of [CoO5nm/CoPt7nm]₅ multilayer films with respect to the post-annealing temperature is shown in Fig 4-1. It is clear that PMA can be developed by annealing, although [CoO5nm/CoPt7nm]₅ film shows a strong LMA in the as-deposited state.

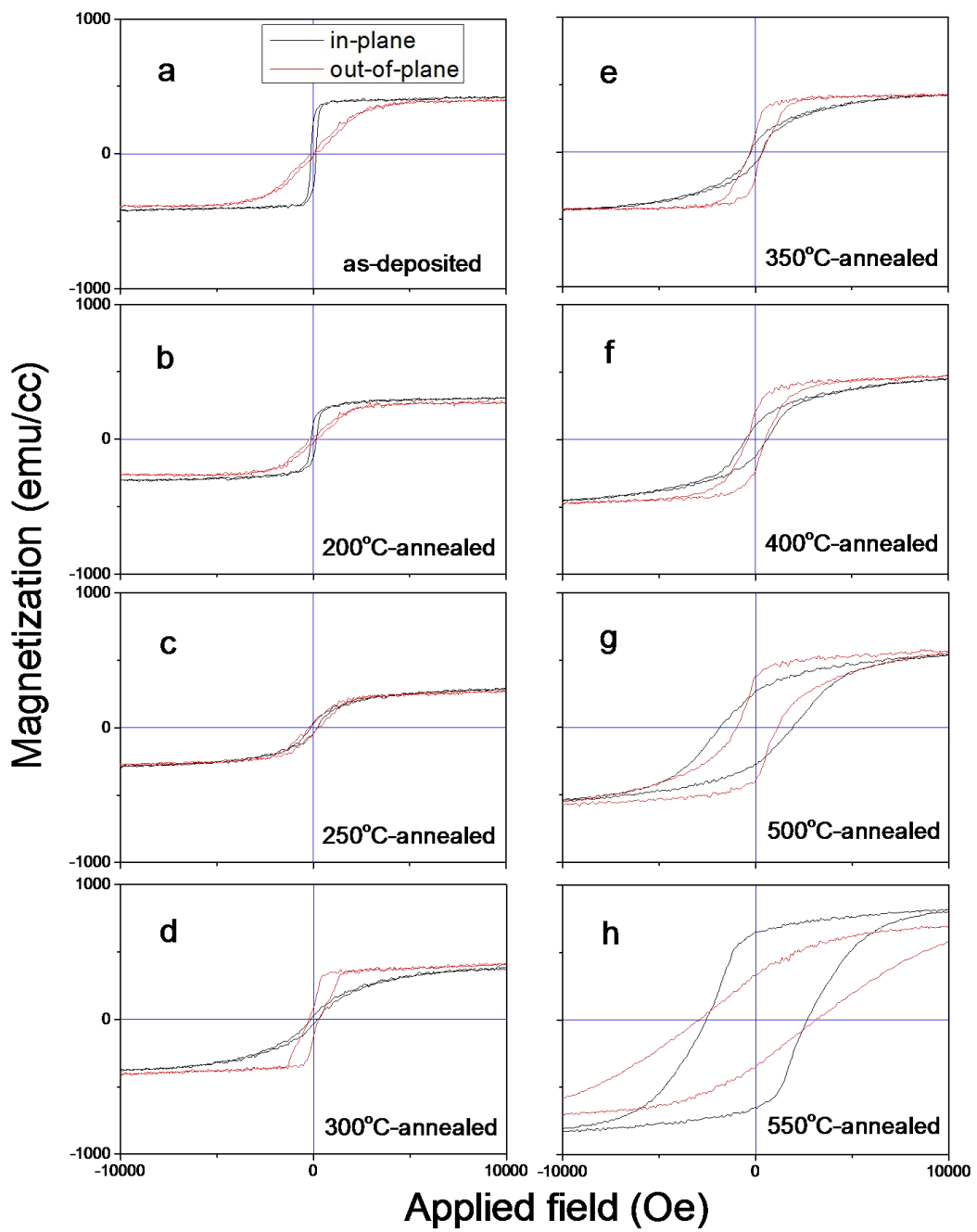


Fig 4-1 Hysteresis loops of a: as-deposited, b: 200°C-annealed, c: 250°C-annealed, d: 300°C-annealed, e: 350°C-annealed, f: 400°C-annealed, g: 500°C-annealed and h: 550°C-annealed [CoO5nm/CoPt7nm]₅ samples (measured at RT).

In detail, with increasing the annealing temperature up to 400°C, [CoO5nm/CoPt7nm]₅ film undergoes a gradual transition from LMA to PMA, and has a stable PMA performance at the temperature region between 300°C and 400°C. However, PMA shows evident degradation tendency when the annealing temperature is above 400°C. As is shown in Fig 4-1(g, h), the squareness of out-of-plane hysteresis loop decreases greatly with increased saturation field, while the squareness of in-plane hysteresis loop improves gradually with enhanced coercivity. It is considered that the degradation of PMA is due to the gradual decomposition of CoO layer at high temperatures. Especially, for the 550°C-annealed sample, its CoO layers are decomposed significantly and it returns to LMA with enhanced saturation magnetization (as is shown in Fig 4-2) and improved coercivity, due to the interaction between CoPt and new generated ferromagnetic Co phase. Compared with the as-deposited sample, the in-plane saturation magnetization of 550°C-annealed sample increases obviously. This is also due to the decomposition of CoO layers and thus the increased total amount of ferromagnetic Co after 550°C-annealing.

Moreover, to compare the magnetic properties of different [CoO5nm/CoPt7nm]₅ samples objectively, the effective PMA energy K_{eff} was calculated based on the M-H hysteresis loops shown in Fig 4-1. As is shown in Fig 4-2, with the increasing of annealing temperature up to 400°C, K_{eff} increases gradually from -0.74MJ/m^3 up to 0.62MJ/m^3 and has a maximum value of

0.86MJ/m³ at 300°C with respect to the strongest PMA. However, K_{eff} decreases evidently when the annealing temperature exceeds 400°C, especially for the 550°C-annealed sample its K_{eff} drops to -0.82MJ/m³.

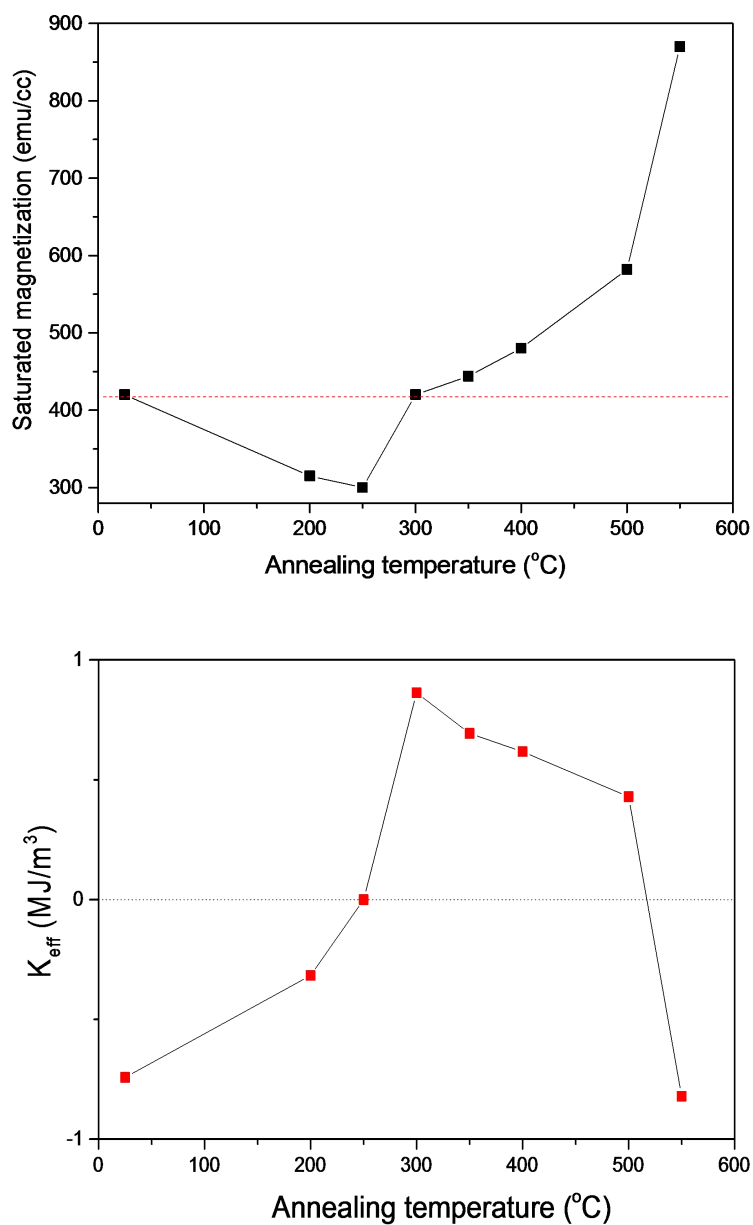


Fig 4-2 Saturation magnetization and effective PMA energy K_{eff} of all [CoO5nm/CoPt7nm]₅ samples.

4.3.2 AFM images of [CoO5nm/CoPt7nm]₅ multilayer films

It is well known that in magnetic multilayer films the effective PMA energy K_{eff} can be written as the sum of interface anisotropy (K_s) and volume anisotropy (K_v) by:

$$K_{eff} = 2K_s / t + K_v$$

where t is the thickness of magnetic layer, $2K_s$ indicates both top and bottom interface anisotropy of magnetic layer [6].

So, in order to find the mechanism responsible for the transition of magnetic anisotropy shown in Fig 4-1, interface anisotropy and volume anisotropy of [CoO5nm/CoPt7nm]₅ were further considered by analyzing CoO/CoPt interface roughness, CoPt layer crystallinity and CoPt layer in-plane stress.

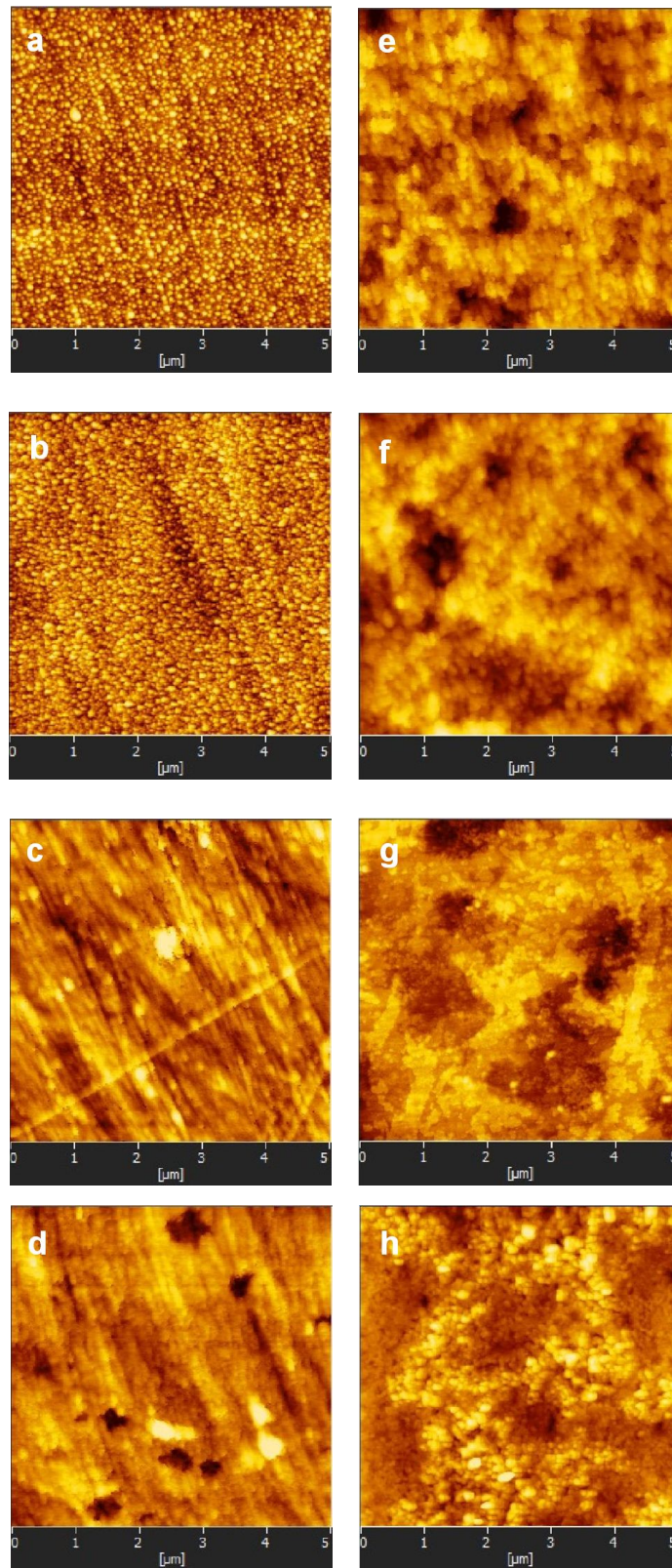


Fig 4-3 Two-dimensional AFM images of a: as-deposited and b: 200°C, c: 250°C, d: 300°C, e: 350°C, f: 400°C, g: 500°C, h: 550°C-annealed $[\text{CoO}5\text{nm}/\text{CoPt}7\text{nm}]_5$ samples.

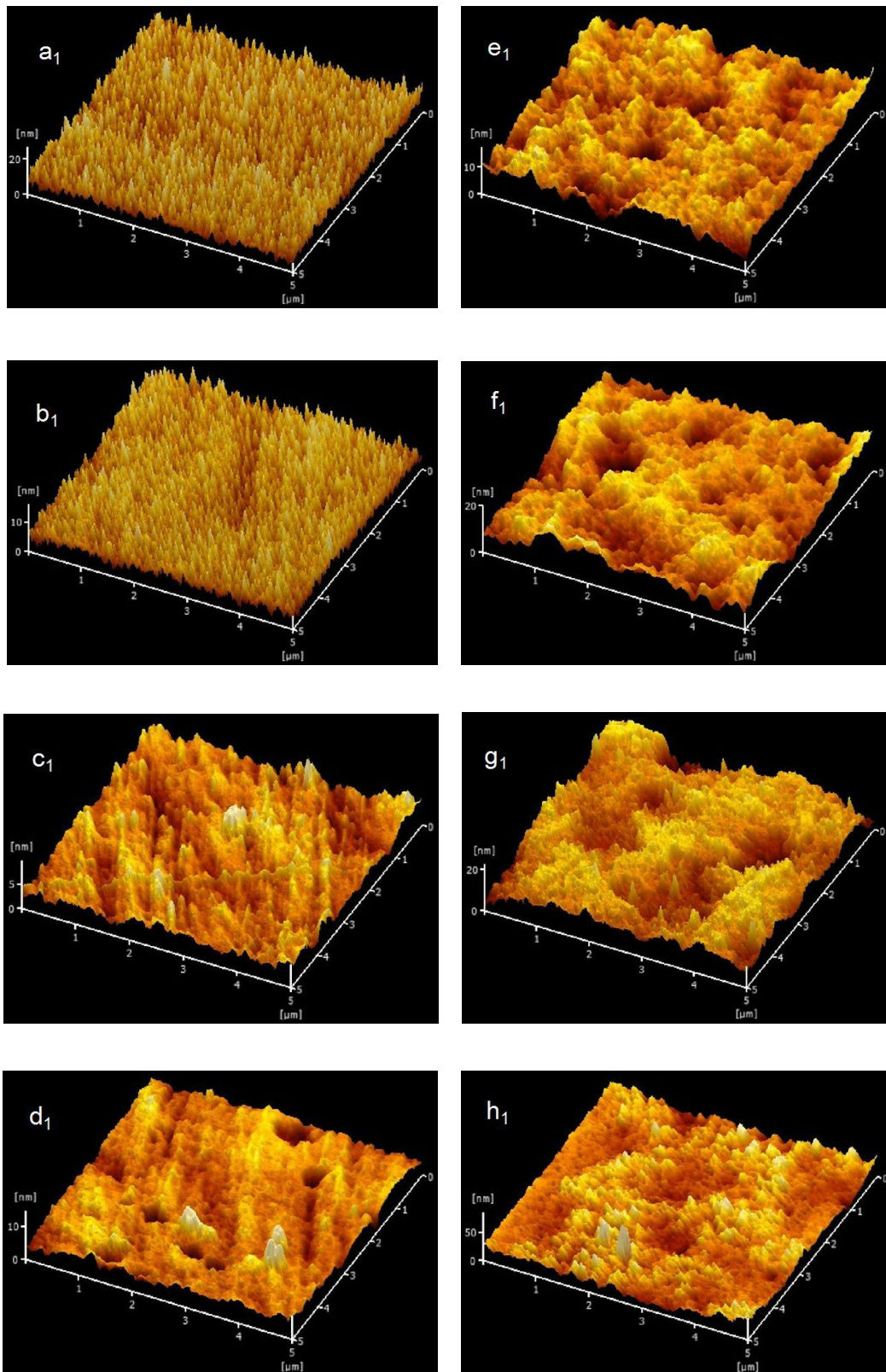
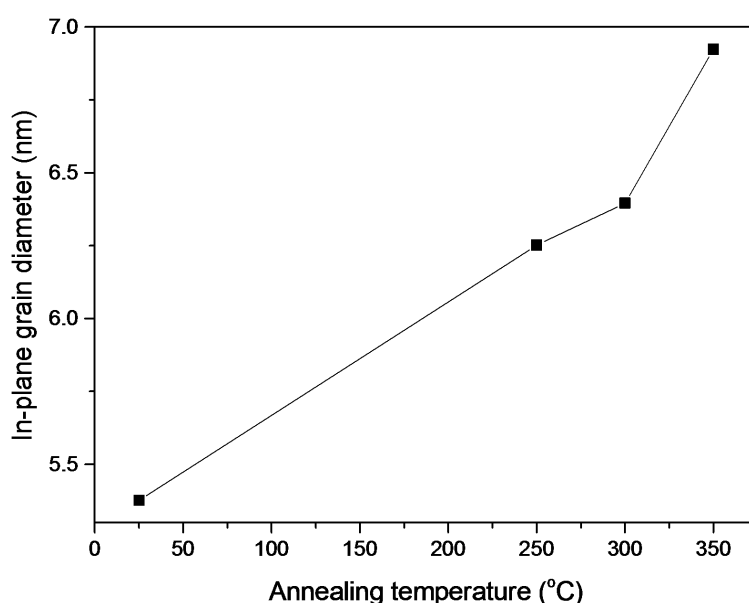


Fig 4-4 Three-dimensional AFM images of as-deposited and 200°C, 250°C, 300°C, 350°C, 400°C, 500°C, 550°C-annealed $[\text{CoO}5\text{nm}/\text{CoPt}7\text{nm}]_5$ samples.

To quantify the post-annealing induced change of interface, [CoO5nm/CoPt7nm]₅ top-surface was measured by AFM as an intuitive reference of CoO/CoPt interfaces. In our opinion, the variation tendency of interfaces should keep consistent with the variation tendency of top-surface.

Fig 4-3 and Fig 4-4 are the related two-dimensional and three-dimensional AFM images of all [CoO5nm/CoPt7nm]₅ samples. It can be seen that the top-surface topography depends greatly on the post-annealing. When the temperature is below 300°C the top-surface roughness can be reduced by annealing due to the coalescence of grains and the removal of defects. On the contrary, when the temperature is above 300°C, the top-surface becomes rougher and rougher, at the same time some black holes also occur. To our knowledge, the rougher interfaces with black holes at high temperatures result from the gradual decomposition of underneath CoO layer.



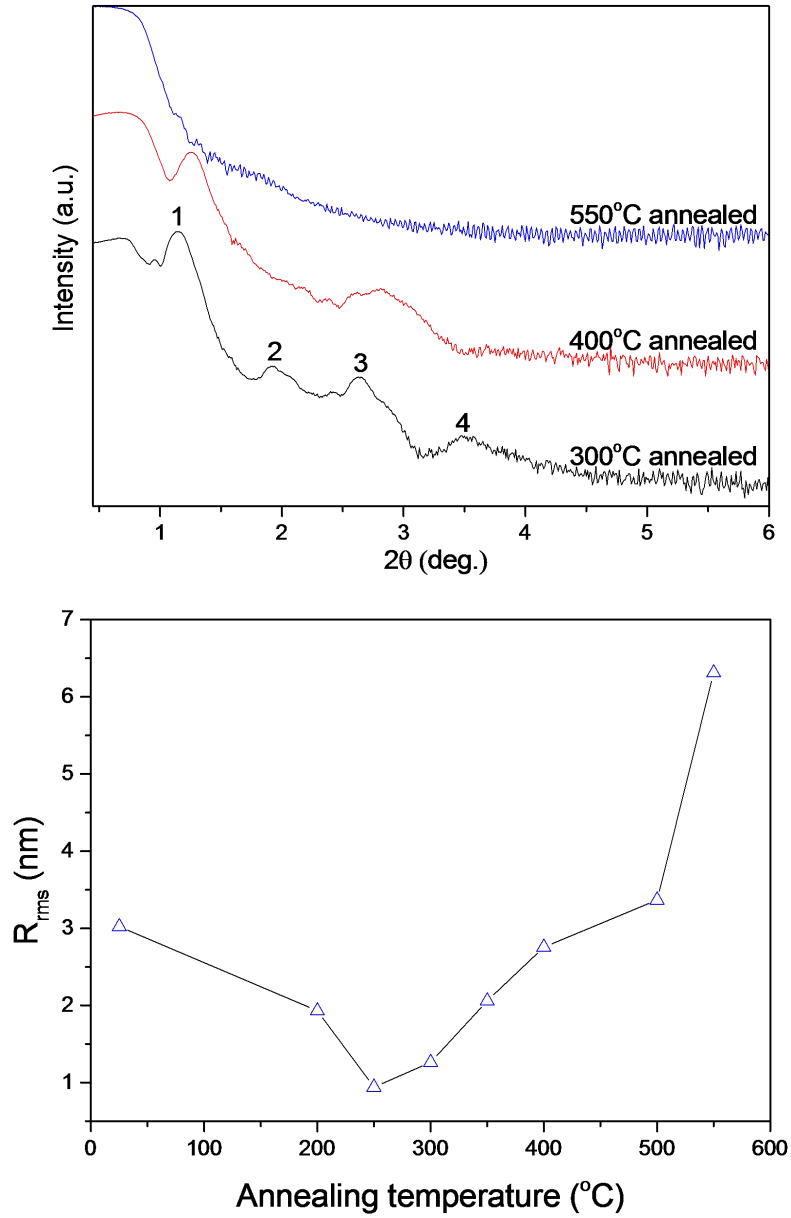


Fig 4-5 CoPt in-plane grain diameter, XRR and top surface roughness R_{rms} of [CoO5nm/CoPt7nm]_s samples.

To confirm the effects of post-annealing on interface quality, CoPt in-plane grain diameter was calculated by Scherrer formula and small angle x-ray reflection (XRR) was further performed. Fig.4-5 shows the calculated CoPt in-plane grain diameters at lower post-annealing temperatures and the measured

XRR profiles at higher post-annealing temperatures.

First, the increasing of CoPt grain diameter at post-annealing temperatures lower than 300°C leads to the smoother interface. As to the XRR profiles, 4 peaks can be observed clearly for the 300°C-annealed sample, indicating the sharp CoO/CoPt interface and good periodicity of layered structure. In contrast, for the 550°C-annealed sample no peak can be observed, and this suggests the destruction of the layered structure caused by CoO layer decomposition.

The root-mean-square roughness (R_{rms}) of [CoO5nm/CoPt7nm]₅ top-surface derived from AFM is also shown in Fig 4-5. Compared with Fig 4-1, we can find the AFM results are in good agreement with the well accepted theory that smooth interfaces (low roughness) are favorable to the enhancement of perpendicular interface anisotropy K_s in multilayer films [7].

4.3.3 XRD of [CoO5nm/CoPt7nm]₅ multilayer films

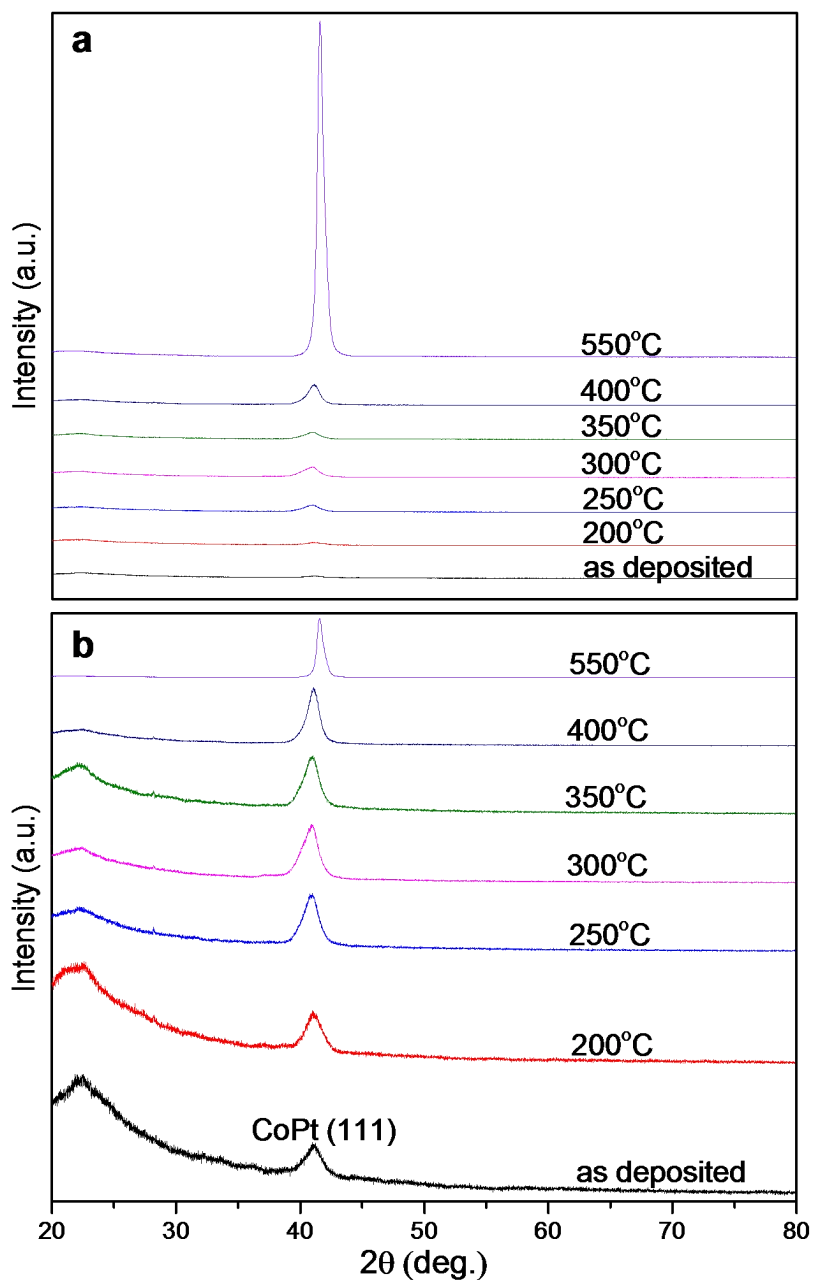


Fig 4-6 a: Out-of-plane XRD b: Intensity normalization of CoPt (111) peak.

Fig 4-6(a) is the out-of-plane XRD profile of [CoO5nm/CoPt7nm]₅. To compare the peak position and confirm the peak center, the corresponding intensity normalization of CoPt (111) peak is listed in Fig 4-6(b). Firstly,

normalized XRD shown in Fig 4-6(b) reveals that all the samples are well crystallized with preferred FCC CoPt (111) orientation. This can be attributed to the addition of Pt, since alloy thin film with Pt component is energetically favorable to form strong (111) texture along the growth direction [8]. Moreover, when the annealing temperature is above 200°C, CoPt (111) peak shows a shift tendency toward higher angle, although it is not that evident. Secondly, in Fig 4-6(a) we can find CoPt (111) peak becomes stronger and stronger with the increase of annealing temperature, indicating the improvement of CoPt crystallinity. Since <111> directions are the easy magnetization axes of FCC CoPt, we believe the stronger <111> orientation is favorable for PMA to some extent. Thirdly, after annealing at 550°C, the CoPt (111) peak becomes sharper and its intensity also increases considerably. This indicates an increased structural coherence length in the perpendicular direction. According to the previous analysis, CoO layer decomposed significantly after annealing at 550°C, and in fact CoPt grains also grew in the perpendicular direction by incorporating new generated Co.

4.3.4 CoPt layer in-plane stress

It is well known the magnetoelastic volume anisotropy of thin films can be correlated with the in-plane stress by magnetoelastic effect: $K_{me} = -\frac{3}{2}\lambda\sigma_{//}$ where K_{me} is the magnetoelastic energy, λ is the magnetostriction constant, $\sigma_{//}$ is the

in-plane stress [9].

In our experiment, CoPt layer has epitaxial relation with CoO layer during the deposition process, so it is inevitable that the lattice mismatch between FCC CoPt ($a_{\text{CoPt}} = 0.38\text{nm}$) and FCC CoO ($a_{\text{CoO}} = 0.43\text{nm}$) will lead to CoPt layer in-plane tensile stress after deposition in $[\text{CoO}5\text{nm}/\text{CoPt}7\text{nm}]_5$ multilayer films [8]. Upon annealing, the as-deposited CoPt layer in-plane tensile stress will be changed considering the different thermal expansion coefficients between CoPt and CoO, the improvement of CoPt crystallinity, the gradual decomposition of CoO, the variation of CoO/CoPt interface as well as the isotropic shrinkage due to the removal of the interior defects [10].

In this work, CoPt layer in-plane tensile stress was calculated by $\sin^2\varphi$ method through analyzing CoPt out-of-plane (111) and in-plane (11-1) lattice distances. So, apart from out-of-plane (111) peak, CoPt (11-1) peak was also measured by tilting $[\text{CoO}5\text{nm}/\text{CoPt}7\text{nm}]_5$ films at 70.5° (Here we denote it as in-plane XRD to make a comparison with out-of-plane XRD, although CoPt (11-1) lattice plane has a dihedral angle = 70.5° to its (111) lattice plane).

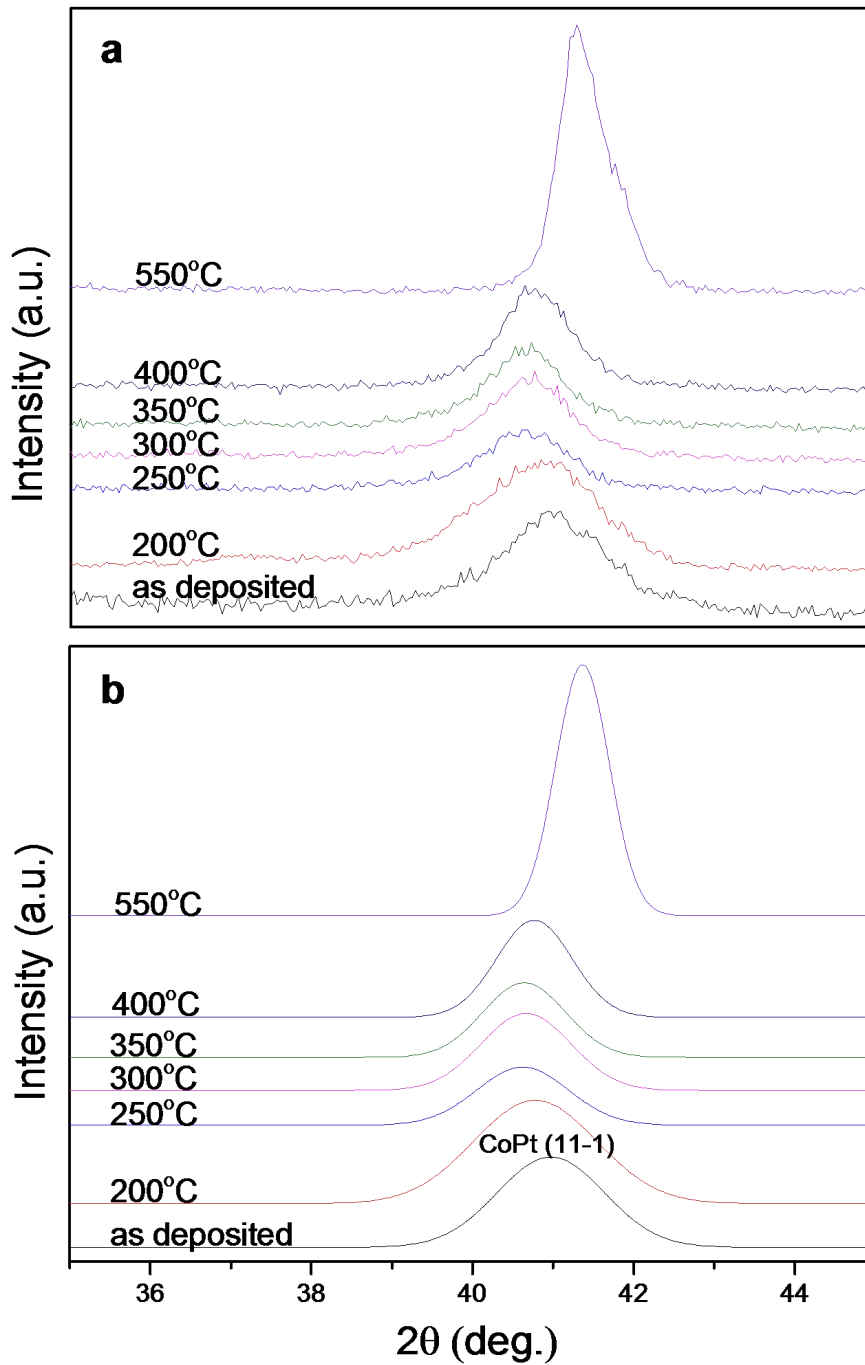


Fig 4-7 a: In-plane XRD b: Gauss fitting of CoPt (11-1) peak.

We can see in Fig 4-7 that upon annealing CoPt (11-1) peak shifts toward lower angle firstly then shifts backward. According to Bragg law, this indicates CoPt (11-1) inter-planar lattice distance increases firstly then decreases. Since there exists a CoPt layer in-plane tensile stress in the as-deposited

[CoO5nm/CoPt7nm]_s which generates from lattice mismatch, it is easy to understand the increase of in-plane CoPt (11-1) inter-planar lattice distance upon annealing will lead to enhanced CoPt layer in-plane tensile stress further.

The $\sin^2\varphi$ method used to calculate CoPt in-plane tensile stress can be expressed as follow: under an assumption of equal-biaxial stress state, we denote the strain at an angle φ to the surface normal as $\varepsilon_{\varphi}^{[111]}$ for the (111) textured FCC CoPt ultra-thin layer, then the strain can be written as:

$$\varepsilon_{\varphi}^{[111]} = \frac{(a_{\varphi} - a_0)}{a_0} = \sigma_{//} \left[\frac{(2S_{11} + 4S_{12} - S_{44})}{3} + \frac{(\sin^2 \varphi \cdot S_{44})}{2} \right]$$

where a_{φ} is the lattice distance along the direction of φ , a_0 is the unstrained lattice distance, $\sigma_{//}$ is the value of stress in the film plane, and S_{ij} is a component of the compliance array with $S_{11} = 6.51 \times 10^{-3} \text{ GPa}^{-1}$, $S_{12} = -2.48 \times 10^{-3} \text{ GPa}^{-1}$ and $S_{44} = 8.06 \times 10^{-3} \text{ GPa}^{-1}$ [10-13]. Then, we can derive the unknown $\sigma_{//}$ by out-of-plane lattice distance $a_{\perp}(\varphi = 0)$ and in-plane lattice distance $a_{//}(\varphi = 70.5^\circ)$.

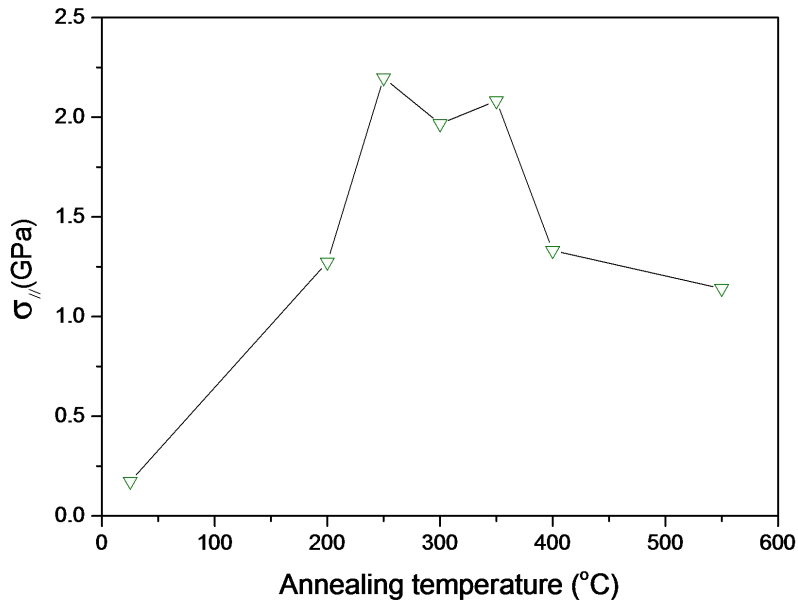


Fig 4-8 CoPt in-plane tensile stress $\sigma_{//}$ of $[\text{CoO}5\text{nm}/\text{CoPt}7\text{nm}]_5$ samples.

It is clear in Fig 4-8 that with the increasing of annealing temperature the calculated CoPt layer in-plane tensile stress $\sigma_{//}$ increases firstly, then it is partially released at high temperature. To our knowledge, the release of tensile stress results from the reduced lattice mismatch between CoPt and the decomposed CoO.

4.3.5 Correlation between K_{eff} and R_{rms} , $\sigma_{//}$

In the past sections, effective perpendicular magnetic anisotropy energy K_{eff} of $[\text{CoO}5\text{nm}/\text{CoPt}7\text{nm}]_5$ films was calculated based on the M-H hysteresis loops, root-mean-square roughness (R_{rms}) of $[\text{CoO}5\text{nm}/\text{CoPt}7\text{nm}]_5$ was derived from AFM, CoPt layer in-plane tensile stress $\sigma_{//}$ was calculated by $\sin^2\varphi$ method.

So, now we can study the correlation between K_{eff} and R_{rms} , $\sigma_{//}$ synthetically,

and further investigate the mechanism responsible for the magnetic anisotropy transition shown in Fig 4-1.

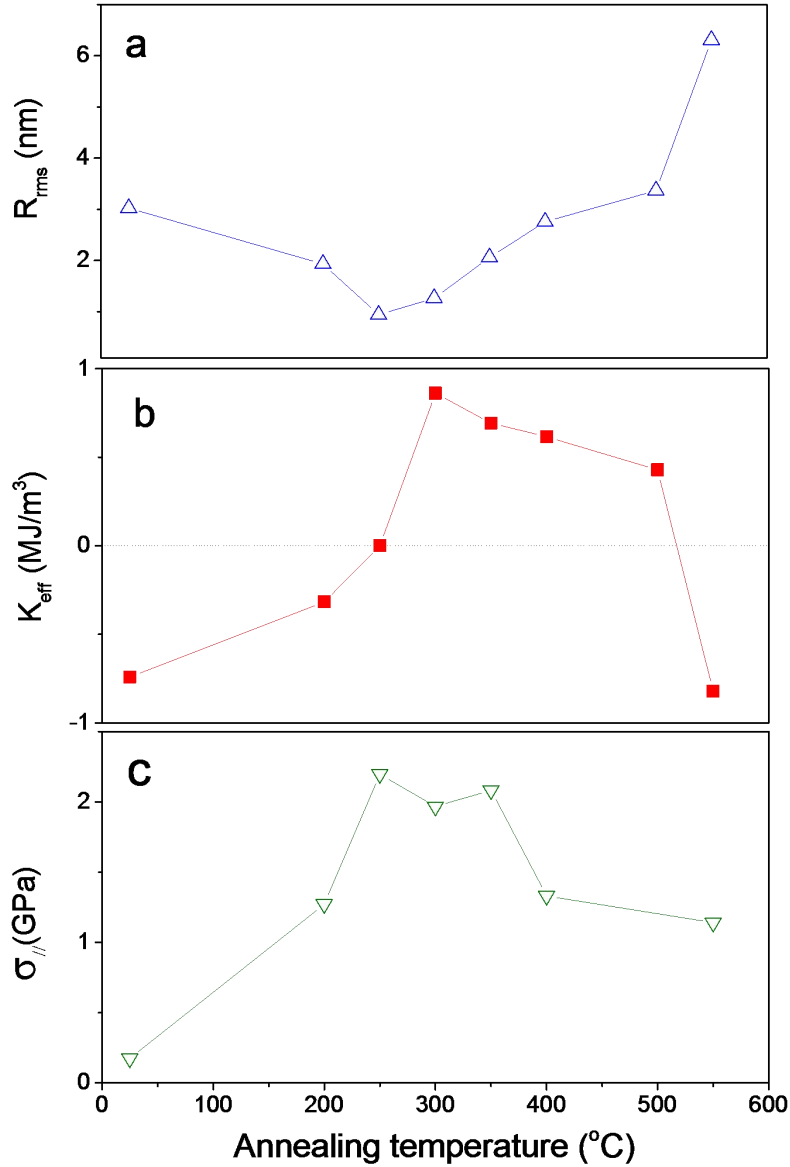


Fig 4-9 Top surface roughness R_{rms} , effective perpendicular magnetic anisotropy energy K_{eff} and CoPt in-plane tensile stress $\sigma_{||}$ of $[\text{CoO}5\text{nm}/\text{CoPt}7\text{nm}]_5$ samples.

Fig 4-9 lists K_{eff} , R_{rms} and $\sigma_{||}$. Comparing Fig 4-9(b) and Fig 4-9(c), we can find the variation tendency of K_{eff} is roughly proportional to the calculated stress $\sigma_{||}$.

According to the magnetoelastic effect $K_{me} = -\frac{3}{2}\lambda\sigma_{||}$ mentioned above, it is

easy to understand that the increase of in-plane tensile stress $\sigma_{//}$ will help promote positive perpendicular magnetoelastic volume anisotropy K_{me} , since CoPt alloy has a negative magnetostriction constant λ along $\langle 111 \rangle$ direction in present work [14]. Comparing Fig 4-9(b) and Fig 4-9(a), we can find the variation tendency of K_{eff} is inversely proportional to the roughness R_{rms} roughly. According to our previous analysis, this inversely proportional relationship between R_{rms} and K_{eff} is in good agreement with the theory that smooth interfaces are favorable to the enhancement of perpendicular interface anisotropy K_s in multilayer films [7].

However, in the foregoing experiments, since it is difficult to control the microstructural parameters selectively in the annealing process, such as CoPt layer crystallinity, CoO layer decomposition, CoO/CoPt interface roughness and CoPt layer internal stress, their precise roles on the magnetic anisotropy transition of $[\text{CoO}5\text{nm}/\text{CoPt}7\text{nm}]_5$ multilayer films still needs further verification.

Different from the previous annealing process, for a specified $[\text{CoO}5\text{nm}/\text{CoPt}7\text{nm}]_5$ sample, CoPt in-plane tensile stress will be changed in the cooling process due to the thermal expansion coefficient differences between CoPt and CoO, but CoPt crystallinity, CoO decomposition and CoO/CoPt interface roughness will be frozen and keep unchanged after cooling. So, to eliminate the influences of CoPt crystallinity, CoO decomposition and CoO/CoPt interface roughness on the magnetic anisotropy transition of

[CoO5nm/CoPt7nm]₅, the selected 200°C-annealed [CoO5nm/CoPt7nm]₅ sample was VSM-measured at RT, -100°C and -192°C successively.

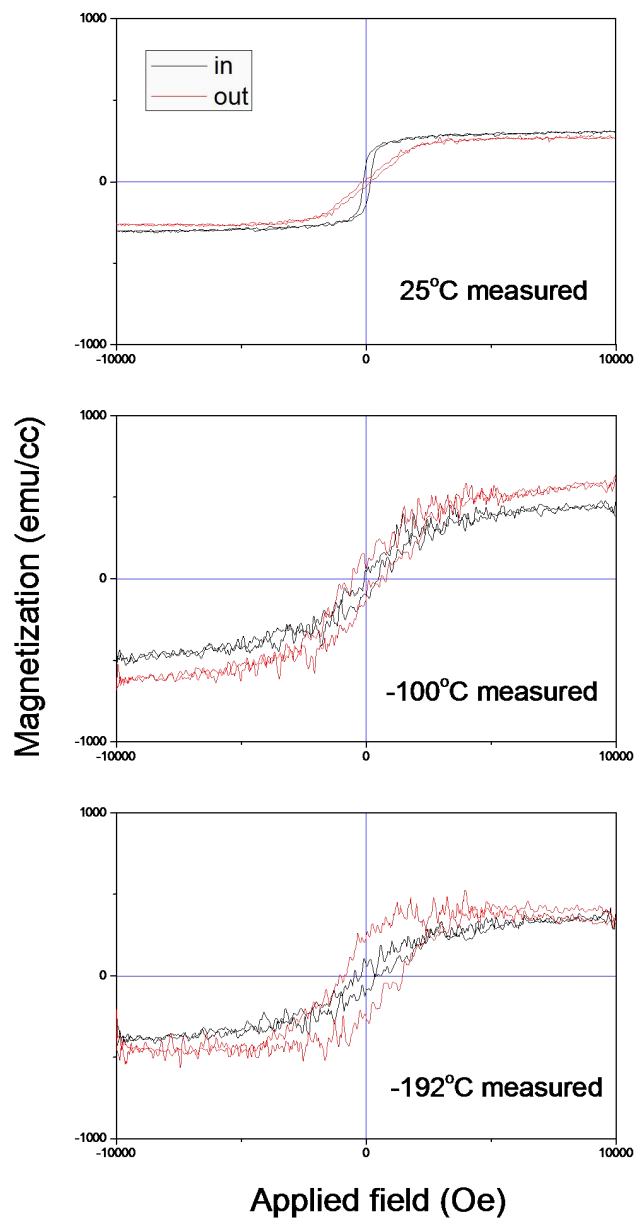


Fig 4-10 Hysteresis loops of 200°C-annealed [CoO5nm/CoPt7nm]₅ sample (measured at a: RT, b: -100°C and c: -192°C successively).

It is interesting in Fig 4-10 that with the decreasing of external temperature 200°C-annealed [CoO5nm/CoPt7nm]₅ undergoes a smooth transition from LMA

to PMA. Since CoPt crystallinity, CoO decomposition and CoO/CoPt interface roughness all are unchanged after cooling for the same sample, here we can affirm the magnetic anisotropy transition of 200°C-annealed [CoO5nm/CoPt7nm]₅ in the cooling process is mainly due to the enlarged CoPt in-plane tensile stress originating from the thermal expansion differences between CoPt and CoO. In other words, in the cooling process it is a magnetoelastically induced magnetic anisotropy transition in 200°C-annealed [CoO5nm/CoPt7nm]₅.

In fact, all the samples shown in Fig 4-1 were measured after cooling from annealing-temperature to RT. For example, in Fig 4-1(b) the as-deposited sample was firstly annealed for 3h to make sure its structure was stable at 200°C, then the sample was cooled down from 200°C to RT. After this cooling process, we measured its hysteresis loops at RT. In our opinion, CoPt layer tensile stress was introduced during this cooling process from 200°C to RT, due to the the thermal expansion mismatch between CoO and CoPt. On the other hand, the low temperature cooling process from RT to -192°C shown in Fig 4-10 can be considered as a successive cooling process. So, during the whole cooling process (200°C→ RT→ -192°C), the change tendency of CoPt layer stress is consistent.

Magnetoelastic effect

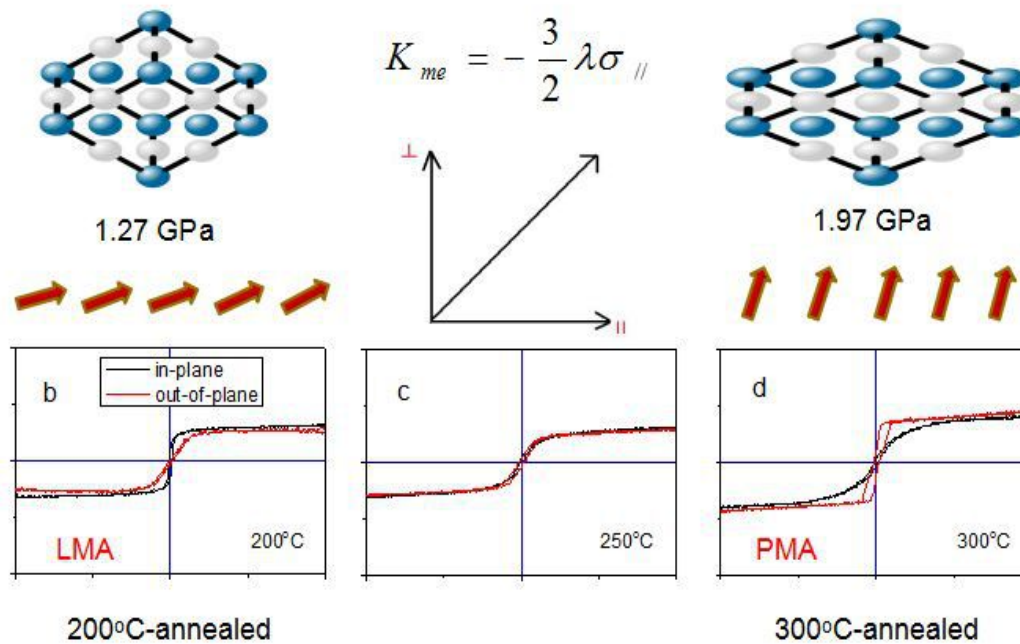


Fig 4-11 Magnetoelastically induced magnetic anisotropy transition in $[\text{CoO}5\text{nm}/\text{CoPt}7\text{nm}]_5$.

Most importantly, it is reasonable to conclude that the change of CoPt in-plane stress is the main reason that leads to the magnetic anisotropy transition in $[\text{CoO}5\text{nm}/\text{CoPt}7\text{nm}]_5$, no matter whether it is after annealing or cooling. As is shown in Fig 4-11, for the 200°C-annealed sample, its Co magnetic moments tend to be parallel to the film due to the weaker CoPt layer in-plane tensile stress, it is LMA. In contrast, for the 300°C-annealed sample, its Co magnetic moments tend to be perpendicular to the film due to the stronger CoPt layer in-plane tensile stress, it is PMA.

In summary, we believe the phenomenon in Fig 4-1 is magnetoelastically induced magnetic anisotropy transition.

4.4 Conclusion

1. The magnetic anisotropy transition of $[\text{CoO}5\text{nm}/\text{CoPt}7\text{nm}]_5$ multilayer film with respect to post-annealing has been studied systematically.
2. The strongest PMA of $[\text{CoO}5\text{nm}/\text{CoPt}7\text{nm}]_5$ is achieved after post-annealing at 300°C and the tolerable annealing temperature with strong PMA is up to 400°C .
3. We demonstrate theoretically and experimentally that the magnetic anisotropy transition in $[\text{CoO}5\text{nm}/\text{CoPt}7\text{nm}]_5$ is mainly attributed to the change of CoPt layer in-plane tensile stress.

References

- [1] P. F. Carcia, A. D. Meinhaldt and A. Suna, *Appl. Phys. Lett.* **47**, (1985) 178.
- [2] C. Chappert and P. Bruno, *J. Appl. Phys.* **64**, (1988) 5736.
- [3] P. F. Carcia, *J. Appl. Phys.* **63**, (1988) 5066.
- [4] M. Sakurai, T. Takahata and I. Moritani, *J. Magn. Soc. Japan* **15**, (1991) 411.
- [5] Y. Hodumi, J. Shi and Y. Nakamura, *Appl. Phys. Lett.* **90**, (2007) 212506.
- [6] Y. X. Yu, J. Shi and Y. Nakamura, *Acta Materialia*. **60**, (2012) 6770.
- [7] C. Zhang, T. Sannomiya, S. Muraishi, J. Shi and Y. Nakamura, *Appl. Phys. A*. **116**, (2014) 1695.
- [8] J. Wang, T. Omi, T. Sannomiya, S. Muraishi, J. Shi and Y. Nakamura, *Appl. Phys. Lett.* **103**, (2013) 042401.
- [9] S. Honda, J. Ago, M. Nawate and N. Morita, *IEEE Trans. Magn.* **28**, (1992) 2677.
- [10] Y. X. Yu, J. Shi and Y. Nakamura, *J. Appl. Phys.* **108**, (2010) 023912.
- [11] M. A. Korhonen and C. A. Paszkiet, *Scr. Met.* **23**, (1989) 1449.
- [12] J. Rouchy and A. Waintal, *Solid State Commun*, **17**, (1975) 1227.
- [13] J. Rouchy, E. T. Lacheisserie, J. C. Genna and A. Waintal, *J. Magn. Magn. Mater.* **21**, (1980) 69.
- [14] H. Takahashi, S. Tsunashima and S. Uchiyama, *J. Magn. Magn. Mater.* **126**, (1993) 282.

Chapter 5 Perpendicular exchange bias of [CoO_x/CoPt_y]_n multilayer films

5.1 Introduction

When a multilayer film with ferromagnetic(FM)/antiferromagnetic(AFM) interfaces is cooled through the Neel temperature (T_N) of AFM in a external magnetic field the shift of FM hysteresis loop (H_{EB}) can be induced, which is so-called exchange bias effect (EB)[1]. Since its discovery in 1956, exchange bias (EB) phenomenon has been widely studied, due to its important roles in the development of fundamental physics, its complicated mechanism and technological application in spintronics field[2].

In fact, in most cases EB was established in the film plane of FM/AFM multilayer, which is so-called longitudinal exchange bias (LEB). In the past few years, with the development of PMA, out-of-plane perpendicular exchange bias (PEB) was also introduced as an active topic since its discovery in 2000[3].

Nowadays, multilayer films with PEB are considered to be a potential effect used in the perpendicular spin valve and perpendicular magnetic tunneling junction e.g. With such industrial background as well as scientific interest, PEB has been widely studied in FM/AFM multilayer systems^[4]. So far, several groups

have shown that some systems with PMA can exhibit PEB after field cooling, such as CoPt/(CoO, FeMn, FeF₂) multilayer films^[3, 5, 6].

However, many aspects of PEB are still controversial or unresolved so far, despite the active research in this field. So, considering its important value both in theory and application, we think it is significant to explore the nature of PEB further.

In this chapter, PEB of [CoO_x/CoPt_y]_n multilayer films has been studied systematically. In order to get the best PEB, the influences of annealing-temperature, CoPt thickness, CoO thickness, repetition period and seed layer on [CoO_x/CoPt_y]_n PEB were studied step by step. According to our experiments, 300°C-annealed [CoO5nm/CoPt5nm]₅ film shows the best PEB performance, having a PEB value of 1060 Oe.

Keywords:

PEB of [CoO_x/CoPt_y]_n multilayer film,

enhancement of PEB after post-annealing treatment,

300°C-annealed [CoO5nm/CoPt5nm]₅ multilayer film.

5.2 Experimental details

5.2.1 Preparation of [CoO_x/CoPt_y]_n multilayer films

In order to find the best PEB performance, a series of [CoO_x/CoPt_y]_n multilayer films with different CoPt thickness, different CoO thickness, different period and different seed layer were prepared. [CoO_x/CoPt_y]_n multilayer films were deposited on glass substrate at room temperature (RT) by magnetron sputtering. Ferromagnetic Co_{0.43}Pt_{0.57} alloy layers were deposited by DC sputtering with 0.8Pa Ar, antiferromagnetic CoO layers were deposited by RF sputtering with gas mixture of 0.8Pa Ar and 0.2Pa O₂, the base pressure before deposition was around 5×10^{-5} Pa. After deposition, [CoO_x/CoPt_y]_n multilayer films were vacuum annealed at different temperatures for 3h, respectively.

The related preparation details of [CoO_x/CoPt_y]_n multilayer films are shown clearly in Table 5-1~Table 5-5.

5.2.2 Characterizations of [CoO_x/CoPt_y]_n multilayer films

It is well known that EB phenomenon is an interfacial phenomenon associated with exchange coupling created at the FM/AFM interface, when the system is field-cooled through AFM Néel temperature (T_N). So, in our experiments PEB was measured at low temperature around 80K, after perpendicular field cooling by liquid N₂ (from RT to 80K in a 5kOe exterior magnetic field) through CoO Néel temperature ($T_N \sim 290K$).

Table 5-1. [CoO_x/CoPt_y]_n with different post-annealing temperature

	25°C-deposited	100°C-annealed	200°C-annealed	250°C-annealed	300°C-annealed	375°C-annealed	400°C-annealed
[CoO _{5nm} /CoPt _{5nm}] ₅	●	●		●	●	●	
[CoO _{5nm} /CoPt _{5nm}] ₁₀	●	●	●		●		●

Table 5-2. [CoO_x/CoPt_y]_n with different CoPt thickness

					300°C-annealed		
[CoO _{5nm} /CoPt _{2.5nm}] ₅					●		
[CoO _{5nm} /CoPt _{5nm}] ₅					●		
[CoO _{5nm} /CoPt _{7nm}] ₅					●		

Table 5-3. [CoO_x/CoPt_y]_n with different CoO thickness

					300°C-annealed		
[CoO _{5nm} /CoPt _{5nm}] ₅					●		
[CoO _{10nm} /CoPt _{5nm}] ₃					●		

Table 5-4. [CoO_x/CoPt_y]_n with different period

					300°C-annealed		
[CoO _{5nm} /CoPt _{5nm}] ₃					●		
[CoO _{5nm} /CoPt _{5nm}] ₅					●		
[CoO _{5nm} /CoPt _{5nm}] ₈					●		
[CoO _{5nm} /CoPt _{5nm}] ₁₀					●		

Table 5-5. [CoPt_y/CoO_x]_n with CoO_{20nm} seed layer

					300°C-annealed	350°C-annealed	
CoO _{20nm} /[CoPt _{5nm} /CoO _{5nm}] ₅					●	●	
CoO _{20nm} /[CoPt _{6nm} /CoO _{5nm}] ₅					●	●	

5.3 Results and Discussion

5.3.1 $[\text{CoO}_x/\text{CoPt}_y]_n$ with different post-annealing temperature

	25°C-deposited	100°C-annealed	200°C-annealed	250°C-annealed	300°C-annealed	375°C-annealed	400°C-annealed
$[\text{CoO}_{5\text{nm}}/\text{CoPt}_{5\text{nm}}]_5$	●	●		●	●	●	
$[\text{CoO}_{5\text{nm}}/\text{CoPt}_{5\text{nm}}]_{10}$	●	●	●		●		●

PEB of $[\text{CoO}_{5\text{nm}}/\text{CoPt}_{5\text{nm}}]_5$ and $[\text{CoO}_{5\text{nm}}/\text{CoPt}_{5\text{nm}}]_{10}$ multilayer films with different post-annealing temperature were studied in section 5.3.1. After perpendicular field cooling by liquid N_2 (from RT to 80K in a 5kOe exterior magnetic field), the out-of-plane M-H hysteresis loops of $[\text{CoO}_{5\text{nm}}/\text{CoPt}_{5\text{nm}}]_5$ and $[\text{CoO}_{5\text{nm}}/\text{CoPt}_{5\text{nm}}]_{10}$ multilayer films were measured at low temperature around 80K by VSM. The related PEB experimental results of $[\text{CoO}_{5\text{nm}}/\text{CoPt}_{5\text{nm}}]_5$ and $[\text{CoO}_{5\text{nm}}/\text{CoPt}_{5\text{nm}}]_{10}$ multilayer films are listed in Fig 5-1 and Fig 5-2, individually.

Firstly, the shift of the out-of-plane hysteresis loop from the origin point demonstrates the PEB effect clearly. Secondly, much stronger PEB can be obtained in the annealed samples. Especially, the strongest PEB is achieved in the 300°C-annealed sample. Thirdly, PEB degrades greatly for the sample annealed above 300°C. In our opinion, the degradation of PEB is due to the decomposition of CoO layer at high temperature and thus the weakened spin coupling between CoPt and CoO.

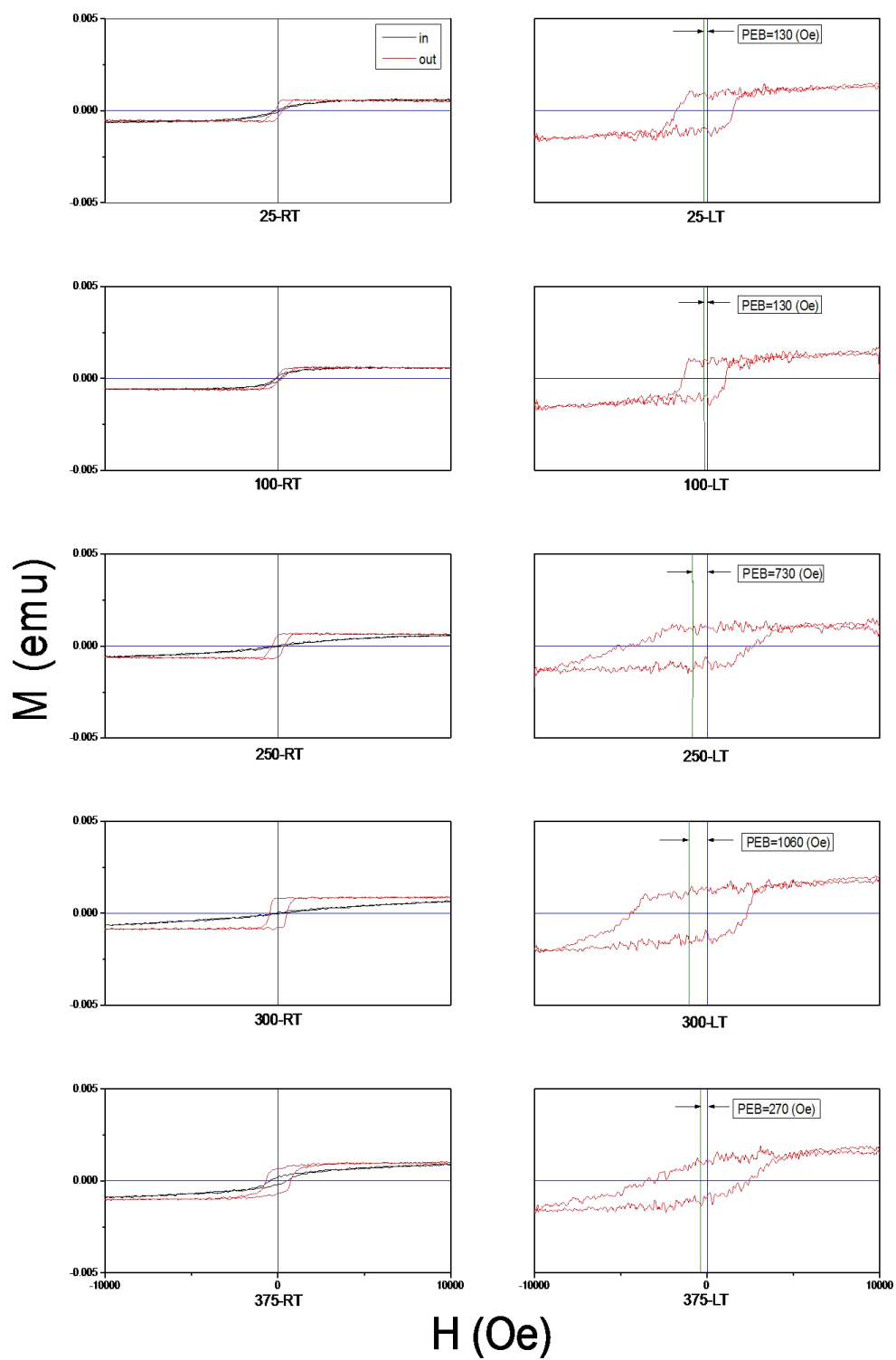


Fig 5-1 PMA (left: measured at RT) and corresponding PEB (right: measured at LT 80K) of as-deposited, 100°C-annealed, 250°C-annealed, 300°C-annealed and 375°C-annealed [CoO5nm/CoPt5nm]₅ samples.

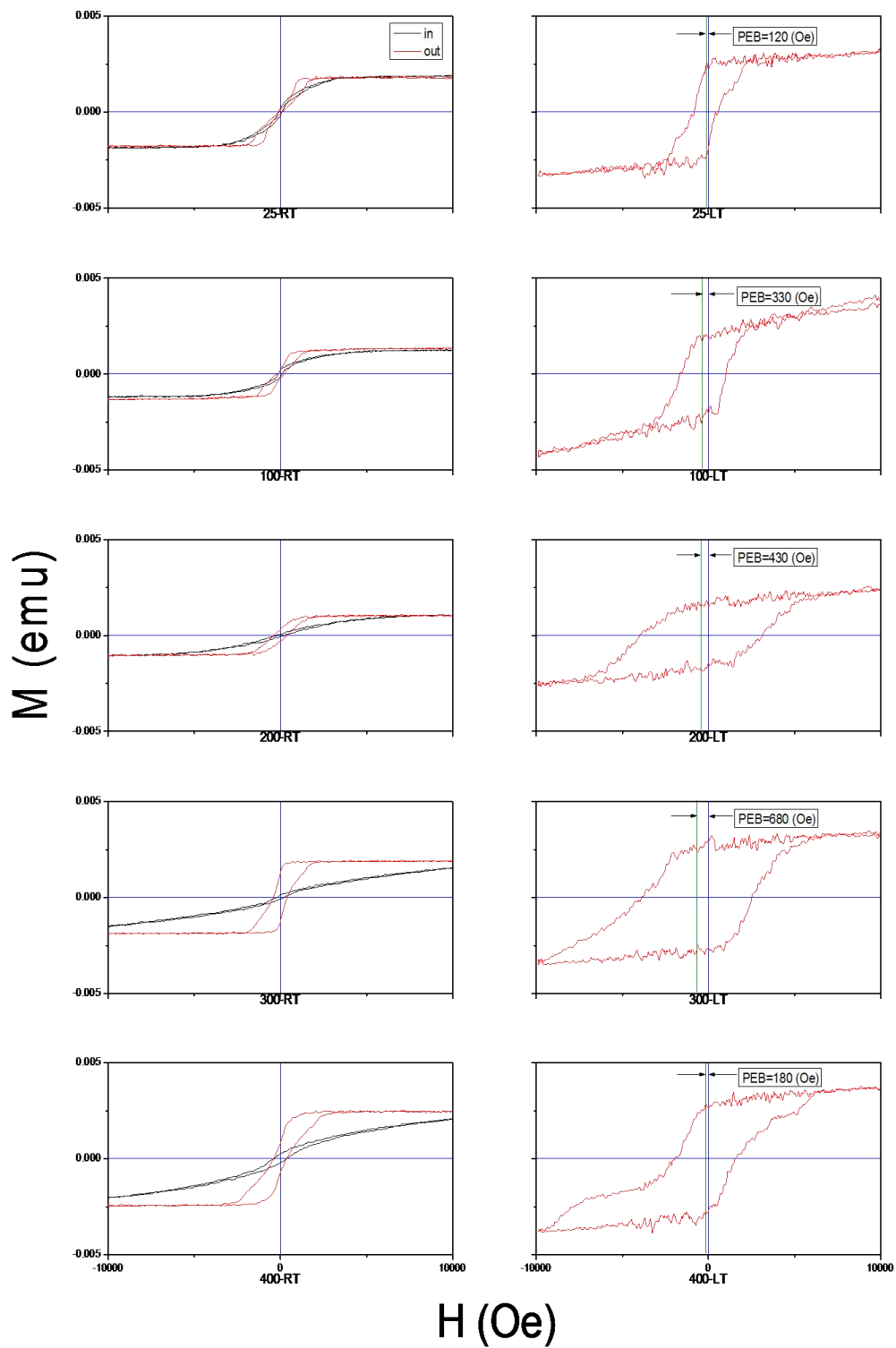


Fig 5-2 PMA (left: measured at RT) and corresponding PEB (right: measured at LT 80K) of as-deposited, 100°C-annealed, 200°C-annealed, 300°C-annealed and 400°C-annealed $[\text{CoO}5\text{nm}/\text{CoPt}5\text{nm}]_{10}$ samples.

5.3.2 [CoO_x/CoPt_y]_n with different CoPt thickness

					300°C-annealed		
[CoO _{5nm} /CoPt _{2.5nm}] ₅					●		
[CoO _{5nm} /CoPt _{5nm}] ₅					●		
[CoO _{5nm} /CoPt _{7nm}] ₅					●		

PEB of 300°C-annealed [CoO_{5nm}/CoPt_y]₅ with different CoPt thickness y=2.5nm, 5nm, 7nm were studied in section 5.3.2. After perpendicular field cooling by liquid N₂ (from RT to 80K in a 5kOe exterior magnetic field), the out-of-plane M-H hysteresis loops of 300°C-annealed [CoO_{5nm}/CoPt_y]₅ were measured at low temperature around 80K by VSM. The related PEB experimental results are listed in Fig 5-3.

Firstly, for 300°C-annealed [CoO_{5nm}/CoPt_y]₅ samples, the thicker the CoPt thickness is the weaker the PEB will become. Secondly, although the PEB value of 300°C-annealed [CoO_{5nm}/CoPt_{2.5nm}]₅ is the maximum, its rising-edge and falling-edge are the roughest. Thirdly, overall consideration we think y=5nm is the optimal CoPt thickness, since 300°C-annealed [CoO_{5nm}/CoPt_{5nm}]₅ has much smoother edges and PEB value of 1060 Oe. In other words, 300°C-annealed [CoO_{5nm}/CoPt_{5nm}]₅ shows the best PEB performance among all [CoO_{5nm}/CoPt_y]₅ in this section.

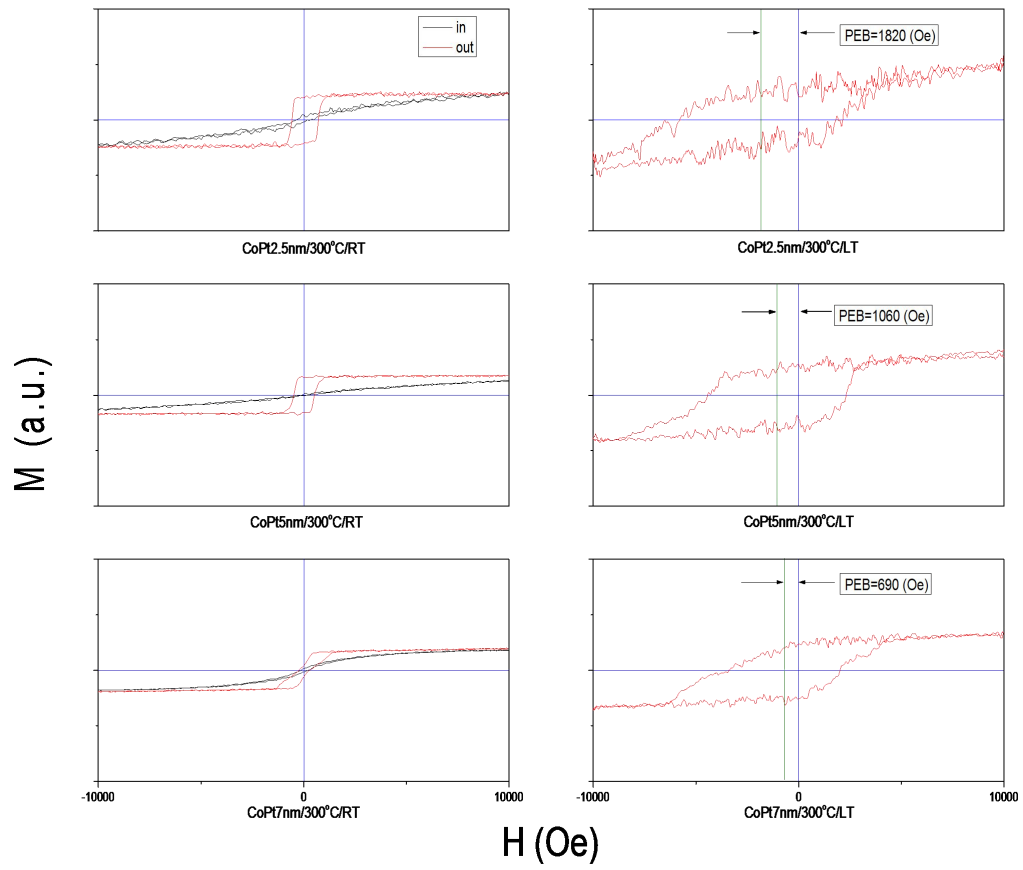


Fig 5-3 PMA (left: measured at RT) and corresponding PEB (right: measured at LT 80K) of 300°C -annealed $[\text{CoO}_{5\text{nm}}/\text{CoPt}_{2.5\text{nm}}]_5$, 300°C -annealed $[\text{CoO}_{5\text{nm}}/\text{CoPt}_{5\text{nm}}]_5$ and 300°C -annealed $[\text{CoO}_{5\text{nm}}/\text{CoPt}_{7\text{nm}}]_5$ samples.

5.3.3 [CoO_x/CoPt_y]_n with different CoO thickness

					300°C-annealed		
[CoO _{5nm} /CoPt _{5nm}] ₅					●		
[CoO _{10nm} /CoPt _{5nm}] ₃					●		

PEB of 300°C-annealed [CoO_{5nm}/CoPt_{5nm}]₅ and 300°C-annealed [CoO_{10nm}/CoPt_{5nm}]₃ with different CoO thickness y=5nm, 10nm were studied in section 5.3.3. After perpendicular field cooling by liquid N₂ (from RT to 80K in a 5kOe exterior magnetic field), the out-of-plane M-H hysteresis loops were measured at low temperature around 80K by VSM. The related PEB experimental results are listed in Fig 5-4.

According to the experimental results, we can find for the 300°C-annealed samples, CoO thickness y=5nm is better for developing strong PEB.

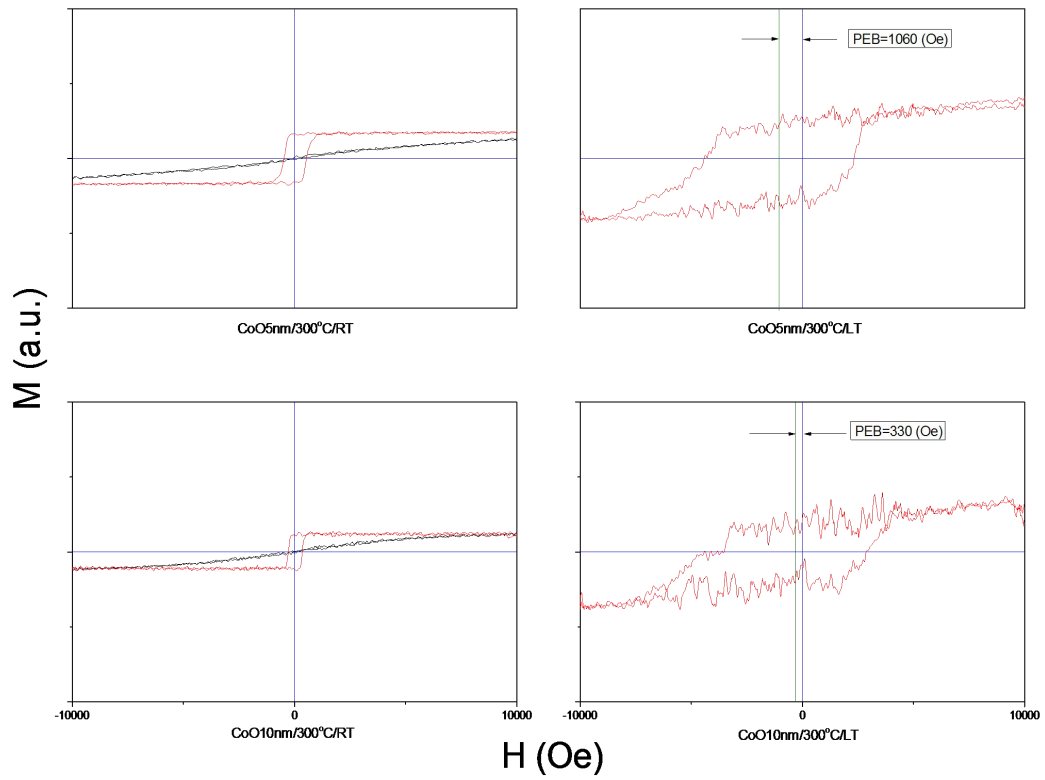


Fig 5-4 PMA (left: measured at RT) and corresponding PEB (right: measured at LT 80K) of 300°C-annealed [CoO5nm/CoPt5nm]5 and 300°C-annealed [CoO10nm/CoPt5nm]3 samples.

5.3.4 [CoO_x/CoPt_y]_n with different period

					300°C-annealed		
[CoO _{5nm} /CoPt _{5nm}] ₃					●		
[CoO _{5nm} /CoPt _{5nm}] ₅					●		
[CoO _{5nm} /CoPt _{5nm}] ₈					●		
[CoO _{5nm} /CoPt _{5nm}] ₁₀					●		

PEB of 300°C-annealed [CoO_{5nm}/CoPt_{5nm}]_n with different repetition period n=3, 5, 8, 10 were studied in section 5.3.4. After perpendicular field cooling by liquid N₂ (from RT to 80K in a 5kOe exterior magnetic field), the out-of-plane M-H hysteresis loops of 300°C-annealed [CoO_{5nm}/CoPt_{5nm}]_n were measured at low temperature around 80K by VSM. The related PEB experimental results are listed in Fig 5-5.

According to the experimental results, we can find for the 300°C-annealed [CoO_{5nm}/CoPt_{5nm}]_n, n=5 is the best repetition period for developing strong PEB.

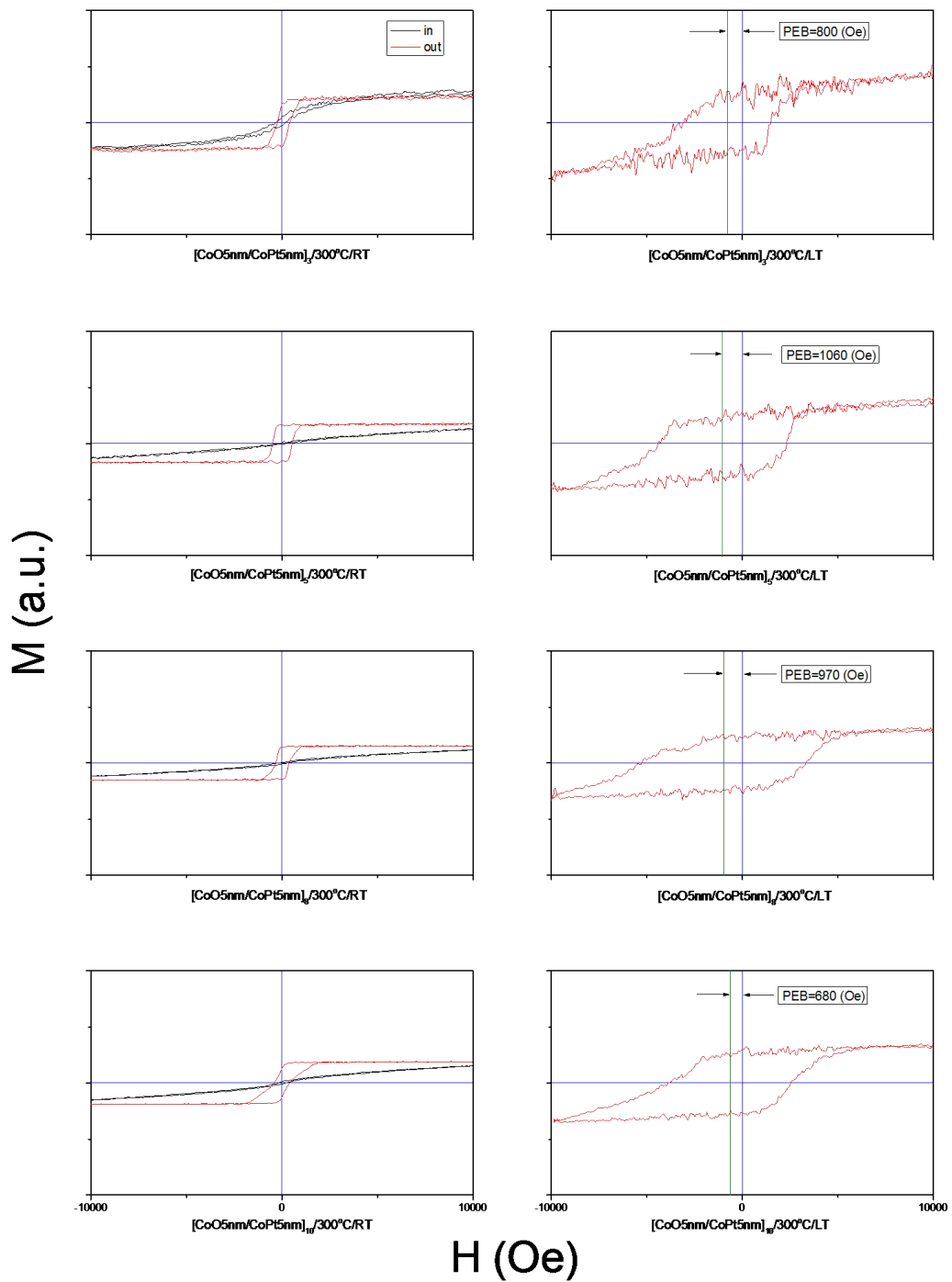


Fig 5-5 PMA (left: measured at RT) and corresponding PEB (right: measured at LT 80K) of 300°C-annealed $[CoO5nm/CoPt5nm]_3$, 300°C-annealed $[CoO5nm/CoPt5nm]_5$, 300°C-annealed $[CoO5nm/CoPt5nm]_8$ and 300°C-annealed $[CoO5nm/CoPt5nm]_{10}$ samples.

5.3.5 [CoPt_y/CoO_x]_n with CoO_{20nm} seed layer

					300°C-annealed	350°C-annealed	
CoO _{20nm} /[CoPt _{5nm} /CoO _{5nm}] ₅					●	●	
CoO _{20nm} /[CoPt _{6nm} /CoO _{5nm}] ₅					●	●	

PEB of CoO_{20nm}/[CoPt_y/CoO_{5nm}]₅ with CoO_{20nm} seed layer but different CoPt thickness $y=5\text{nm}$, 6nm were studied in section 5.3.5. After perpendicular field cooling by liquid N₂ (from RT to 80K in a 5kOe exterior magnetic field), the out-of-plane M-H hysteresis loops of 300°C-annealed and 350°C-annealed CoO_{20nm}/[CoPt_y/CoO_{5nm}]₅ were measured at low temperature around 80K by VSM. The related PEB experimental results are listed in Fig 5-6.

According to the experimental results, we can find for the CoO_{20nm}/[CoPt_y/CoO_{5nm}]₅ films with CoO_{20nm} seed layer, it is hard to get strong PEB with clear rising-edge and falling-edge, although their PMA are very strong after annealing at 300°C and 350°C.

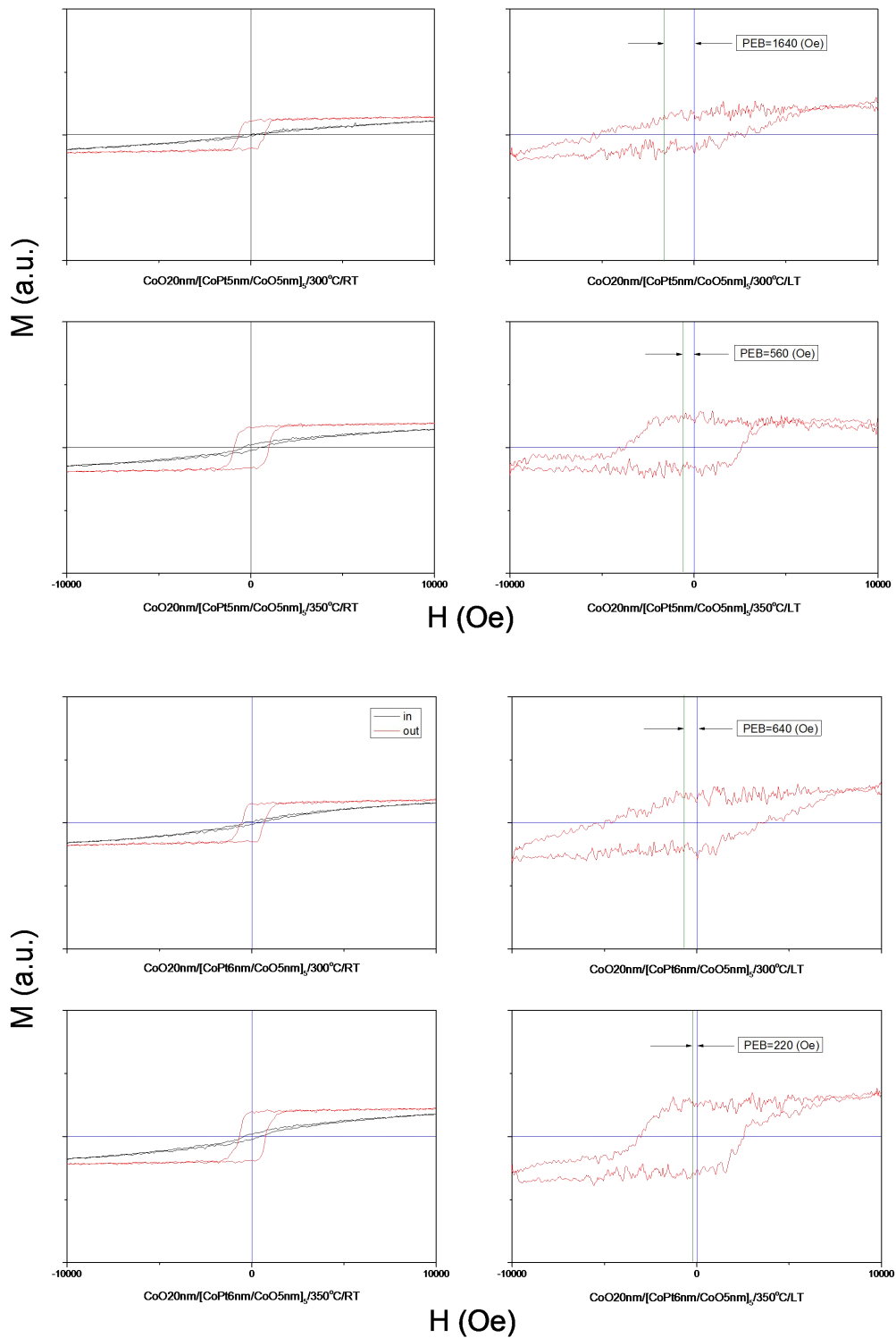


Fig 5-6 PMA (left: measured at RT) and corresponding PEB (right: measured at LT 80K) of 300°C/350°C-annealed $\text{CoO20nm}/[\text{CoPt5nm}/\text{CoO5nm}]_5$ and 300°C/350°C-annealed $\text{CoO20nm}/[\text{CoPt6nm}/\text{CoO5nm}]_5$ samples.

5.4 Conclusion

1. To get the best PBE in $[\text{CoO}_x/\text{CoPt}_y]_n$ multilayer films, the influences of post-annealing temperature, CoPt thickness y , CoO thickness x , repetition period n and CoO seed layer on PEB of $[\text{CoO}_x/\text{CoPt}_y]_n$ multilayer films have been studied systematically.
2. Enhanced PEB can be obtained in the annealed $[\text{CoO}_x/\text{CoPt}_y]_n$ multilayer films. Especially, the strongest PEB can be obtained in the 300°C-annealed $[\text{CoO}_x/\text{CoPt}_y]_n$ multilayer films.
3. According to our experiments, 300°C-annealed $[\text{CoO}_{5\text{nm}}/\text{CoPt}_{5\text{nm}}]_5$ multilayer film (Fig 5-1) shows the best PEB performance, having a PEB value of 1060 Oe with clear rising-edge and falling-edge.

References

- [1] J. Nogues and I. K. Schuller, *J. Magn. Mater.* 192, (1999) 203.
- [2] S. N. Dong, X. H. Huang and X. G. Li, *Materials China*, 30, 46, 2011.
- [3] Brown, Elliot and Wormington, Matthew, *The International Centre for Diffraction Data*. pp. 290–294. 2011.
- [4] L. Guo, Y. Wang, J. Wang, S. Muraishi, T. Sannomiya, Y. Nakamura and J. Shi, *J. Magn. Mater.* 394, (2015) 349.
- [5] R. Coehoorn, *Giant magnetoresistance and magnetic interactions in exchange-biased spin-valves*. Technische Universiteit Eindhoven. 2011.
- [6] B. C. Dodrill, B. J. Kelley, *Magnetic In-line Metrology for GMR Spin-Valve Sensors*, 2011.

Chapter 6 Magnetoelastically induced perpendicular magnetic anisotropy and perpendicular exchange bias of [CoO5nm/CoPt5nm]₅ multilayer films

6.1 Introduction

Perpendicular exchange bias (PEB) was introduced as an active topic in the past few years with the development of perpendicular magnetic anisotropy (PMA). After perpendicular field cooling, PEB has been established in (CoPt)/(CoO, FeMn, FeF₂) multilayer films with PMA [1-3]. Since its discovery, extrinsic control of PEB has been proposed, due to its scientific significance in spintronic devices and potential application in high density magnetic random access memory with perpendicular magnetic tunneling junction (p-MTJ).

At present, the researches aiming to control PEB so far are focused mainly on enhancing the interfacial exchange coupling by adjusting the FM/AFM interface roughness, or optimizing the crystalline structures of FM or AFM layer by employing different seed layers [4,5]. In fact, during the epitaxial growth process of FM/AFM multilayer films in-plane stress will be introduced inevitably, due to the lattice mismatch between FM and AFM layer. As is known, the in-plane stress is considered to be an important physical origin of PMA in FM/AFM multilayer films, which is so called magnetoelastically induced PMA [6,7].

In this chapter, the effects of magnetoelastically induced PMA on PEB have been studied in [CoO5nm/CoPt5nm]₅ multilayer films. We find the PMA strength of CoPt layer plays an important role on PEB at CoO/CoPt interfaces and it is effective to control PEB of [CoO5nm/CoPt5nm]₅ multilayer films by changing the magnetoelastically induced PMA strength of CoPt layer.

After deposition at room temperature, [CoO5nm/CoPt5nm]₅ multilayer films were post annealed at 100°C, 250°C, 300°C and 375°C for 3h, respectively. In-plane tensile stress of CoPt layer was calculated by $\sin^2 \varphi$ method, and we found it increased gradually upon annealing from 0.99 GPa (as-deposited) up to 3.02 GPa (300°C-annealed). As to the magnetic property, significant enhancement of PMA was achieved in [CoO5nm/CoPt5nm]₅ multilayer films after annealing due to the increase of CoPt layer in-plane tensile stress. With the enhancement of magnetoelastically induced PMA, great improvement of PEB was also achieved in [CoO5nm/CoPt5nm]₅ multilayer films, which increased from 130 Oe (as-deposited) up to 1060 Oe (300°C-annealed), showing the same change tendency as PMA and the strong correlation with CoPt layer in-plane tensile stress.

We consider it is the increase of CoPt layer in-plane tensile stress that leads to the enhancement of CoPt layer PMA, which is favorable for the spins in CoPt layer aligning to a more perpendicular direction. And thus the enhanced PMA with more perpendicular spins alignment in CoPt layer results in the improved

PEB in [CoO5nm/CoPt5nm]₅ multilayer films through enhanced perpendicular spins coupling at CoO/CoPt interfaces.

Keywords:

[CoO5nm/CoPt5nm]₅ multilayer film,
magnetoelastic effect,
perpendicular exchange bias,
perpendicular magnetic anisotropy,
correlation between PEB and PMA.

6.2 Experimental details

6.2.1 Preparation of [CoO5nm/CoPt5nm]₅ multilayer films

[CoO5nm/CoPt5nm]₅ multilayer films were deposited by magnetron sputtering on fused quartz substrate at room temperature (RT). The base pressure before deposition was around 5×10^{-5} Pa, ferromagnetic Co_{0.43}Pt_{0.57} solid solution layer was DC deposited with 0.8Pa Ar, antiferromagnetic CoO layer was RF deposited with gas mixture of 0.8Pa Ar and 0.2Pa O₂. After deposition at room temperature, the [CoO5nm/CoPt5nm]₅ multilayer films were vacuum annealed at 100°C, 250°C, 300°C and 375°C for 3h, respectively.

6.2.2 Characterizations of [CoO5nm/CoPt5nm]₅ multilayer films

The microstructure characterizations of [CoO5nm/CoPt5nm]₅ multilayer films including cross-section, crystallinity and top surface were carried out by transmission electron microscopy (TEM), x-ray diffraction (XRD) and atomic force microscope (AFM), respectively. By $\sin^2 \varphi$ method, residual stress in CoPt layer was calculated through analyzing its in-plane (11-1) and out-of-plane (111) lattice parameters. PMA was determined directly at RT with vibrating sample magnetometer (VSM), PEB was determined at low temperature around 80K after perpendicular field cooling through CoO Néel temperature ($T_N \sim 290\text{K}$) in a 5kOe exterior magnetic field.

6.3 Results and discussion

6.3.1 PMA of [CoO5nm/CoPt5nm]₅ multilayer films

PMA M-H hysteresis loops of [CoO5nm/CoPt5nm]₅ multilayer films were determined directly at RT using VSM. Fig 6-1 shows the dependence of PMA on post-annealing temperature.

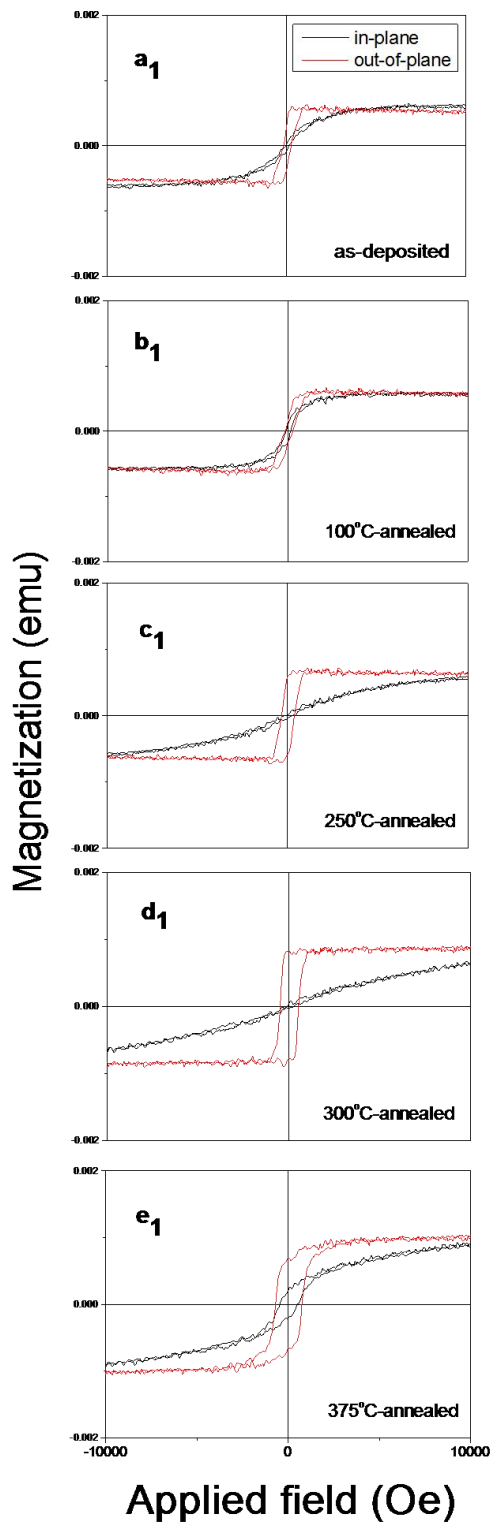


Fig 6-1 PMA M-H hysteresis loops of as-deposited, 100°C, 250°C, 300°C and 375°C annealed [CoO5nm/CoPt5nm]₅ samples (measured at RT).

It can be seen that PMA is enhanced after annealing even the as-deposited sample has already shown PMA. When the sample is annealed up to 300°C, the squareness of the out-of-plane hysteresis loop is improved gradually with enhanced coercivity, while the in-plane hysteresis loop becomes more and more slanted with increased saturation field. As shown in Fig 6-1(d₁), the strongest PMA is achieved when the sample is annealed at 300°C. However, PMA shows degradation tendency when the annealing temperature is above 350°C and we can see in Fig 6-1(e₁) that PMA becomes weaker for the sample annealed at 375°C. According to our previous experience, this is due to the decomposition of CoO layer at high temperature. As to the 400°C annealed sample (not shown here), CoO layer is greatly decomposed and it becomes magnetic isotropic due to the interaction of CoPt layer and the increased soft ferromagnetic Co phase.

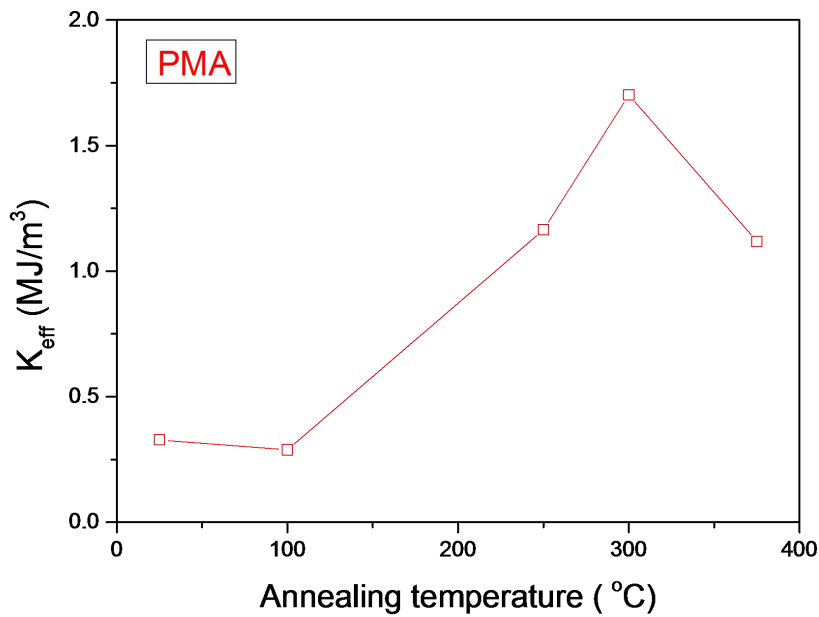


Fig 6-2 K_{eff} of all [CoO5nm/CoPt5nm]₅ calculated from PMA M-H hysteresis loops.

Moreover, to compare the magnetic properties of different [CoO5nm/CoPt5nm]₅ samples objectively, the effective PMA energy (K_{eff}) was calculated based on the M-H hysteresis loops shown in Fig 6-1.

As is shown in Fig 6-2, with the increasing of annealing temperature up to 300°C, K_{eff} increases gradually from 0.33MJ/m³ up to 1.70MJ/m³. However, K_{eff} decreases evidently when the annealing temperature exceeds 300°C due to the decomposition of CoO layer. Especially for the 375°C-annealed sample, its K_{eff} drops to 1.12MJ/m³.

6.3.2 PEB of [CoO5nm/CoPt5nm]₅ multilayer films

On the other hand, exchange bias is an interfacial phenomenon associated with exchange coupling created at the FM/AFM interface, when the system is field-cooled through AFM Néel temperature (T_N). So, in the case of [CoO5nm/CoPt5nm]₅ multilayer films here, their PEB was determined at low temperature around 80K, after perpendicular field cooling by liquid N₂ through CoO Néel temperature $T_N \sim 290K$ (cooled from RT to 80K in a 5kOe exterior magnetic field).

In this section, PEB out-of-plane M-H hysteresis loops of [CoO5nm/CoPt5nm]₅ samples are shown in Fig 6-3. The dependence of PEB values on post-annealing temperatures are shown in Fig 6-4.

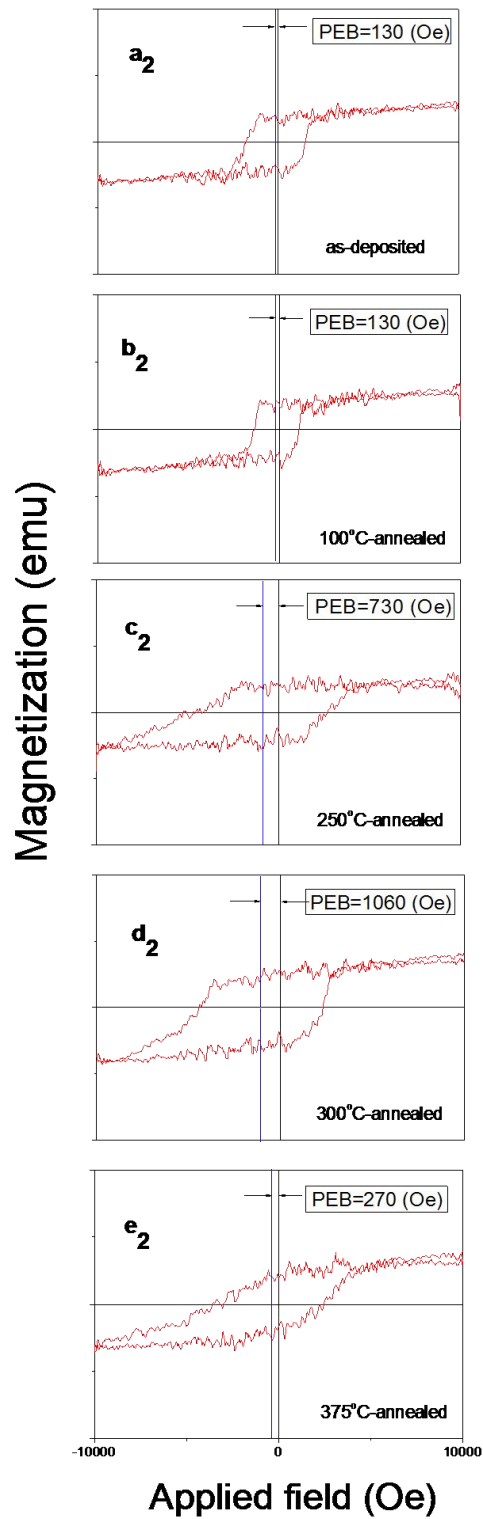


Fig 6-3 PEB out-of-plane M-H hysteresis loops of $[\text{CoO}5\text{nm}/\text{CoPt}5\text{nm}]_5$ samples (measured at 80K after perpendicular field cooling).

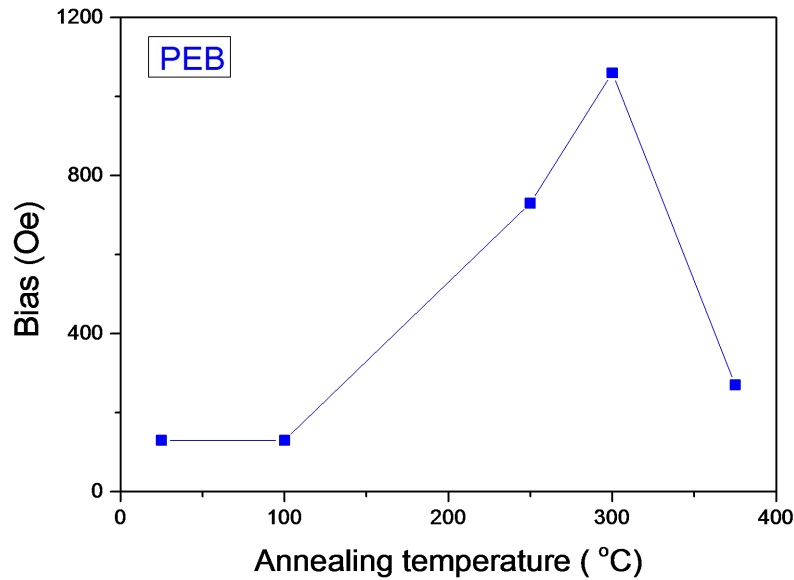


Fig 6-4 Bias values of all [CoO5nm/CoPt5nm]₅ samples derived from PEB out-of-plane M-H hysteresis loops.

We can find that the shift of the out-of-plane hysteresis loop from the origin shown in Fig 6-3 demonstrates the PEB effect clearly. Similar with PMA, PEB increases from 130Oe to 1060Oe when the samples are annealed up to 300°C, then it degrades greatly when the annealing temperature is above 350°C. In our opinion, the degradation of PEB for the 375°C annealed sample is also due to the decomposition of CoO layer and thus the weakened spin coupling between CoPt and CoO.

6.3.3 Cross-section TEM and top-surface AFM

In order to characterize the microstructure of [CoO5nm/CoPt5nm]₅ multilayer films, cross-section TEM and top-surface AFM measurements were carried out firstly.

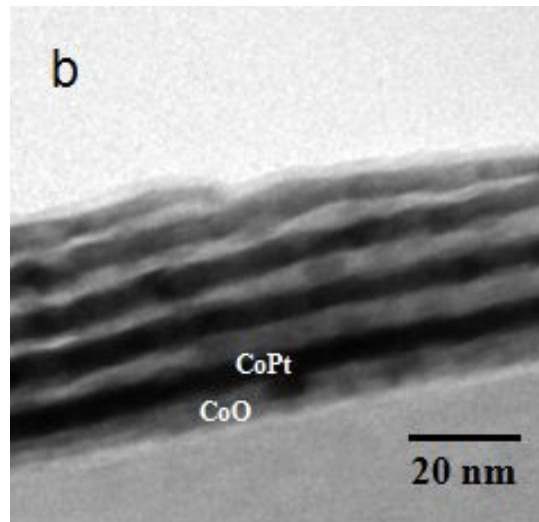
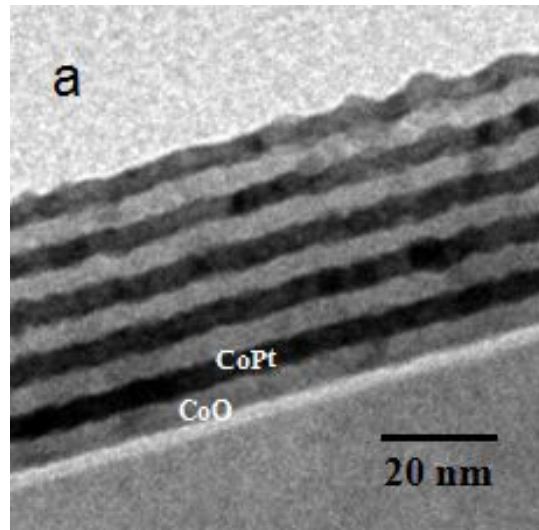


Fig 6-5 Cross-section TEM images of as-deposited (a) and 300°C-annealed (b) $[\text{CoO}5\text{nm}/\text{CoPt}5\text{nm}]_5$ samples.

In Fig 6-5(a), the continuous multilayer structure with sharp component transition at $\text{CoO}5\text{nm}/\text{CoPt}5\text{nm}$ interfaces can be identified clearly in the as-deposited sample. However, in Fig 6-5(b) CoO layers become fuzzy after 3h annealing at 300°C. To our knowledge, this is due to the slight decomposition of CoO at higher temperature .

Generally, the FM/AFM interface roughness plays important roles in

determining the magnetic properties of FM/AFM multilayer films [8]. As an intuitive reference of CoO/CoPt interface, the topography change of $[\text{CoO}5\text{nm}/\text{CoPt}5\text{nm}]_5$ top-surface versus annealing was observed using AFM.

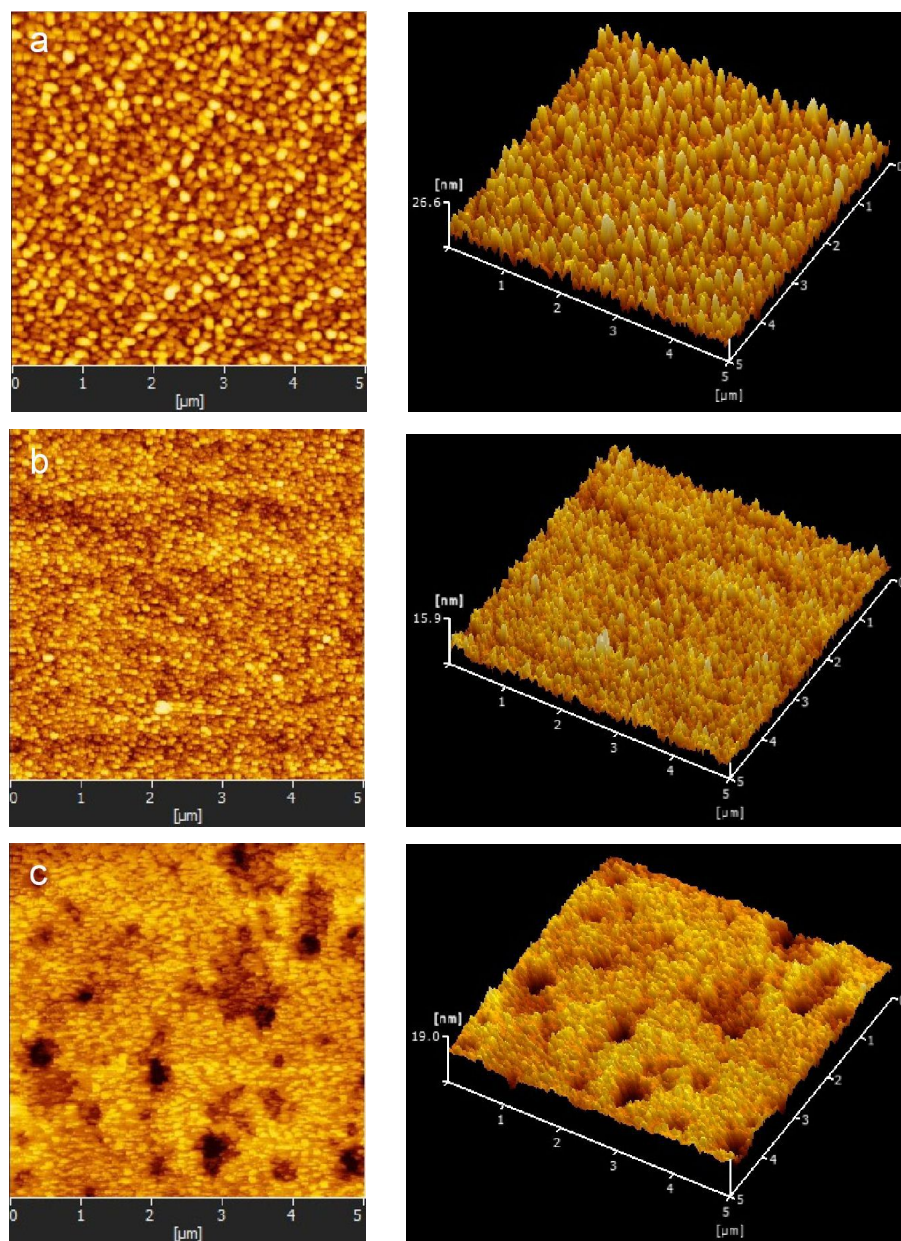


Fig 6-6 2D (left) and 3D (right) AFM images of as-deposited (a), 300°C-annealed (b) and 375°C-annealed (c) $[\text{CoO}5\text{nm}/\text{CoPt}5\text{nm}]_5$ samples.

Fig 6-6 shows the top surface profiles of as-deposited, 300°C-annealed and 375°C-annealed samples. The derived roughness value from AFM images are

3.862nm (as-deposited), 1.534nm (300°C-annealed) and 1.844nm (375°C-annealed) respectively. First, with the improvement of the top surface flatness (roughness value changes from 3.862 nm to 1.534 nm after annealing at 300°C) we can confirm the flatness of CoO/CoPt interfaces should be improved simultaneously, due to the removal of defects and the coalescence of grains. It is well known the improvement of FM/AFM interface flatness is favorable to the enhancement of PMA [9]. Second, it can be seen that in 375°C-annealed sample the decomposition of underneath CoO has great influence on the CoPt top layer, resulting in the quite different top surface topography with black holes. In our opinion, this is the main reason that leads to the degradation of PMA and PEB mentioned above.

6.3.4 XRD and CoPt layer in-plane stress

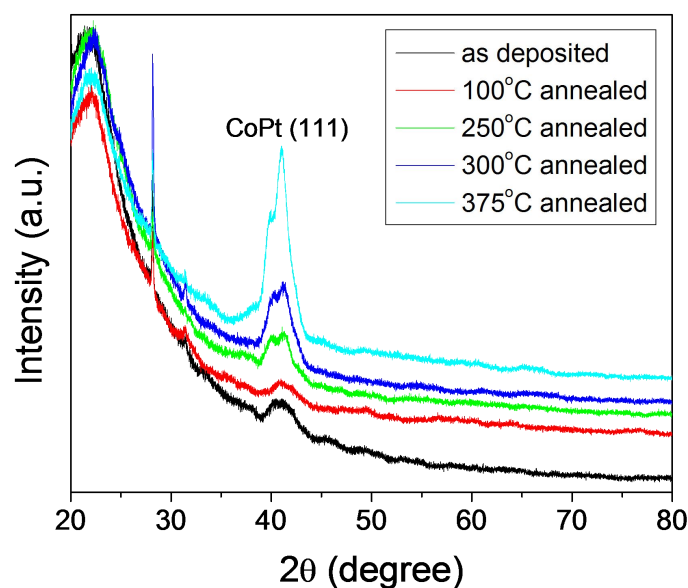


Fig 6-7 Out-of-plane XRD of all [CoO5nm/CoPt5nm]₅ samples.

XRD results shown in Fig 6-7 reveal that all the samples are well crystallized with preferred FCC CoPt (111) orientation. This can be attributed to the addition of Pt, since alloy thin film with Pt component is energetically favorable to form strong (111) texture along the growth direction [9]. With the increasing of annealing temperature, CoPt (111) peak becomes stronger and stronger. According to our previous analysis, stronger CoPt (111) texture is helpful for the enhancement of PMA to some extent. Moreover, the multilayer structure can be confirmed by the satellite peaks around CoPt (111) main peak.

In fact, the lattice mismatch between FCC CoPt ($a_{\text{CoPt}} = 0.38\text{nm}$) and FCC CoO ($a_{\text{CoO}} = 0.43\text{nm}$) is around 12% [9]. This will lead to CoPt layer in-plane tensile stress since CoPt is locally epitaxial growth on CoO layer in the $[\text{CoO}5\text{nm}/\text{CoPt}5\text{nm}]_5$ multilayer films. Upon annealing, the in-plane tensile stress will be changed considering the different thermal expansion coefficients between CoPt and CoO, the change of interfaces, the decomposition of CoO as well as the isotropic shrinkage due to the removal of the interior defects such as the release of dissolved gas atoms [6].

CoPt in-plane tensile stress was calculated by $\sin^2 \varphi$ method through analyzing CoPt in-plane (11-1) and out-of-plane (111) lattice parameters [10]. In order to determine CoPt layer in-plane tensile stress, CoPt (11-1) peak was further measured by *in-plane XRD* (Here we denote it as in-plane XRD, although CoPt (11-1) lattice plane has a dihedral angle = 70.5° to its (111) lattice plane.).

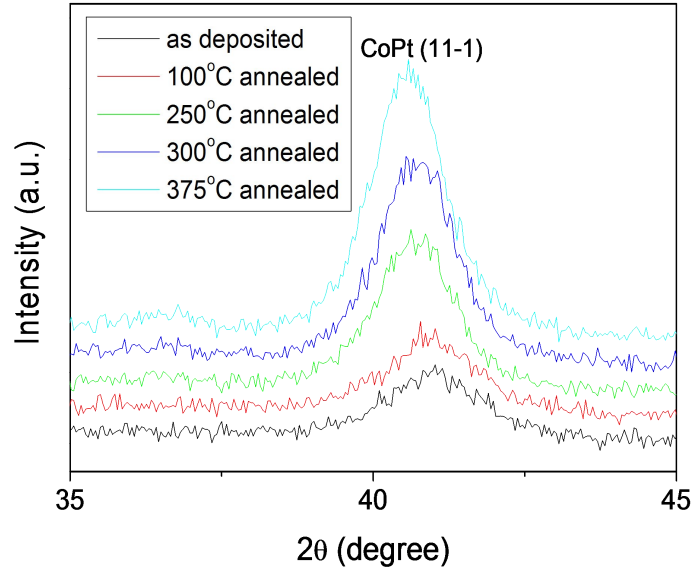


Fig 6-8 In-plane XRD of all [CoO5nm/CoPt5nm]_s samples.

In Fig 6-8, we can find the CoPt (11-1) peak shifts toward lower angle gradually upon annealing. In other words, this indicates the CoPt (11-1) inter-planar distance increases gradually upon annealing, and it will lead to the increasing of CoPt layer in-plane tensile stress inevitably.

Under an assumption of equal-biaxial stress state, we denote the strain at an angle φ to the surface normal as $\varepsilon_{\varphi}^{[111]}$ for the (111) textured fcc CoPt ultra-thin layer, then the strain can be expressed as:

$$\varepsilon_{\varphi}^{[111]} = \frac{(a_{\varphi} - a_0)}{a_0} = \sigma_{//} \left[\frac{(2S_{11} + 4S_{12} - S_{44})}{3} + \frac{(\sin^2 \varphi \cdot S_{44})}{2} \right]$$

where a_{φ} is the lattice parameter along the direction of φ , a_0 is the unstrained lattice parameter, $\sigma_{//}$ is the value of stress in the film plane, and S_{ij} is a component of the compliance array with $S_{11} = 6.51 \times 10^{-3} \text{ GPa}^{-1}$, $S_{12} =$

$-2.48 \times 10^{-3} \text{ GPa}^{-1}$ and $S_{44} = 8.06 \times 10^{-3} \text{ GPa}^{-1}$ [6,11,12]. Then, we can derive the unknown $\sigma_{//}$ by out-of-plane lattice parameter $a_{\perp}(\varphi = 0)$ and in-plane lattice parameter $a_{//}(\varphi = 70.5^{\circ})$.

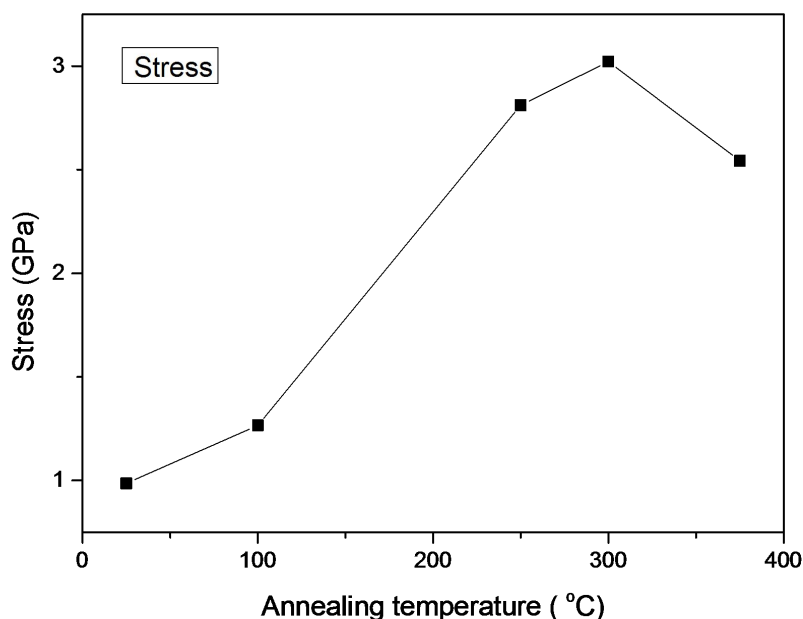


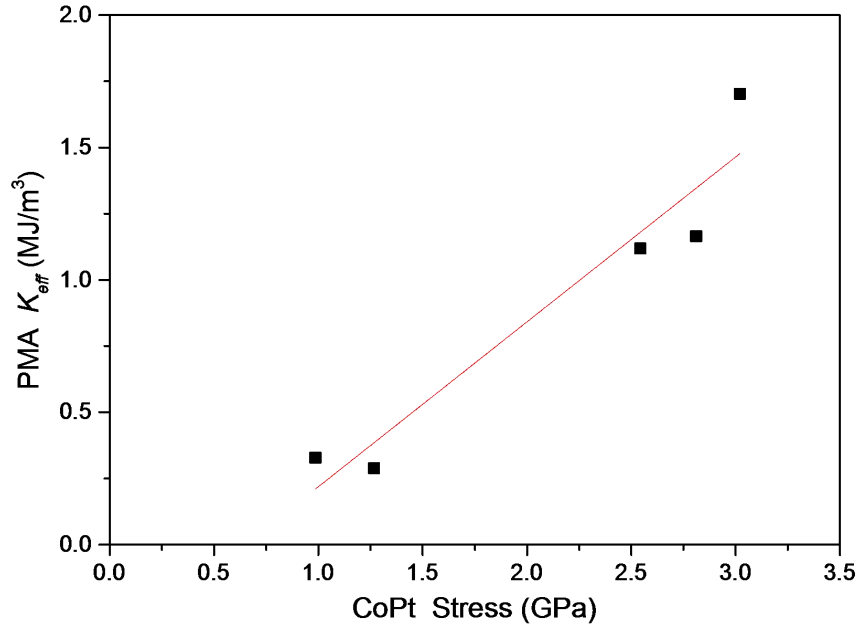
Fig 6-9 CoPt in-plane tensile stress calculated by $\sin^2\phi$ method.

As we can see in Fig 6-9, with the increasing of annealing temperature the calculated tensile stress increases gradually from 0.99GPa to 3.02GPa, but is partially released at 375°C. According to our previous analysis, the release of tensile stress results from the reduced lattice mismatch between CoPt and the decomposed CoO.

6.3.5 Correlation between CoPt layer stress, PMA and PEB

In order to find the mechanism responsible for the enhancement of PEB in $[\text{CoO}5\text{nm}/\text{CoPt}5\text{nm}]_5$, the correlation between CoPt layer stress, PMA and PEB

is further studied.



Magnetoelastic effect

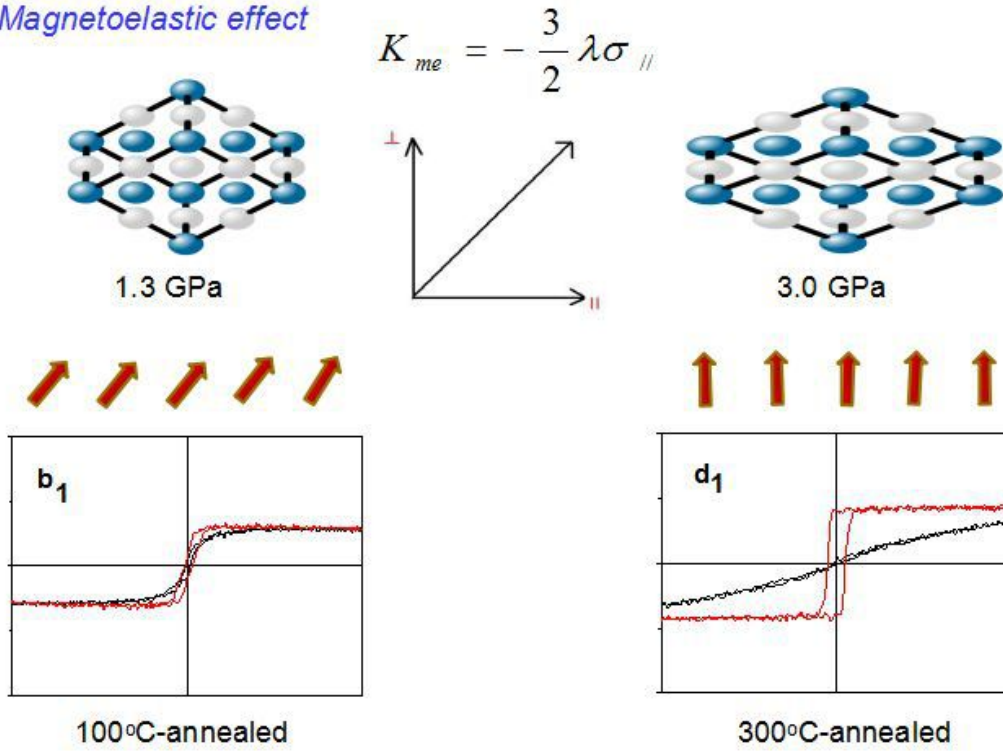


Fig 6-10 CoPt layer in-plane tensile stress and effective PMA energy.

It is well known the magnetoelastic anisotropy of thin films can be correlated with the in-plane stress by magnetoelastic effect:

$$K_{me} = -\frac{3}{2}\lambda\sigma_{//}$$

where K_{me} is the magnetoelastic energy, λ is the magnetostriction constant, $\sigma_{//}$ is the in-plane stress [13]. Since CoPt alloy has a negative magnetostriction constant λ along $\langle 111 \rangle$ direction, an in-plane tensile stress $\sigma_{//}$ will help promote positive magnetoelastic energy K_{me} [14]. As is shown in Fig 6-10, the strong proportional-correlation between CoPt layer in-plane tensile stress and effective PMA energy (K_{eff}) also indicates the enhancement of PMA shown in Fig 6-1 is mainly from the enhanced CoPt layer in-plane tensile stress.

On the other hand, it is generally accepted that PEB is essentially a spin-spin interaction generating from the perpendicular spin coupling between FM and uncompensated AFM at the FM/AFM interface. Therefore, PEB is very sensitive to the perpendicular spin alignment at the FM/AFM interface and any kind of modification of the interfacial spin configuration will affect the strength of the spin coupling and thus the strength of PEB [15,16].

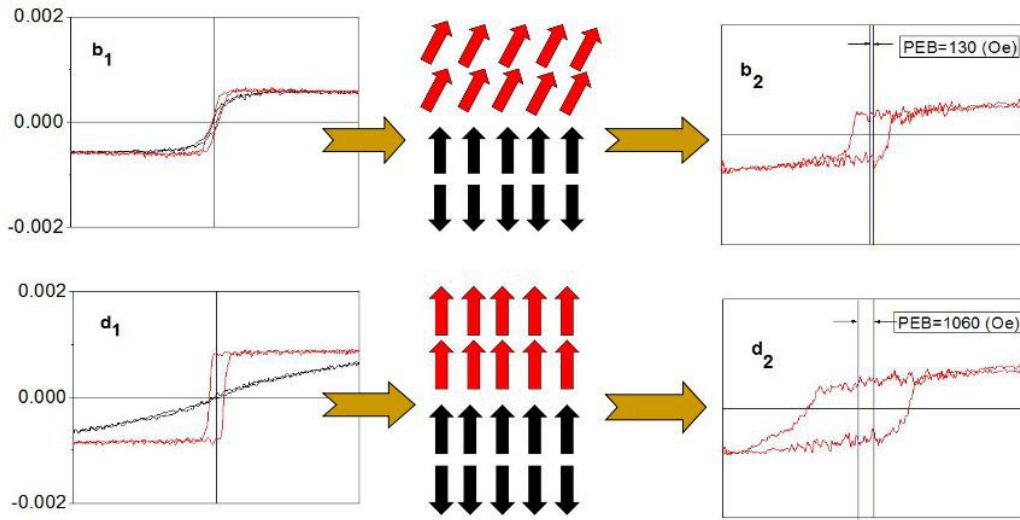


Fig 6-11 Schematic diagrams of Co magnetic moments arrangement at CoO/CoPt interface in $[\text{CoO}5\text{nm}/\text{CoPt}5\text{nm}]_5$ (**b**: is 100°C-annealed sample, **d**: is 300°C-annealed sample).

As is shown in Fig 6-11, in the ideal state, we assume the CoO/CoPt interface is purely smooth, CoPt layer is single domain, Co magnetic moments of CoO layer near to the interface is 100% perpendicular to the CoO/CoPt interface. Under this ideal state, it is easy to understand the enhanced PMA with more perpendicular Co magnetic moments in CoPt layer will result in the improved PEB at CoO/CoPt interface through enhanced perpendicular spins coupling between CoPt and CoO.

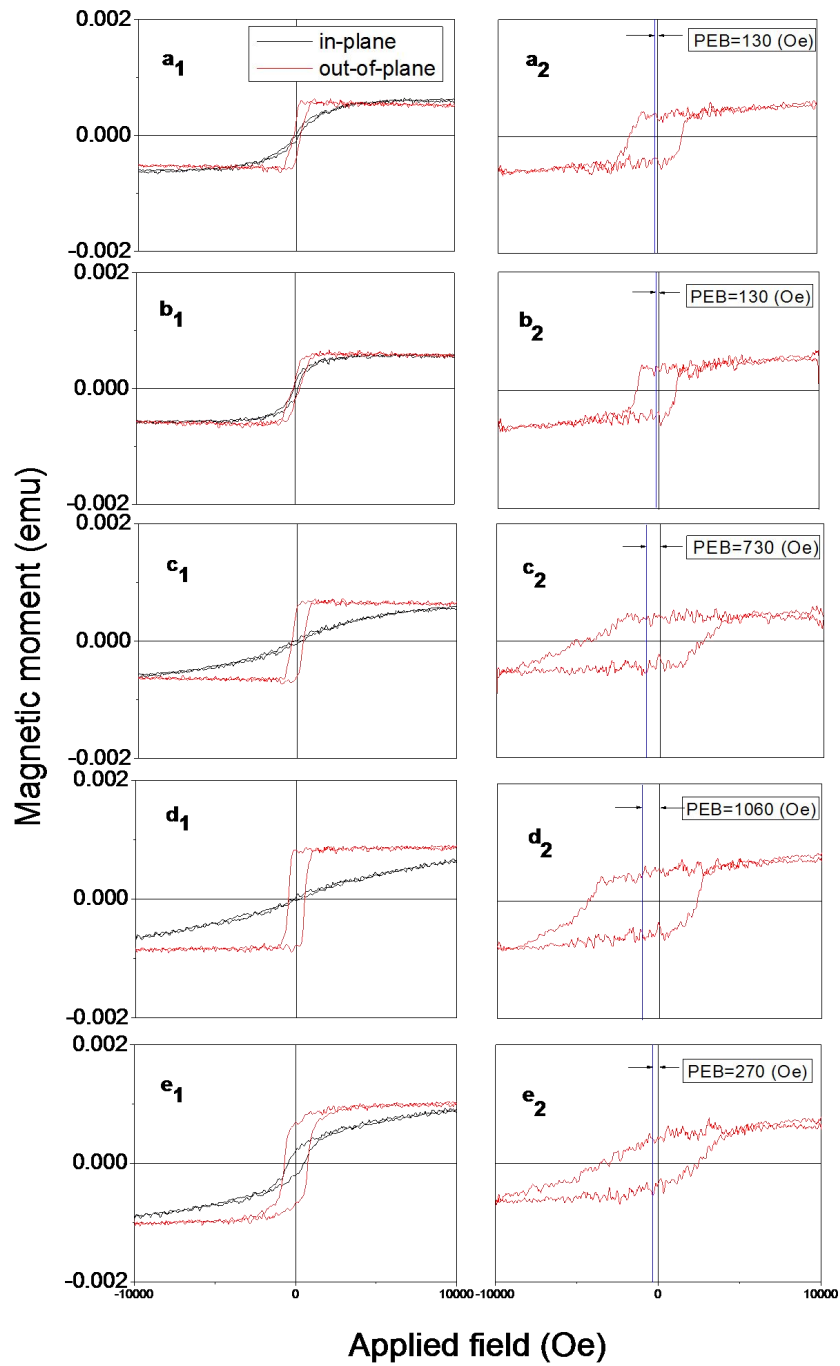


Fig 6-12 Correlation between PMA and PEB.

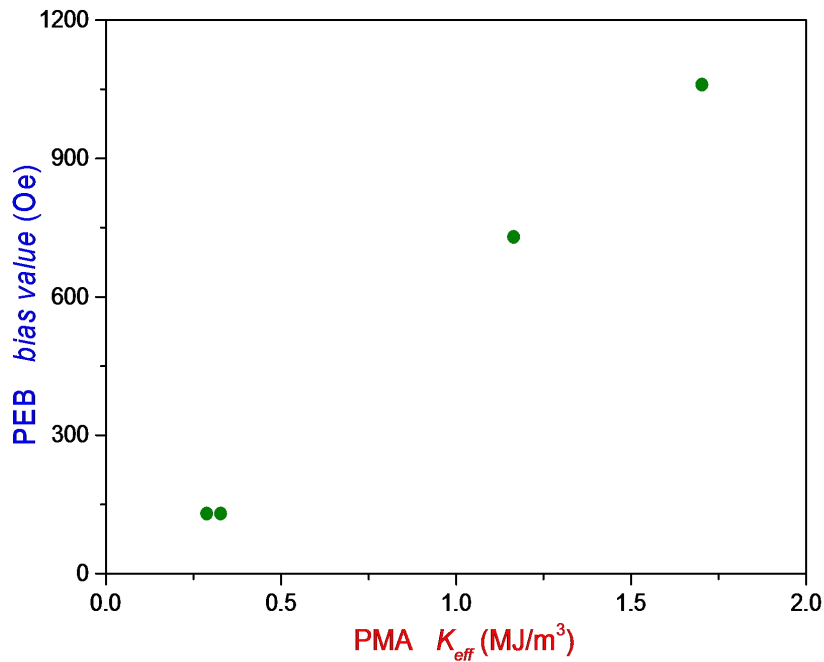


Fig 6-13 Correlation between effective PMA energy and PEB value.

In summary, it is reasonable to conclude that in [CoO5nm/CoPt5nm]₅ multilayer films, enhanced CoPt in-plane tensile stress upon annealing leads to enhanced PMA, which is favorable for the Co magnetic moments in CoPt layer aligning to a more perpendicular direction. The more perpendicular Co magnetic moments alignment in CoPt layer leads to the improved PEB through enhanced perpendicular spins coupling at the CoO/CoPt interface.

Finally, the strong proportional-correlation between PEB value and effective PMA energy (shown in Fig 6-13) also demonstrates the improvement of PEB in [CoO5nm/CoPt5nm]₅ multilayer films results from the magnetoelastically induced PMA enhancement.

6.4 Conclusion

1. The effects of magnetoelastically induced PMA on PEB have been explored in $[\text{CoO}5\text{nm}/\text{CoPt}5\text{nm}]_5$ multilayer films.

2. We find the PMA strength of FM layer plays an important role on PEB at the FM/AFM interface and it is effective to control PEB of $[\text{CoO}5\text{nm}/\text{CoPt}5\text{nm}]_5$ multilayer films by changing the PMA strength of CoPt layer.

3. We demonstrate that the PEB improvement in $[\text{CoO}5\text{nm}/\text{CoPt}5\text{nm}]_5$ multilayer films is mainly due to the magnetoelastically induced PMA enhancement and thus the enhanced perpendicular spins coupling at the CoO/CoPt interface.

4. The positive effect of PMA on PEB at FM/AFM interface in $[\text{CoO}5\text{nm}/\text{CoPt}5\text{nm}]_5$ multilayer films is reported for the first time to our knowledge.

5. We think the controllable PEB should have potential applications in high density magnetic random access memory with perpendicular magnetic tunneling junction.

References

- [1] F. Garcia, G. Casali, S. Auffret, and B. Dieny, *J. Appl. Phys.* **91**, (2002) 6905.
- [2] S. Maat, K. Takano, S. S. P. Parkin and E. E. Fullerton, *Phys. Rev. Lett.* **87**, (2001) 087202.
- [3] B. Kagerer, C. Binck and W. Kleemann, *J. Magn. Magn. Mater.* **217**, (2000) 139.
- [4] L. Lin, N. Thiyagarajah, H. W. Joo, J. Heo, K. A. Lee and S. Bae, *Appl. Phys. Lett.* **97**, (2010) 242514.
- [5] J. Wang, T. Sannomiya, J. Shi and Y. Nakamura, *J. Appl. Phys.* **113**, (2013) 17D707.
- [6] Y. X. Yu, J. Shi and Y. Nakamura, *J. Appl. Phys.* **108**, (2010) 023912 .
- [7] B. N. Engel, C. D. England, R. A. Van leeuwen, M. H. Wiedmann and C. M. Falco, *Phys. Rev. Lett.* **67**, (1991) 1910.
- [8] R. L. Stamps, *J. Phys. D: Appl. Phys.* **33** (2000) R247–R268.
- [9] J. Wang, T. Omi, T. Sannomiya, S. Muraishi, J. Shi and Y. Nakamura, *Appl. Phys. Lett.* **103**, (2013) 042401.
- [10] M. A. Korhonen and C. A. Paszkiet, *Scr. Met.* **23**, (1989) 1449.
- [11] J. Rouchy and A. Waintal, *Solid State Commun.* **17**, (1975) 1227.
- [12] J. Rouchy, E. T. Lacheisserie, and A. Waintal, *J. Magn. Magn. Mater.* **21**, (1980) 69.
- [13] S. Honda, J. Ago, M. Nawate and N. Morita, *IEEE Trans. Magn.* **28**, (1992) 2677.
- [14] H. Takahashi, S. Tsunashima and S. Uchiyama, *J. Magn. Magn. Mater.* **126**, (1993) 282.
- [15] J. Nogues and I. K. Schuller, *J. Magn. Magn. Mater.* **192**, (1999) 203.
- [16] W. H. Meiklejohn and C. P. Bean, *Phys. Rev.* **105**, (1957) 904.

Chapter 7 Conclusions

Perpendicular magnetic anisotropy (PMA) and perpendicular exchange bias (PEB) of $[\text{CoO}_x/\text{CoPt}_y]_n$ multilayer films have been studied systematically in this thesis. In order to get the best PMA and the best PEB in $[\text{CoO}_x/\text{CoPt}_y]_n$ multilayer films, the influences of post-annealing temperature, CoPt thickness, CoO thickness, repetition period and CoO seed layer on PMA and PEB were studied step by step.

According to our experiments, $\text{CoO}_{20\text{nm}}/[\text{CoPt}_{5\text{nm}}/\text{CoO}_{5\text{nm}}]_5$ multilayer films show the best PMA performance and possess the highest thermal stability at the temperature region between -192°C and 400°C . This indicates $\text{CoO}_{20\text{nm}}/[\text{CoPt}_{5\text{nm}}/\text{CoO}_{5\text{nm}}]_5$ multilayer films could be a potential candidate for the PMA application at elevated temperatures, in particular when they need to be processed at the middle high temperature region between 300°C and 400°C .

After perpendicular field cooling, PEB was also obtained in $[\text{CoO}_x/\text{CoPt}_y]_n$ multilayer films. According to our experiments, 300°C -annealed $[\text{CoO}_{5\text{nm}}/\text{CoPt}_{5\text{nm}}]_5$ film shows the best PEB performance, having a PEB value of 1060Oe. We hope this 300°C -annealed $[\text{CoO}_{5\text{nm}}/\text{CoPt}_{5\text{nm}}]_5$ multilayer film can have some potential applications in perpendicular magnetic tunneling junction.

The mechanism responsible for the magnetic anisotropy transition in $[\text{CoO}_{5\text{nm}}/\text{CoPt}_{7\text{nm}}]_5$ multilayer films has been studied in detail by analyzing

CoO/CoPt interface and CoPt layer internal stress. $[\text{CoO}_{5\text{nm}}/\text{CoPt}_{7\text{nm}}]_5$ undergoes a smooth transition from longitudinal magnetic anisotropy (LMA) to PMA upon annealing and returns backward to LMA at high temperature of 550°C. It is found the effective PMA energy is proportional to the in-plane tensile stress of CoPt layer but is inversely proportional to the roughness of CoO/CoPt interface. By means of low temperature experiment, we demonstrate the magnetic anisotropy transition observed in $[\text{CoO}_{5\text{nm}}/\text{CoPt}_{7\text{nm}}]_5$ multilayer film is mainly attributed to the change of CoPt layer in-plane tensile stress.

The effects of magnetoelastically induced PMA on PEB have been studied in $[\text{CoO}_{5\text{nm}}/\text{CoPt}_{5\text{nm}}]_5$ multilayer films. In-plane tensile stress of CoPt layer was calculated by $\sin^2 \varphi$ method, and we found it increased gradually upon annealing from 0.99 GPa (as-deposited) up to 3.02 GPa (300°C-annealed) in $[\text{CoO}_{5\text{nm}}/\text{CoPt}_{5\text{nm}}]_5$ multilayer films. Significant enhancement of PMA was achieved in $[\text{CoO}_{5\text{nm}}/\text{CoPt}_{5\text{nm}}]_5$ multilayer films after annealing due to the increase of CoPt layer in-plane tensile stress. With the enhancement of magnetoelastically induced PMA, great improvement of PEB was also achieved in $[\text{CoO}_{5\text{nm}}/\text{CoPt}_{5\text{nm}}]_5$ multilayer films, which increased from 130 Oe (as-deposited) up to 1060 Oe (300°C-annealed), showing the same change tendency as PMA and the strong correlation with CoPt layer in-plane tensile stress. We consider it is the increase of CoPt layer in-plane tensile stress that leads to the enhancement of CoPt layer PMA, which is favorable for the spins in

CoPt layer aligning to a more perpendicular direction. And thus the enhanced PMA with more perpendicular spins alignment in CoPt layer results in the improved PEB in $[\text{CoO}_{5\text{nm}}/\text{CoPt}_{5\text{nm}}]_5$ multilayer films through enhanced perpendicular spins coupling at CoO/CoPt interfaces.

To our knowledge, the PMA surviving at temperature region between 300°C and 400°C in $[\text{CoO}_x/\text{CoPt}_y]_n$ multilayer film is obtained for the first time. On the other hand, the positive effect of PMA on PEB at FM/AFM interface in $[\text{CoO}_x/\text{CoPt}_y]_n$ multilayer films is also reported for the first time.

Publications

1. L. Guo, Y. Wang, J. Wang, S. Muraishi, T. Sannomiya, Y. Nakamura and J. Shi, Magnetoelastically induced perpendicular magnetic anisotropy and perpendicular exchange bias of CoO/CoPt multilayer films, *Journal of Magnetism and Magnetic Materials*, **394**, 349-353, (2015).
2. L. Guo, T. Harumoto, T. Sannomiya, S. Muraishi, Y. Nakamura and J. Shi, Magnetoelastically induced magnetic anisotropy transition in $[\text{CoO}_{5\text{nm}}/\text{CoPt}_{7\text{nm}}]_5$ multilayer films, *Journal of Magnetism and Magnetic Materials*, **407**, 148-154, (2016).

Presentations

1. L. Guo, J. Wang, J. Shi and Y. Nakamura, Magnetic Anisotropy in CoO/CoPt Multilayers, The Workshop on Education and Research Center for Materials Innovation, Tokyo Institute of Technology, Japan, February 6, 2014.
2. L. Guo, Y. Wang, J. Shi and Y. Nakamura, Perpendicular magnetic anisotropy and perpendicular exchange bias in CoO/CoPt multilayer films, 17th International Conference on Magnetism and Magnetic Materials, Barcelona, Spain, August 17-18, 2015.
3. L. Guo, J. Shi and Y. Nakamura, Magnetoelastically induced perpendicular magnetic anisotropy and perpendicular exchange bias of CoO/CoPt multilayer films, 日本電子材料技術協会第 52 回秋期講演大会, Tokyo, Japan, November 13, 2015.

Acknowledgements

First of all, I would like to express my sincere gratitude to my supervisor, Prof. Shi, for accepting me as a PhD candidate in Tokyo Institute of Technology. I am deeply grateful of his thoughtful instructions and kind suggestions throughout my study, his help in the completion of my PhD. I am also greatly indebted to my supervisor, Prof. Nakamura, who have instructed and helped me a lot in XRD and XRR. His broad knowledge and instructive advice on crystal structure and TEM really gave me useful edification. Moreover, I greatly appreciate my supervisors, Prof. Nakamura and Prof. Shi, for their kind help and valuable recommendation letter on my job-hunting in Japan.

I would like to thank Associate Prof. Muraishi, Assistant Prof. Sannomiya and Lecturer Harumoto for their kind help in my study and instructive advice on my papers.

I would like to thank PhD Hongyu An, PhD Tenghua Gao, PhD Yue Wang, PhD Cong Zhang and Master Omi for their help in my study. Special thanks to all members of Nakamura-Shi lab for their kind supports.

Last but not the least, grateful acknowledgement is made to my family members who have been assisting, supporting and caring for me all the time.

December 2015